bioRxiv preprint doi: https://doi.org/10.1101/2025.08.02.668269; this version posted November 10, 2026. The copyright holder for this preprint (which was not certified by peer review) is the author/funder, who has granted bioRxiv a license to display the preprint in perpetuity. It is made available under a CC-BY 4.0 International license.

Protein sequence evolution underlies interspecies incompatibility of a cell fate determinant

Emily L. Rivard,[1,2] John R. Srouji,[1,3] Anastasia Repouliou,[1,4] Cassandra G. Extavour[1,5,6,7*]

[1]Department of Molecular and Cellular Biology, Harvard University, Cambridge, MA, USA

[2]Currently: Department of Molecular Biology and Genetics, Cornell University, Ithaca, NY, USA

[3]Currently: BioNTech SE, Cambridge, MA, USA

[4]Currently: Department of Biological Engineering, Massachusetts Institute of Technology, Cambridge, MA, USA

[5]Department of Organismic and Evolutionary Biology, Harvard University, Cambridge, MA, USA

[6]Howard Hughes Medical Institute, Chevy Chase, MD, USA

[7]Lead contact

*Correspondence: extavour@oeb.harvard.edu

bioRxiv preprint doi: https://doi.org/10.1101/2025.08.02.668269; this version posted November 10, 2026. The copyright holder for this preprint (which was not certified by peer review) is the author/funder, who has granted bioRxiv a license to display the preprint in perpetuity. It is made available under a CC-BY 4.0 International license.

Abstract

Novel and rapidly evolving genes can integrate into conserved gene networks and play critical roles in development. Understanding how sequence variation in the orthologs of such genes influences functional interactions with the molecular products of older, more conserved genes requires investigation at the level of protein function. Here, we ask this question using the *oskar* gene as a case study. *oskar* is essential for primordial germ cell specification and embryonic patterning in fruit flies. Previous work showed functional incompatibility between *oskar* orthologs from the congeneric fruit fly species *Drosophila melanogaster* and *Drosophila virilis*. However, the region(s) of Oskar in which protein-coding sequence evolution led to this incompatibility, and the molecular mechanisms underlying it, remained unknown. To address these questions, we generated chimeric versions of *oskar* comprising different combinations of Oskar protein domains from each species, expressed these chimeric *oskar* sequences in *D. melanogaster*, and quantified their ability to assemble functional germ line and abdominal patterning determinants (germ plasm). We found that a specific portion of *D. virilis* Oskar, namely the OSK domain, was primarily responsible for the cross-species incompatibility of Oskar. In the absence of endogenous *D. melanogaster* Oskar, chimeras containing the *D. virilis* OSK domain could not localize posterior germ plasm well enough to generate primordial germ cells, but were sufficient to specify the anteroposterior axis. We also found that the *D. virilis* OSK domain had dominant-negative effects on *D. melanogaster* Oskar's ability to localize germ plasm mRNAs, resulting in severe axial patterning defects. Both *in vivo* and *in silico* analyses support the hypothesis that evolved changes in the ability of the OSK domain to interact with conserved germ plasm mRNAs played a significant role in the evolution of interspecies incompatibility of Oskar. Under this hypothesis, an essential germ line determinant evolved to be incompatible across species of the same genus in less than 50 million years, while retaining functional within-species molecular interactions. Thus, by investigating *in vivo* protein function, we link genomic and molecular evolution with phenotypic variation and fitness at higher scales.

Keywords: *oskar*, *Drosophila melanogaster*, *Drosophila virilis*, germ line, germ plasm, pole cells, axial patterning

bioRxiv preprint doi: https://doi.org/10.1101/2025.08.02.668269; this version posted November 10, 2026. The copyright holder for this preprint (which was not certified by peer review) is the author/funder, who has granted bioRxiv a license to display the preprint in perpetuity. It is made available under a CC-BY 4.0 International license.

Introduction

Genes with essential roles in development often exhibit strong sequence conservation [1–3]. However, others undergo rapid sequence evolution despite being critical for development [4–7]. While *cis*-regulatory sequence changes frequently drive phenotypic evolution [8–11], evolution in protein-coding sequences can also have dramatic functional consequences for development [12–14]. Unfortunately, simply identifying amino acid substitutions that arise during evolution cannot tell us whether or how they generate phenotypic change [15–17]. Studying the evolution of protein function *in vivo* at a molecular scale—through altered interactions with other molecules, localization patterns, or enzymatic activity—can provide data needed to link sequence changes with biological consequences at cellular and organismal levels.

Germ cell specification is critical not only for the development of an organism, but also for the continuity of its lineage. A suite of ancient, conserved genes function in germ line segregation across metazoans [18,19]. However, multiple convergently evolved lineage-specific and quickly evolving genes have become integrated into this core germ line gene network and acquired essential roles in germ line specification. The best studied example of such a gene is the gene *oskar*, which arose in insects at least 325 million years ago [20,21] and subsequently gained a role in germ cell specification in some species, including *Drosophila melanogaster*. Oskar protein is the only factor necessary and sufficient for assembly of the germ plasm, the specialized cytoplasm at the egg posterior comprised of maternally provided germ line and abdominal patterning molecules [22]. Specifically, Oskar nucleates formation of granules containing these molecules, and the cytoplasm containing these granules acts as a germ line determinant. Thus, cells inheriting these granules, called pole cells, are specified as the primordial germ cells [23].

bioRxiv preprint doi: https://doi.org/10.1101/2025.08.02.668269; this version posted November 10, 2026. The copyright holder for this preprint (which was not certified by peer review) is the author/funder, who has granted bioRxiv a license to display the preprint in perpetuity. It is made available under a CC-BY 4.0 International license.

D. melanogaster Oskar protein structure and function have been interrogated with genetic and biochemical assays over the last several decades. Oskar has two ordered domains, an N-terminal LOTUS domain and a C-terminal hydrolase-like OSK domain (Fig. 1B) [24–26]. The LOTUS domain binds to Vasa protein *in vitro*, and Vasa recruitment to the germ plasm by Oskar is required for germ cell formation [27–29]. The LOTUS domain of Oskar dimerizes *in vitro*, a capacity that could be relevant for its function in *D. melanogaster* [24–26]. The OSK domain binds germ plasm mRNAs *in vitro* [24,25] and is required for proper recruitment of multiple germ plasm mRNAs *in vivo* [30]. An intrinsically disordered region linking LOTUS and OSK may mediate interactions with several additional germ line molecules [31–33]. Finally, while the aforementioned regions comprise the shorter translational isoform of Oskar that nucleates germ granules, there is a longer Oskar isoform with an additional N-terminal disordered domain called the Long Osk domain (Fig. S1B) [34]. Rather than interact with germ granule components, the Long Oskar isoform is required for correct anchoring of *oskar* RNA/protein and mitochondria at the posterior [35,36]. The Long Osk domain also modulates F-actin dynamics and endocytic activity at the posterior cortex of the oocyte, both of which influence how well germ plasm is anchored [37–40].

Despite its essential role in germ plasm assembly, which largely relies on direct interactions with other germ plasm molecules, *oskar* exhibits rapid protein sequence divergence compared with other *Drosophila* germ line genes [6,7]. Indeed, even within the genus *Drosophila*, *oskar* has diverged so much that some orthologs are no longer functionally interchangeable [41,42]. The ortholog of *oskar* from *D. virilis*, a species 40-50 million years diverged from *D. melanogaster* [43], was previously reported to rescue abdominal patterning defects, but not the loss of germ cells, when expressed in *D. melanogaster oskar* protein null flies (*osk[2]* (also called *osk[84]*) or *osk[6]* (also called *osk[166]*)) [42]. Further, the same study reported that *D. virilis*

bioRxiv preprint doi: https://doi.org/10.1101/2025.08.02.668269; this version posted November 10, 2026. The copyright holder for this preprint (which was not certified by peer review) is the author/funder, who has granted bioRxiv a license to display the preprint in perpetuity. It is made available under a CC-BY 4.0 International license.

oskar induced dominant-negative patterning defects in a wild-type background [42]. However, this study raised at least three open questions, which have remained unanswered to date. First, did the trans-species expression vector used yield correct translation or localization of *D. virilis* Oskar protein in *D. melanogaster*? Second, what was the mechanism underlying the dominant-negative impacts of *D. virilis oskar* expression? Third, which region(s) of *D. virilis* Oskar were responsible for its failure to drive pole cell formation in *D. melanogaster*?

While there is substantial evidence that all four major domains of the Oskar protein play important germ plasm assembly roles, the sequence changes that prevent *D. virilis oskar* from specifying germ cells in *D. melanogaster* are unknown. Although evidence suggests that the OSK domain interacts with germ plasm mRNAs [24,25,30], the LOTUS domain interacts with Vasa protein [27–29], the interdomain interacts with Actin-binding proteins [32], and the Long Oskar domain contributes to mitochondrial localization [35], none of these reported domain abilities in *D. melanogaster* indicate that evolved changes in their sequences should or should not be expected to prevent *D. virilis* Oskar from carrying out these functions in a *D. melanogaster* context. Thus, given the essential roles of all four domains of the Oskar protein, it is not clear *a priori* whether any one of these domains might be more of a contributor than others, to inter-species incompatibility.

In principle, inter-species incompatibility of Oskar could be due to evolutionary changes in the sequences of interacting germ plasm mRNAs, rather than in the Oskar protein itself. Indeed, mRNA sequence divergence between lineages can cause changes in germ granule composition for some mRNAs [44]. However, several previous observations lead us to hypothesize that evolutionary divergence in the Oskar protein is more likely to explain why *D. virilis* Oskar cannot assemble functional germ plasm in *D. melanogaster*. First, *D. virilis nanos* mRNA can be

bioRxiv preprint doi: https://doi.org/10.1101/2025.08.02.668269; this version posted November 10, 2026. The copyright holder for this preprint (which was not certified by peer review) is the author/funder, who has granted bioRxiv a license to display the preprint in perpetuity. It is made available under a CC-BY 4.0 International license.

effectively localized to the posterior in *D. melanogaster* embryos (presumably by *D. melanogaster* Oskar), and the 3'UTR of *nanos* mRNA shows high conservation between these two species [45]. Furthermore, unlike *oskar*, *D. virilis nanos* can functionally substitute for *D. melanogaster nanos* [46]. In addition, previous studies have failed to find conserved 3'UTR signatures of germ plasm localization shared across all known mRNA germ plasm components [47,48]. Taken together, these data suggest that evolutionary divergence of germ plasm mRNA UTR sequences is unlikely to provide a simple answer to explain why *D. virilis* Oskar protein cannot assemble functional germ plasm in *D. melanogaster*.

We posit that investigating the basis of this incompatibility could shed light on the larger problem of the evolution of complex molecular regulatory networks whose members have very different molecular evolutionary dynamics, and potentially also on the functional significance of specific portions of *oskar*. Here, we elucidate how protein-coding sequence evolution in *oskar* between these two species influences its ability to assemble functional germ plasm and mediate germ cell specification and abdominal patterning. By expressing *D. melanogaster–D. virilis* chimeric *oskar* sequences in *D. melanogaster* and characterizing their ability to perform Oskar's functions, we identified Oskar protein domains from *D. virilis* that cause failure to form germ cells and impede recruitment of some germ plasm mRNAs to the posterior. We also identified portions of the *D. virilis* Oskar protein with dominant-negative effects on *D. melanogaster* Oskar's ability to recruit germ plasm mRNA and mediate germ cell formation and axial patterning. Finally, we characterized Oskar-driven changes in how germ granules form and localize at the posterior in *D. virilis* and *D. melanogaster*. This evolution-informed mutagenesis strategy sheds new light on structure-function relationships *in vivo* for an important developmental gene. Furthermore, our findings suggest that even within a conserved gene

bioRxiv preprint doi: https://doi.org/10.1101/2025.08.02.668269; this version posted November 10, 2026. The copyright holder for this preprint (which was not certified by peer review) is the author/funder, who has granted bioRxiv a license to display the preprint in perpetuity. It is made available under a CC-BY 4.0 International license.

network, molecular interactions among gene products can evolve in species-specific ways. This highlights the molecular flexibility of developmental programs and underscores the importance of continued investigation at the molecular mechanistic studies to understand interspecies variation in development.

Results

Germ plasm molecules recruited by Oskar in D. melanogaster *are also localized to the posterior in* D. virilis

We first asked how germ plasm assembly, primordial germ cell formation, and Oskar's predicted structure compare between wild-type *D. virilis* and *D. melanogaster*. We used hybridization chain reaction (HCR) *in situ* hybridization and immunofluorescence to determine whether several key germ plasm molecules in *D. melanogaster* localize to the germ plasm of oocytes and embryos of *D. virilis*. We found that, as in *D. melanogaster*, *D. virilis oskar* mRNA and protein localize to the posterior end of oocytes and cleavage stage embryos (Fig. 1A, Fig. S1A). We also observed Vasa protein, mitochondria (detected with an anti-ATP5A antibody), and *nanos, polar granule component* (*pgc*), and *germ cell-less* (*gcl*) mRNAs enriched at the posterior of *D. virilis* eggs (Fig. 1A, Fig. S1A). These data demonstrate that several of the molecules that Oskar recruits to germ plasm in *D. melanogaster* are also found in *D. virilis* germ plasm.

We also used anti-Vasa antibody staining to label and count pole cells in stage 5 embryos from both species. We found that *D. virilis* has significantly fewer pole cells at this stage than *D. melanogaster* (Fig. 1B). This may result from the reduced expression of some germ line

bioRxiv preprint doi: https://doi.org/10.1101/2025.08.02.668269; this version posted November 10, 2026. The copyright holder for this preprint (which was not certified by peer review) is the author/funder, who has granted bioRxiv a license to display the preprint in perpetuity. It is made available under a CC-BY 4.0 International license.

163 determinants in this species [44] or from differences in the composition, organization, or function
164 of germ plasm.

165 Having established that *D. virilis* germ plasm contains known Oskar interaction partners,
166 and that germ cells appear to be spatially and temporally specified in the same way, albeit in
167 different quantities, we next investigated differences in Oskar primary sequence and predicted
168 secondary and tertiary structure between these species. We found that the AlphaFold3 [49]
169 structural predictions for *D. melanogaster* and *D. virilis* Oskar share a domain architecture
170 consisting of four distinct regions (Fig. 1C, Fig. S1A–B). The longer of Oskar's two translational
171 isoforms starts with an N-terminal disordered region called Long Osk, which is 22 amino acids
172 longer in *D. virilis* than in *D. melanogaster* and contains two additional predicted alpha helices
173 (Fig. 1C, Fig. S1A–B). The first folded domain, LOTUS, exhibits a high degree of structural
174 similarity between these species (RMSD = 0.263) and shares 69% amino acid identity (Fig.
175 S1B–C). The disordered interdomain that links Oskar's two folded domains is 33 amino acids
176 shorter in *D. virilis* than in *D. melanogaster* and lacks much secondary structure (Fig. S1B–C).
177 The C-terminal folded domain, OSK, is also structurally similar between the two species (RMSD
178 = 0.297) and shares 76% identity (Fig. S1B–C). Thus, the modular organization of Oskar is
179 similar between *D. melanogaster* and *D. virilis,* with higher sequence and structural similarity
180 within the folded regions and greater variability in the disordered portions of the protein.

181 This shared organization suggested that designing chimeric *D. melanogaster–D. virilis*
182 Oskar proteins with different combinations of the four domains could be an effective strategy for
183 determining the region(s) of Oskar where evolutionary divergence was responsible for the
184 interspecies incompatibility (Fig. 1D). We therefore generated sixteen chimeric versions of
185 Oskar by swapping its four domains between the two species in all possible combinations. To

bioRxiv preprint doi: https://doi.org/10.1101/2025.08.02.668269; this version posted November 10, 2026. The copyright holder for this preprint (which was not certified by peer review) is the author/funder, who has granted bioRxiv a license to display the preprint in perpetuity. It is made available under a CC-BY 4.0 International license.

test the function of these chimeric Oskar proteins in *D. melanogaster,* we expressed these constructs in *D. melanogaster* under the control of the *D. melanogaster* genomic regulatory region. We evaluated the abilities of these chimeric Oskar proteins in two genetic backgrounds: 1) an *oskar* RNA null background to evaluate the chimera's ability to rescue the *oskar* null, and 2) a background with endogenous *oskar* present to assess potential interactions with *D. melanogaster oskar.*

We performed several experiments to ask whether the behaviors of our chimeric Oskar proteins were sufficiently similar to those of endogenous *D. melanogaster* Oskar, to allow us to make inferences about the functional impacts of interspecies protein sequence divergence. First, we quantified enrichment of each chimera at the posterior, and found that despite some variation in detectable expression levels (Figs. S2, S3), this did not correlate with any of the germ plasm component, pole cell formation, or axial patterning phenotypes that we assessed. Further, we determined that chimeric *oskar* mRNAs and proteins localized correctly to the oocyte posterior (Fig. S2, S4, Table S1). In *D. melanogaster*, *oskar* mRNA splicing contributes to its correct localization [50–52]. Although we did not explicitly analyze chimeric *oskar* mRNA processing, we confirmed that correct localization, as well as localization and translation of chimeric Oskar proteins, occurred in all chimeras (Figs. S2–S4). Moreover, all chimeras permitted oogenesis to proceed normally, which does not happen when *D. melanogaster oskar* splicing is disrupted [50,53,54]. Thus, we were able to attribute the germ plasm, pole cell, and body patterning phenotypes we assessed, to species-specific protein domain abilities in the experiments described below.

bioRxiv preprint doi: https://doi.org/10.1101/2025.08.02.668269; this version posted November 10, 2026. The copyright holder for this preprint (which was not certified by peer review) is the author/funder, who has granted bioRxiv a license to display the preprint in perpetuity. It is made available under a CC-BY 4.0 International license.

207 *The* D. virilis *OSK domain impedes germ plasm assembly in* D. melanogaster

208 We first tested whether the chimeric Oskar proteins could induce pole cell formation at
209 the posterior of stage 5 embryos. Consistent with previous studies using a *D. melanogaster oskar*
210 protein null (*osk[2]* (also called *osk[84]*) or *osk[6]* (also called *osk[166]*)) background [42], we
211 found that *D. virilis* Oskar completely failed to specify pole cells in *D. melanogaster oskar* RNA
212 null embryos *(y[1] sc[*] v[1]; Kr[If-1]/CyO; TI{w[+mC]=TI}osk[0.EGFP]*[55]; Fig. 2A–B).
213 Oskar (marked by the HA tag on our transgenes) and Vasa proteins were detected in posterior
214 somatic blastoderm cells (Fig. 2A). Only nine chimeric Oskar proteins could induce any pole
215 cells to form, and only three of those could induce as many pole cells as *D. melanogaster* Oskar
216 (Fig. 2B, Table S2). Notably, inclusion of the *D. virilis* OSK domain caused near (two of eight)
217 or complete (six of eight) failure to generate pole cells (Fig. 2B), suggesting that this domain is
218 an important contributor to *D. virilis oskar*'s functional incompatibility in *D. melanogaster.* We
219 also observed some reduction in pole cell number by chimeras containing the LOTUS domain
220 from *D. virilis* in combination with the interdomain from *D. melanogaster* (Fig. 2B). These
221 reductions did not occur in chimeras that had the *D. virilis* LOTUS and *D. virilis* interdomains
222 together (Fig. 2B), suggesting that the functional properties of Oskar's individual domains may
223 be influenced by neighboring protein sequence.

224 As previously reported [42], we found that although *D. virilis oskar* cannot mediate pole
225 cell formation, it can perform *oskar*'s axial patterning role. Specifically, first instar larval
226 progeny of mothers expressing *D. virilis oskar* exhibited wild-type abdominal patterning (Fig.
227 2C). This result suggests that *D. virilis oskar* can successfully recruit abdominal patterning
228 determinants to the posterior for abdominal specification.

229

bioRxiv preprint doi: https://doi.org/10.1101/2025.08.02.668269; this version posted November 10, 2026. The copyright holder for this preprint (which was not certified by peer review) is the author/funder, who has granted bioRxiv a license to display the preprint in perpetuity. It is made available under a CC-BY 4.0 International license.

D. virilis *Oskar and chimeric Oskar proteins effectively recruit Vasa but not mRNAs to germ plasm*

To better understand how the chimeras either succeeded or failed to perform Oskar's roles in cell fate specification, we examined the localization of a selection of germ plasm molecules that are normally recruited by *D. melanogaster* Oskar to the posterior. Specifically, we measured the integrated enrichment of signal for the 15% posterior-most portion of the egg in immunofluorescence and HCR experiments designed to detect particular germ plasm components (Figs. 3, 5, S5, S6). We also assessed colocalization of the chimeric Oskar proteins with each germ plasm molecule by calculating the Pearson correlation for the signal intensity between HA and another germ plasm molecule, for the pixels in the 15% posterior-most end of the embryo that had HA intensity values two standard deviations over the mean (Fig. S7).

The germ line protein Vasa requires Oskar for its posterior localization [56,57] and directly interacts with *D. melanogaster* Oskar via the LOTUS domain based both on crystal structures and on *in vitro* assays [27,28]. We wished to determine whether failure to accumulate sufficient Vasa in the germ plasm could account for the inability of some of the tested chimeras to induce pole cell formation. In stage 10 oocytes, we found no significant difference in Vasa posterior enrichment between animals expressing *D. melanogaster* or *D. virilis oskar* (Figs. 3, S5A, Table S3). In contrast, for most chimeras we observed reduced Vasa posterior enrichment in oocytes (Fig. 3), suggesting that combinations of sequences from the two species have a deleterious effect on initial recruitment of Vasa to the posterior of the oocyte. However, in cleavage stage embryos, we found that nearly all chimeras enriched Vasa at least as well as *D. melanogaster* Oskar, suggesting that sufficient Vasa protein can accumulate with additional time (Figs. 3, S5B, Table S3). Indeed, embryos expressing several chimeras, as well as full length *D. virilis oskar,*

bioRxiv preprint doi: https://doi.org/10.1101/2025.08.02.668269; this version posted November 10, 2026. The copyright holder for this preprint (which was not certified by peer review) is the author/funder, who has granted bioRxiv a license to display the preprint in perpetuity. It is made available under a CC-BY 4.0 International license.

had significantly higher Vasa enrichment at the posterior than that observed with *D. melanogaster oskar* (Figs. 3, S5B, Table S3). Furthermore, we found that nearly all chimeras had correlation coefficients at least as high as those observed between *D. melanogaster* Oskar and Vasa in embryos (Fig. S7). Structural predictions of *D. virilis* Oskar protein interacting with *D. melanogaster* Vasa generated with AlphaFold3 [49] suggest these proteins would form the same interface observed in both predicted and crystallography-resolved structures of *D. melanogaster* Oskar LOTUS in complex with the RecA-like domain of Vasa (Fig. S8A) [27]. These results suggest that failure to interact with Vasa is unlikely to explain why *D. virilis oskar* cannot rescue pole cell formation in a *D. melanogaster oskar* null background.

We then examined the distribution of the germ plasm mRNAs *nanos* and *germ cell-less* (*gcl*), suggested based on *in vitro* evidence to directly interact with the OSK domain of Oskar as a mechanism for their localization to the posterior [24,25]. Despite the inability of most chimeras to form pole cells (Fig. 2), and the known role of *gcl* in pole cell formation [58], we did not find evidence of reductions in posterior enrichment of *gcl* in embryos from mothers expressing most of the chimeras (Figs. 3, S5D, Table S3). However, we did find significantly reduced enrichment of *nanos* in embryos laid by mothers expressing several chimeras with one or both of the *D. virilis* LOTUS or OSK domains (Figs. 3, S5C, Table S3). Thus, *D. virilis* protein sequence from either of the two folded Oskar domains may prevent *nanos* mRNA from accumulating at the posterior to wild-type levels in *D. melanogaster*.

Furthermore, we found that the *D. virilis oskar* line showed significantly reduced correlation between HA and *nanos* (Fig. S7, Table S3), suggesting that *D. virilis* Oskar may not interact with *nanos* mRNA in the same way as *D. melanogaster* Oskar. All chimeras with the *D. virilis* OSK domain also showed this reduced co-localization, as well as most chimeras with the

bioRxiv preprint doi: https://doi.org/10.1101/2025.08.02.668269; this version posted November 10, 2026. The copyright holder for this preprint (which was not certified by peer review) is the author/funder, who has granted bioRxiv a license to display the preprint in perpetuity. It is made available under a CC-BY 4.0 International license.

D. virilis LOTUS domain, and the chimera with both folded domains from *D. melanogaster* but the two intrinsically disordered domains from *D. virilis* (Fig. S7, Table S3).

The OSK domain has long been considered a putative mRNA binding domain based on *in vitro* experiments [24,25], and an *oskar* allele lacking the OSK domain entirely (ΔOSK) expressed at the anterior pole of fly embryos fails to recruit germ plasm mRNAs [26,30]. To generate hypotheses about the potential RNA-binding ability of this domain in each species, we generated electrostatic maps of the OSK domain (Fig. S8B). These maps suggest that the *D. virilis* OSK domain is less positively charged on the surface than the *D. melanogaster* OSK domain, perhaps indicating reduced RNA-binding ability. However, swaps of the OSK domain alone were not the only chimeric features that led to reduced mRNA enrichment or co-localization, again highlighting the complex and potentially not strictly modular nature of Oskar's molecular interactions.

Together, these data suggest that failure to recruit Vasa is not responsible for the lack of germ cells in *D. virilis oskar* rescue experiments. Instead, differential interactions with germ plasm mRNAs may contribute to functional differences in Oskar protein between *D. virilis* and *D. melanogaster*.

D. virilis *Oskar has dominant-negative effects on* D. melanogaster *Oskar function*

Oskar-mediated germ plasm assembly requires multiple complex molecular interactions, both homotypic [26] and heterotypic [59]. We therefore hypothesized that the presence of *D. virilis* Oskar and/or chimeric Oskar proteins might disrupt the germ plasm assembly abilities of endogenous *D. melanogaster* Oskar. To test this hypothesis, we introduced chimeric Oskar proteins into a genetic background with endogenous *oskar*.

bioRxiv preprint doi: https://doi.org/10.1101/2025.08.02.668269; this version posted November 10, 2026. The copyright holder for this preprint (which was not certified by peer review) is the author/funder, who has granted bioRxiv a license to display the preprint in perpetuity. It is made available under a CC-BY 4.0 International license.

We first assessed the impact of these chimeras on wild-type germ plasm function by counting the number of pole cells specified. While over-expressing *D. melanogaster oskar* at the posterior led to significantly more pole cells compared to wild-type controls (expressing only endogenous *oskar*), *D. virilis oskar* caused fewer pole cells to be specified by embryonic stage 5 (Fig. 4A–B, Table S4). All but two chimeras caused reductions in pole cell number compared to *D. melanogaster oskar*, suggesting that all of Oskar's domains can contribute to pole cell formation in this background (Fig. 4A–B, Table S4). Notably, all chimeras containing the *D. virilis* OSK domain had significantly fewer pole cells than the *D. melanogaster oskar* positive control, and half of these chimeras exhibited dominant-negative effects on endogenous Oskar's ability to specify pole cells (Fig. 4B, Table S4). In particular, the chimera with just the LOTUS and OSK domains from *D. virilis* generated significantly fewer pole cells than any other chimera, and even fewer than full length *D. virilis* Oskar (Fig. 4A–B, Table S4), suggesting that this combination of domains has a particularly potent negative effect on endogenous *oskar*'s function.

Strikingly, expression of *D. virilis oskar* or of two of the chimeric Oskar proteins in the presence of *D. melanogaster oskar* caused dominant female sterility (Fig. 4B). This finding is consistent with previous work showing sterility in *D. melanogaster* lines expressing full-length *D. virilis oskar* [42]. We collected unhatched first instar larvae produced by females expressing *D. virilis oskar* and found that these embryos were bicaudal [60], a severe patterning defect in which the head and thoracic segments are replaced by a mirror image duplication of the posterior abdominal segments and telson (Fig. 4C). Examination of the chimeric *oskar* genotypes revealed three additional chimeras with these strong anterior defects (Fig. 4D, Table S4): the chimera with LOTUS and OSK from *D. virilis,* the chimera with all domains from *D. virilis* except LOTUS,

bioRxiv preprint doi: https://doi.org/10.1101/2025.08.02.668269; this version posted November 10, 2026. The copyright holder for this preprint (which was not certified by peer review) is the author/funder, who has granted bioRxiv a license to display the preprint in perpetuity. It is made available under a CC-BY 4.0 International license.

and the chimera with OSK and Long Osk from *D. virilis.* We observed low, but not statistically significant, levels of partial posterior duplications in eight other chimeric genotypes, three of which contained the *D. virilis* OSK domain (Fig. 4D, Table S4).

Bicaudal phenotypes can result from deficient or insufficient posterior localization of multiple determinant molecules [61–65] , including the germ plasm component *nanos* mRNA [66]. We therefore hypothesized that *nanos* mRNA might be mislocalized in the embryos derived from mothers expressing chimeras that yielded bicaudal larvae, thus causing the patterning defects described above (Fig. 4C–D). To test this, we compared the localization of *nanos* mRNA in embryos derived from mothers expressing either *D. virilis* or *D. melanogaster oskar* (Fig. 4E). When expressing *D. melanogaster oskar*, *nanos* was tightly localized at the posterior in cleavage stage embryos, and was specifically detected in pole cells later in embryogenesis (Fig. 4E). In contrast, *nanos* was mislocalized in *D. virilis oskar* embryos. Specifically, there was reduced *nanos* enrichment at the posterior of preblastoderm embryos, low levels of *nanos* expression throughout the blastoderm, and loss of *nanos* expression in germ cells later in embryogenesis (Fig. 4E).

We then examined the localization of several additional germ plasm molecules recruited in the presence of Oskar chimeras in a background with endogenous *D. melanogaster oskar*. We noted that, in contrast to our observations in an *oskar* null background (Fig. 2), most chimeras were able to produce at least some pole cells in a background with endogenous *D. melanogaster oskar* (Fig 4). In addition to Vasa protein and *nanos* mRNA, we therefore chose to quantify the mRNA of germ plasm component *pgc*, rather than that of *gcl*, which we had chosen for the null background experiments based on its known role in pole cell formation [58]. As in the *oskar* null rescue experiments (Fig. 3), we found that both *D. melanogaster* Oskar and *D. virilis* Oskar

bioRxiv preprint doi: https://doi.org/10.1101/2025.08.02.668269; this version posted November 10, 2026. The copyright holder for this preprint (which was not certified by peer review) is the author/funder, who has granted bioRxiv a license to display the preprint in perpetuity. It is made available under a CC-BY 4.0 International license.

increased Vasa enrichment at the posterior in stage 10 oocytes and stage 1–2 embryos (Figs. 5, S6A–B, Table S5). However, *D. virilis* Oskar failed to localize the germ plasm mRNAs *nanos* and *pgc* to the posterior as well as *D. melanogaster* Oskar (Figs. 5, S6C–D, Table S5). In fact, enrichment of both *nanos* and *pgc* mRNAs was significantly reduced by the expression of *D. virilis* Oskar relative to enrichment in animals only expressing endogenous *oskar*. We therefore hypothesize that expression of *D. virilis oskar* leads to dominant-negative effects on *D. melanogaster oskar*'s ability to recruit germ plasm mRNAs. Chimeras containing the *D. virilis* OSK domain also exhibited significant defects in both *nanos* and *pgc* mRNA enrichment at the posterior, and half of these chimeras had reduced *nanos* and *pgc* enrichment at the posterior relative to endogenous *oskar* alone (Figs. 5, S6C–D, Table S5). These observations may implicate the OSK domain specifically in *D. virilis* Oskar's possible dominant-negative effect on *D. melanogaster* Oskar-mediated germ plasm assembly. In addition, the finding that *D. virilis oskar* cannot enrich germ plasm mRNAs at the posterior is consistent with the observed strong axial patterning defect (Fig. 4C–D) and may contribute to the reduction in pole cells (Fig. 4A–B).

We wished to gain further insight into the potential mechanisms underlying the dominant-negative patterning defect. To this end, we quantified the accumulation and localization of chimeric Oskar protein, endogenous Oskar protein, and Nanos protein in wild-type oocytes and embryos (containing endogenous *oskar*) expressing full length *D. virilis oskar*, or expressing chimeras containing the *D. virilis* OSK domain. In these conditions, we detected at least as much chimeric or *D. virilis* Oskar protein at the posterior, as in controls (Figs. S3, S9, S10; Tables S6, S7). Moreover, the localization of the chimeric or *D. virilis* Oskar proteins closely matched that of endogenous Oskar protein, being tightly localized to the posterior in both

bioRxiv preprint doi: https://doi.org/10.1101/2025.08.02.668269; this version posted November 10, 2026. The copyright holder for this preprint (which was not certified by peer review) is the author/funder, who has granted bioRxiv a license to display the preprint in perpetuity. It is made available under a CC-BY 4.0 International license.

stage 10 oocytes and embryos (Figs. S9, S10). As noted above, chimeric *oskar* mRNAs, including chimera Dm123Dv4 containing the *D. virilis* OSK domain, also localized correctly to the oocyte posterior (Fig. S4, Table S1). This suggests that chimeric *oskars* were translated and localized correctly, and that the observed patterning defects are unlikely to be due to insufficient quantity or localization of the chimeric Oskar proteins.

Endogenous Oskar protein was enriched at the posterior of stage 10 oocytes to at least the same degree as in controls (Fig. S9; Table S6). The posterior localization of endogenous Oskar in stage 10 oocytes in the presence of these chimeras was also similar to controls (Fig. S9). By stages 1–2 of embryogenesis, posterior enrichment of endogenous Oskar was statistically indistinguishable from controls in flies containing both endogenous *D. melanogaster* Oskar and full length *D. virilis* Oskar, as well as in flies containing both endogenous *D. melanogaster* Oskar and chimera Dm13Dv24 (Fig. S9; Table S6). This chimera, which contains the *D. virilis* LOTUS and OSK domains, induced the highest proportion (92%) of dominant-negative bicaudal defects, of all chimeric Oskar proteins (Fig. 4D). The second highest proportion (52%) of dominant-negative bicaudal defects was induced by chimera Dm2Dv134, which contains the *D. virilis* Long Oskar, linker and OSK domains (Fig. 4D). Stage 1–2 embryos containing this chimera as well as endogenous *D. melanogaster oskar*, had significantly less endogenous Oskar protein than controls, even though they had contained significantly more endogenous Oskar when they were stage 10 oocytes (Fig. S9; Table S6). Based on these observations, it could be the case that reduction of endogenous Oskar at the posterior could contribute to the dominant-negative AP patterning defects observed in the presence of chimera Dm2Dv134.

As noted above, full-length *D. virilis oskar*, and chimeras containing the *D. virilis* OSK domain, were unable to accumulate normal levels of *nanos* mRNA at the posterior in a wild-type

bioRxiv preprint doi: https://doi.org/10.1101/2025.08.02.668269; this version posted November 10, 2026. The copyright holder for this preprint (which was not certified by peer review) is the author/funder, who has granted bioRxiv a license to display the preprint in perpetuity. It is made available under a CC-BY 4.0 International license.

391 background (Figs. 5, S10, Table S7). We examined the quantities and localization of Nanos
392 protein in these genotypes, and found that Nanos protein enrichment did not always scale with
393 *nanos* mRNA enrichment in a simple way. Specifically, we detected at least as much Nanos
394 protein at the posterior as in controls, in the presence either of full-length *D. virilis* Oskar, or of
395 chimeras containing the *D. virilis* OSK domain (Fig. S10B; Table S7). In accordance with our
396 observations that ectopic *nanos* mRNA was sometimes detectable anterior to the normal
397 posterior localization site (Fig. 4E), we detected similar regions of ectopic Nanos protein further
398 anterior than in controls, especially at earlier embryonic stages (Fig. S10J). Further, we detected
399 higher levels of Nanos protein at more anterior positions than in controls, in embryos with both
400 endogenous *D. melanogaster oskar* and either full length *D. virilis* Oskar or chimeras containing
401 the *D. virilis* OSK domain (Fig. S10I; Table S7). We observed strong colocalization of these
402 chimeric proteins and *nanos* mRNA (Fig. S10D, J), but weaker colocalization of these chimeras
403 and Nanos protein (Fig. S10E, J). We did not find evidence for mislocalization or absence of
404 Smaug protein in embryos expressing *D. virilis* OSK-containing chimeras in a background with
405 endogenous *D. melanogaster oskar*, suggesting that the observed patterning defects were not
406 explained by the absence of Smaug-dependent degradation of repression of *nanos* (Fig. S11;
407 Table S8). Taken together, these observations are consistent with the interpretation that
408 inappropriately anteriorly localized Nanos protein contributed to the dominant-negative bicaudal
409 patterning defects observed with these chimeras.

410 In *D. melanogaster*, Oskar is involved in a positive feedback loop between polarity
411 maintenance, Oskar mRNA localization, and Oskar protein translation [67,68]. We therefore asked
412 whether defects in polarity maintenance might contribute to some of the apparent functional
413 failures of chimeric Oskar. To do this, we assessed the behavior of the Par-1 protein, a kinase

bioRxiv preprint doi: https://doi.org/10.1101/2025.08.02.668269; this version posted November 10, 2026. The copyright holder for this preprint (which was not certified by peer review) is the author/funder, who has granted bioRxiv a license to display the preprint in perpetuity. It is made available under a CC-BY 4.0 International license.

with a conserved role in eukaryotic cell polarity [69], which is normally enriched at the posterior pole of *D. melanogaster* oocytes and contributes to Oskar localization [70–76]. We quantified the enrichment of Par-1 protein, its co-localization with chimeric Oskar, and its localization pattern in *oskar* null oocytes expressing selected Oskar chimeras, as well as in wild-type oocytes (containing endogenous *D. melanogaster* Oskar) expressing either full length *D. melanogaster oskar*, or full length *D. virilis oskar*. We found that in a wild-type background, there were no significant alterations to Par-1 enrichment, co-localization with Oskar, or localization pattern in the presence of *D. virilis* Oskar (Fig. S12D–E, Table S9). Par-1 also appeared unaffected in *oskar* null oocytes expressing chimeras containing the *D virilis* LOTUS or interdomains (Fig. S12A–C, Table S10). Interestingly, however, we noted that *oskar* null oocytes expressing chimeras containing the *D. virilis* Long Oskar or OSK domains did not accumulate as much Par-1 at the posterior as controls (Fig. S12B, Table S10). However, in *oskar* null embryos, four out the seven chimeras containing the *D. virilis* Long Oskar domain were able to support pole cell formation (Fig. 2), and all of them showed at least as much Vasa enrichment as controls (Fig. 3). Further, although none of the seven chimeras containing the *D. virilis* OSK domain were able to support pole cell formation in *oskar* null embryos (Fig. 2), most of them nevertheless accumulated appropriate levels of Vasa protein, *nos* and *gcl* mRNAs (Fig. 3). Moreover, we did not observe defects in *oskar* mRNA or protein localization in the chimeras we examined (Figs. S4, S9). Given these data, we cannot exclude the interpretation that some of the germ plasm and patterning defects we report here, may be partially caused by a disruption of the positive feedback loop that maintains oocyte polarity [67,68]. However, we speculate that in many cases, even if polarity is initially disrupted in oocyte stages, this defect is corrected by the time of embryonic germ plasm accumulation.

bioRxiv preprint doi: https://doi.org/10.1101/2025.08.02.668269; this version posted November 10, 2026. The copyright holder for this preprint (which was not certified by peer review) is the author/funder, who has granted bioRxiv a license to display the preprint in perpetuity. It is made available under a CC-BY 4.0 International license.

437

438 D. virilis *Oskar nucleates granules with distinct localization and size compared to those*

439 *nucleated by* D. melanogaster *Oskar*

440 In addition to regulating germ plasm assembly and localization [59], previous reports

441 suggest that Oskar also regulates the specific morphology and localization of germ granules [41].

442 Germ granule morphology, including size, shape and localization, are strikingly variable across

443 insects [77,78] including within the genus *Drosophila* [79–82], but the molecular mechanistic basis of

444 Oskar's regulation of these granule properties remains unknown. Previous histological reports

445 described *D. virilis* germ plasm as having fewer, larger granules than *D. melanogaster* [79]. We

446 developed an antibody against *D. virilis* Oskar, and then used species-specific anti-Oskar

447 antibodies to compare the localization pattern of wild-type *D. virilis* and *D. melanogaster* Oskar

448 in their native context. We found that endogenous *D. melanogaster* Oskar in wild-type *Oregon R*

449 embryos was distributed through the posterior cytoplasm (Fig. 6B–C, Table S11), similar to the

450 distribution of electron-dense germ plasm granules reported for this species [80,83]. However, in its

451 native context *D. virilis* Oskar was significantly more enriched in the posterior cortical

452 cytoplasm of the embryo, and appeared to form fewer, larger granules, than those observed for

453 *D. melanogaster* Oskar (Fig. 6B–C, Table S11), again consistent with previous observations [79].

454 We then compared the localization of *D. melanogaster* Oskar and *D. virilis* Oskar

455 expressed in *D. melanogaster oskar* null (*y[1] sc[*] v[1]]; Kr[If-1]/CyO;*

456 *TI{w[+mC]=TI}osk[0.EGFP]*) oocytes and embryos by imaging embryos stained for HA, the

457 tag we used for our chimeric *oskar* constructs (Fig. 6A). In mid-oogenesis (stage 10), *D.*

458 *melanogaster* and *D. virilis* Oskar had indistinguishable HA localization patterns, suggesting that

459 *D. virilis oskar* mRNA was successfully localized and then translated at the posterior (Fig. 6A).

bioRxiv preprint doi: https://doi.org/10.1101/2025.08.02.668269; this version posted November 10, 2026. The copyright holder for this preprint (which was not certified by peer review) is the author/funder, who has granted bioRxiv a license to display the preprint in perpetuity. It is made available under a CC-BY 4.0 International license.

460 However, in cleavage stage embryos, *D. virilis* Oskar was detected over a broader region of the
461 embryo than *D. melanogaster* Oskar (Fig. 6A). In addition, we saw *D. virilis* Oskar protein
462 accumulation far from the posterior in apparently random ectopic locations in 36% of embryos
463 (Fig. S13A–B). In the cellular blastoderm, *D. melanogaster* Oskar was localized to the pole cells,
464 while *D. virilis* Oskar was detected in the cytoplasm of presumably somatic blastoderm cells at
465 the posterior end of the embryo (Fig. 6A).

466 Examining the granular distribution of *D. virilis* Oskar within the posterior of *D.*
467 *melanogaster* oocytes and early embryos revealed a fascinating pattern. In stage 10 oocytes, *D.*
468 *melanogaster* and *D. virilis* Oskar localized similarly along the edge of the *D. melanogaster*
469 oocyte membrane (Fig. S13D). However, we observed a difference in the HA signal distribution
470 between species in cleavage stage embryos. *D. virilis* Oskar was tightly associated with the
471 posterior embryonic membrane at this stage, while the signal for *D. melanogaster* Oskar was
472 distributed throughout the posterior cytoplasm (Fig. 6B–C, Fig. S13C).

473 Finally, we saw gross morphological differences in the Oskar-containing granules of *D.*
474 *melanogaster* expressing *D. virilis* or *D. melanogaster* Oskar. Specifically, HA signal appeared
475 in fewer, larger foci when expressing *D. virilis* Oskar compared to the numerous small puncta of
476 *D. melanogaster* Oskar-containing granules (Fig. 6D). Chimeric Oskar proteins possessing the
477 OSK domain from *D. virilis* formed granules resembling, but not identical to, those formed by *D.*
478 *virilis* Oskar (Fig. 6D), In other words, granules generated in *D. melanogaster* by *D. virilis* Oskar
479 protein more closely resembled those of wild-type *D. virilis* than those of *D. melanogaster* (Fig.
480 6D). Further, granules generated by chimeric Oskar proteins containing the *D. virilis* OSK
481 domain were also similar to the *D. virilis* granule type, suggesting that evolved changes to this
482 domain may drive species-specific granule size and localization (Fig. 6D).

bioRxiv preprint doi: https://doi.org/10.1101/2025.08.02.668269; this version posted November 10, 2026. The copyright holder for this preprint (which was not certified by peer review) is the author/funder, who has granted bioRxiv a license to display the preprint in perpetuity. It is made available under a CC-BY 4.0 International license.

The potential for evolved changes in Oskar protein to influence mRNA or protein interactions

We found that *D. virilis* Oskar successfully enriched the germ plasm protein Vasa at the posterior of embryos but exhibited defects in its recruitment of some, but not all, germ plasm mRNAs (Fig. 3; Fig. S2). This result led us to consider whether Vasa and germ plasm mRNAs might compete for Oskar binding sites. To explore this possibility *in silico*, we compared AlphaFold3 [49] predictions of *D. melanogaster* or *D. virilis* Oskar in complex with *D. melanogaster* Vasa, and with the *D. melanogaster nanos* 3'UTR (Fig. S8C–D). We found that regions of the *D. melanogaster* OSK domain that potentially interact with the *nanos* 3'UTR were not predicted to do so in *D. virilis* Oskar (Fig. S8C–D).

As a second *in silico* approach to asking whether evolved changes in RNA interacting ability might explain the differences between *D. virilis* and *D. melanogaster* proteins *in vivo*, we used GPSite [84], a machine-learning model for predicting protein binding sites with various other molecules, to predict binding residues for *D. melanogaster* and *D. virilis* Oskar protein with protein and RNA. We considered residues with predicted binding scores greater than a threshold of 0.5 to be putative binding sites. We observed that while the overall pattern of predicted residue binding affinity was similar between the two orthologs, *D. virilis* Oskar exhibited higher protein-binding scores than *D. melanogaster* Oskar within the LOTUS domain, while *D. melanogaster* Oskar protein-binding affinity exhibited higher peaks than *D. virilis* within the interdomain (Fig. S14A, C). *D. melanogaster* Oskar exhibited higher RNA-binding scores than *D. virilis* Oskar throughout the protein (Figs. S14B, D, S15B). Indeed, *D. virilis* Oskar was not predicted to have any residues over the threshold for confident RNA-binding in its Long Oskar

bioRxiv preprint doi: https://doi.org/10.1101/2025.08.02.668269; this version posted November 10, 2026. The copyright holder for this preprint (which was not certified by peer review) is the author/funder, who has granted bioRxiv a license to display the preprint in perpetuity. It is made available under a CC-BY 4.0 International license.

505 isoform, and only two residues over the threshold for its Short Oskar isoform, compared to the
506 thirteen in *D. melanogaster* Short Oskar. (Fig. S14B, D).

507 We compared the overall protein-binding and RNA-binding scores for each of our
508 chimeric Oskar protein sequences. We found that all chimeric Oskar proteins had overall protein-
509 binding scores over the threshold, but chimeras with their LOTUS domain from *D. virilis* had
510 consistently higher protein-binding scores (Fig. S15A, C). In terms of predicted RNA-binding
511 ability, while *D. melanogaster* Oskar and several additional chimeras had RNA-binding scores
512 over 0.5, *D. virilis* Oskar and a host of other chimeric proteins were below this threshold for the
513 Long Oskar isoform (Fig. S14B, D). Intriguingly, the three chimeric proteins with the lowest
514 RNA-binding scores for short Oskar exhibited patterning defects and severe defects in mRNA
515 enrichment in our experiments conducted in a background with endogenous Oskar (Fig. S15D).

516 Our AlphaFold3 predictions suggested that the *D. virilis* OSK domain should exhibit a
517 greater interaction with Vasa than the OSK domain of *D. melanogaster* (Fig. S8C–D). Using
518 GPsite [84] to examine the relationship between RNA-binding and protein-binding scores, we
519 found a clear pattern of *D. virilis* LOTUS leading to high protein-binding score, regardless of the
520 other domains present (Fig. S15E, F). The predicted RNA-binding score was less tightly
521 associated with any specific protein domain. However, the *D. virilis* OSK domain appeared in
522 nearly all of the lowest ranked short Oskar chimeras (Fig. S15F). We notably observed that the
523 short Oskar chimeras with all *D. melanogaster* and all *D. virilis* sequence were found in the most
524 extreme corners of the correlation plot, with *D. melanogaster* Oskar displaying high RNA-
525 binding and lower protein-binding scores, while *D. virilis* Oskar has high protein-binding and
526 low RNA-binding scores (Fig. S15). Taken together, these *in silico* observations are consistent
527 with our *in vivo* experiments in supporting the hypothesis that evolved differences in the OSK

bioRxiv preprint doi: https://doi.org/10.1101/2025.08.02.668269; this version posted November 10, 2026. The copyright holder for this preprint (which was not certified by peer review) is the author/funder, who has granted bioRxiv a license to display the preprint in perpetuity. It is made available under a CC-BY 4.0 International license.

528 domain change this domain's ability to interact with germ plasm mRNAs in species-specific
529 ways, which are a major cause of interspecies incompatibility of Oskar's germ line determinant
530 role.
531
532 **Discussion**
533 We have used domain swapping between orthologous genes to obtain insight into the
534 evolutionary changes that can affect protein function, even between closely related species, as
535 well as the functional roles of that protein's domains in its native context. We uncovered the
536 basis for the functional incompatibility of *D. virilis oskar* in *D. melanogaster* by expressing
537 sixteen chimeric versions of *oskar* in *D. melanogaster* and testing their ability to perform *oskar*
538 function (Fig. 1D). Our data suggest that the *D. virilis oskar* and chimeras containing the *D.*
539 *virilis* OSK domain fail to rescue germ cell formation (Fig. 2A–B), but that all chimeras can
540 successfully restore abdominal patterning in *oskar* null embryos (Fig. 2C). We observed a
541 complex relationship between Oskar sequence and its ability to recruit germ plasm molecules. *D.*
542 *virilis oskar* can successfully enrich Vasa at the posterior but exhibits defects in its interactions
543 with some germ plasm mRNAs, and these defects are often associated with the presence of the
544 *D. virilis* OSK domain (Fig. 3). In addition, *D. virilis oskar* has a dominant-negative effect on *D.*
545 *melanogaster oskar* function that is also at least partially due to the *D. virilis* OSK domain (Figs.
546 4–5), which appears to lead to inappropriately anterior accumulation of Nanos protein (Fig. S10),
547 resulting in patterning defects including bicaudal embryos (Fig. 4). Finally, we identify
548 differences in the localization and size of *D. virilis* and *D. melanogaster* Oskar-containing
549 granules that are linked at least partially to the presence of the OSK domain, and that we

bioRxiv preprint doi: https://doi.org/10.1101/2025.08.02.668269; this version posted November 10, 2026. The copyright holder for this preprint (which was not certified by peer review) is the author/funder, who has granted bioRxiv a license to display the preprint in perpetuity. It is made available under a CC-BY 4.0 International license.

speculate may influence their ability to mediate downstream functions (Fig. 6). Thus, our results shed light on the evolution of a key germ line protein.

Maintenance of Oskar at the posterior

In the first reported test of the function of a non-*D. melanogaster* oskar ortholog, Webster and colleagues [42] observed reduced maintenance of *D. virilis oskar* mRNA at the posterior of *D. melanogaster* embryos (their Fig. 3D) relative to *D. melanogaster oskar* mRNA. They also reported more diffuse localization of *D. melanogaster oskar* mRNA (their Fig. 3C) and protein (their Fig. 3J) when both *D. melanogaster* and *D. virilis oskar* were expressed in the same *D. melanogaster* embryo. The authors proposed a model for Oskar protein function in which one domain of Oskar anchors it to the posterior cortex, while one or more distinct domains bind to germ plasm molecules [42]. They speculated that *D. virilis* Oskar could interact with *D. melanogaster* posterior patterning determinants but could not anchor itself to the posterior, thereby dragging these determinants away from the pole [42].

In the three decades since that work was published, we have learned that Oskar indeed has a domain with a distinct role in anchoring itself to the posterior, namely the Long Osk domain [36]. However, our data do not suggest that swapping the *D. melanogaster* Long Osk domain with *D. virilis* Long Osk sequence leads to severe defects in the posterior maintenance of *oskar* or other germ plasm molecules (Fig. 3). In fact, Webster and colleagues [42] concluded their study by describing a *D. melanogaster–D. virilis oskar* chimeric protein that they expressed at the anterior pole of *D. melanogaster* embryos. This chimera was described as having 188 amino acids of N-terminal *D. melanogaster* sequence, which corresponds to the Long Osk domain and a portion of the LOTUS domain (Fig. S1B), with the remainder of the sequence derived from *D.*

bioRxiv preprint doi: https://doi.org/10.1101/2025.08.02.668269; this version posted November 10, 2026. The copyright holder for this preprint (which was not certified by peer review) is the author/funder, who has granted bioRxiv a license to display the preprint in perpetuity. It is made available under a CC-BY 4.0 International license.

573 *virilis*. They reported (as "data not shown") that that this chimera failed to specify pole cells at
574 the anterior of the embryo [42]. This finding is consistent with our results, which show that the
575 chimera possessing only *D. melanogaster* Long Osk cannot specify pole cells in *D.*
576 *melanogaster*, nor can most other chimeras that possess the *D. virilis* OSK domain (Fig. 2B).
577 Together, these data suggest that *D. virilis* Oskar's failure to localize tightly to the posterior in *D.*
578 *melanogaster* is not solely based on a difference in the Long Osk domain itself. However, it is
579 possible that changes to another domain within the Long Oskar isoform may influence its
580 activity, given that Long Oskar contains all the domains found in the shorter isoform.
581 Alternatively, Short Oskar's function in germ granule assembly may also affect Oskar
582 localization at the posterior. For instance, Oskar failing to interact with germ plasm mRNA could
583 in principle influence granule size or biophysical properties in a way that allows diffusion away
584 from the posterior more readily. To our knowledge, no other domain of Oskar has been directly
585 implicated in posterior localization, and further work will be needed to test this new hypothesis
586 about how Oskar might be retained at the posterior pole.
587
588 *Oskar's inferred interactions with germ granule components*
589 Although the LOTUS domain is classically associated with Vasa interactions and the
590 OSK domain with mRNA binding, *in vivo* studies challenge the strict modularity of Oskar's
591 domains, suggesting the LOTUS domain may also contribute to mRNA interactions [26]. If Vasa
592 and germ plasm mRNAs indeed interact with Oskar via some of the same residues, then reduced
593 interaction with mRNA could in principle enable more interaction with Vasa. Conversely,
594 greater affinity for Vasa could preclude interaction with mRNA. Our data cannot distinguish
595 between these possibilities, but are consistent with the hypothesis that Oskar's interactions with

bioRxiv preprint doi: https://doi.org/10.1101/2025.08.02.668269; this version posted November 10, 2026. The copyright holder for this preprint (which was not certified by peer review) is the author/funder, who has granted bioRxiv a license to display the preprint in perpetuity. It is made available under a CC-BY 4.0 International license.

596 germ plasm molecules *in vivo* are complex and potentially non-modular in nature. Future work
597 could examine the specific intermolecular interactions of cross-species germ plasm components
598 using quantitative analysis of single-molecule imaging, or assessing RNA translation dynamics.

599 Recent work demonstrated that degrading germ plasm mRNAs increases the size of
600 Oskar-labeled germ granules, suggesting a relationship between protein and mRNA
601 incorporation in granules [30]. We found that the Oskar-labeled granules from *D. virilis* appeared
602 in larger foci than the small Oskar-labeled granules nucleated by *D. melanogaster* Oskar (Fig.
603 6D). We speculate that the reduced mRNA co-localization and increase in Vasa co-localization
604 effected by *D. virilis* Oskar (Fig. S7) could contribute to the apparent difference in Oskar-labeled
605 germ granule size.

606 The germ granules that form upon expression of *D. virilis* Oskar in *D. melanogaster*
607 resemble those detectable in *D. virilis* using an anti-*D. virilis* Oskar antibody (Fig. 6D). *D. virilis*
608 germ granules are distinct from those of *D. melanogaster* both morphologically and in terms of
609 molecular content. In her classic comparative study of *Drosophila* germ granules, Sheila Counce
610 described *D. virilis* granules as fused into short strings, in contrast to the small, individual
611 droplets observed in *D. melanogaster* [79]. In addition, a recent study found that *D. virilis* exhibits
612 lower expression levels of several germ plasm mRNAs and has fewer transcripts within granules
613 than *D. melanogaster* [44]. This difference in germ plasm mRNA abundance might explain why *D.*
614 *virilis* embryos form fewer pole cells than *D. melanogaster* (Fig. 1B). It is also possible that
615 variable germ plasm mRNA amount, or other differences in the composition of *D. virilis* germ
616 granules relative to those of *D. melanogaster*, may explain the morphological differences in the
617 granules between these species. Further examination of pole bud formation, pole cell divisions,

bioRxiv preprint doi: https://doi.org/10.1101/2025.08.02.668269; this version posted November 10, 2026. The copyright holder for this preprint (which was not certified by peer review) is the author/funder, who has granted bioRxiv a license to display the preprint in perpetuity. It is made available under a CC-BY 4.0 International license.

and the contents and biophysical properties of germ granules in both species, will be needed to rigorously test this hypothesis.

The origin and functional consequences of the variation in germ granule morphology and composition across *Drosophila* species remain unclear [44,79,80]. While previous work suggested that mRNA position within germ granules is independent of the onset of translation or degradation [85], a recent study found a correlation between the positioning of mRNAs within germ granules and their translational status [86]. It is possible that species-specific differences in germ granule structure or morphology could influence the post-transcriptional regulation of germ granule components. In the case of the germ granules nucleated by *D. virilis* Oskar in *D. melanogaster*, possible changes in the proportions or spatial organization of germ plasm components within the granule could disrupt the onset of gene expression patterns that regulate pole cell formation and other precisely timed developmental processes.

Different germ plasm requirements for pole cell specification and axial patterning

We found that *D. virilis* Oskar was able to rescue the abdominal patterning but not the pole cell specification defects of *D. melanogaster oskar* null embryos (Fig. 2), consistent with previous reports [42]. This may be because *D. virilis* Oskar can interact sufficiently with abdominal patterning determinants but insufficiently with germ cell determinants in *D. melanogaster*. Alternatively, this finding may reflect a difference in the dose dependency or sensitivity of these processes to changes in posterior localization of germ plasm.

Oskar directs the localization of the posterior patterning determinant *nanos*, which establishes a posterior gradient of Nanos protein that inhibits translation of *hunchback* at the posterior and enables proper axial patterning [87,88]. However, *nanos* is not required for germ cell

bioRxiv preprint doi: https://doi.org/10.1101/2025.08.02.668269; this version posted November 10, 2026. The copyright holder for this preprint (which was not certified by peer review) is the author/funder, who has granted bioRxiv a license to display the preprint in perpetuity. It is made available under a CC-BY 4.0 International license.

specification [66,89], although it is required for their subsequent migration and survival [90–93]. We observed no striking differences in the predicted interactions between *D. melanogaster* and *D. virilis* Oskar and the three germ plasm proteins Lasp, Valois, and Smaug (Figs. S11, S16), for which direct interactions have been proposed based on yeast two hybrid, GST-pull down and cell culture-based assays [31–33]. It is possible that other, untested molecules required for germ cell specification fail to assemble in the *D. melanogaster* germ plasm with *D. virilis oskar* expression.

It may also be the case that pole cell formation requires more stringent posterior localization and a higher concentration of germ granule components than is necessary for *nanos* to mediate proper axial patterning. The role of germ granules in pole cell specification is tightly associated with the posterior pole, where granules mediate complex processes allowing pole buds to form, including changes in the phospholipid composition of the membrane and the actin cytoskeleton network [94,95]. The species-specific differences in *D. virilis* Oskar localization at the posterior (Fig. 6) may impact the dynamic process transporting germ granules into the germ cells as they form [96]. Future studies deploying high-resolution live imaging of embryos at the time of pole budding may offer new insights into how germ cell formation is disrupted upon expression of *D. virilis oskar.*

Jongens and colleagues [97] reported that ectopic expression of *gcl* at the anterior led to formation of ectopic anterior pole buds . This might initially appear incompatible with our observation that some chimeras with levels of *gcl* that were comparable to controls, were nonetheless unable to form pole cells (Figures 2, 3). However, Jongens and colleagues [97] noted that the ectopic pole buds formed by anteriorly localized *gcl* did not pinch off to form pole cells. This was consistent with their report that other germ plasm components did not ectopically

bioRxiv preprint doi: https://doi.org/10.1101/2025.08.02.668269; this version posted November 10, 2026. The copyright holder for this preprint (which was not certified by peer review) is the author/funder, who has granted bioRxiv a license to display the preprint in perpetuity. It is made available under a CC-BY 4.0 International license.

664 localize to the anterior in response to anterior *gcl* expression (a report described in the text of
665 their results section, but with data indicated as "not shown" page 2128 in 97. They interpreted their
666 results to mean that "the level of *gcl* activity required for the induction of pole bud formation
667 may be much less than that required to complete pole cell formation" page 2132 in 97 . We did not, as
668 did Jongens and colleagues [97], quantify pole bud formation by examining embryos at stages
669 earlier than the end of stage 5. Instead, we only included late stage 5 embryos with well-formed
670 pole cells in our quantification (Fig. 2). Many chimeras that failed to drive pole cell formation
671 despite apparently unaffected *gcl* levels, nevertheless showed alterations in the levels of at least
672 some of the other germ plasm components that we quantified. Our observation is thus consistent
673 with the interpretation of Jongens and colleagues, that "*gcl* activity alone is not sufficient for
674 pole cell formation or maintenance page 2133 in 97. In sum, while many of the individual molecules
675 found in wild-type germ plasm clearly play important roles in establishing some of the molecular
676 and cellular characteristics of pole cells (e.g. *gcl* for pole bud formation, *nanos* for somatic state
677 repression, *oskar* for granule nucleation), establishing robustly cellularized PGCs that can
678 maintain germ cell fate, requires a complex interaction of many, if not all, of these components.
679
680 *Dominant-negative effect of* D. virilis oskar *on* D. melanogaster oskar *function*
681 We observed that expression of *D. virilis oskar* in a background with endogenous *D.*
682 *melanogaster oskar* had dominant-negative effects on axial patterning, pole cell number, and
683 germ plasm mRNA enrichment (Fig. 4–5). In fact, the mRNA enrichment defects were more
684 severe in a background with both *D. melanogaster* and *D. virilis oskar* than in an *oskar* null
685 background, leading to development of bicaudal embryos, (Fig. 4–5) a phenotype which does not
686 occur when expressing *D. virilis oskar* in *oskar* RNA null embryos (Fig. 2). There is precedent

bioRxiv preprint doi: https://doi.org/10.1101/2025.08.02.668269; this version posted November 10, 2026. The copyright holder for this preprint (which was not certified by peer review) is the author/funder, who has granted bioRxiv a license to display the preprint in perpetuity. It is made available under a CC-BY 4.0 International license.

for dominant-negative effects arising from expression of a wild-type gene from another species in a non-native context. For example, expression of homologs of the *matrimony* gene from multiple *Drosophila* species in wild-type *D. melanogaster* embryos causes severe developmental defects [98]. Furthermore, expression of the *D. melanogaster* Serum Response Factor ortholog (*blistered*) in mammalian cells has a dominant-negative effect on the activity of the endogenous mammalian factor, which appears to occur via dimerization between the endogenous and transfected proteins [99].

One possible molecular explanation for the strong dominant-negative effect of *D. virilis* Oskar could be the formation of heterodimers between *D. virilis* and *D. melanogaster* Oskar that have a deleterious effect on Oskar function. *D. melanogaster* Oskar's LOTUS domain dimerizes in crystal structures [24–26], and AlphaFold3 [49] consistently predicts interactions between *D. melanogaster* Short Oskar monomers at the same interface observed in the reported crystal structures (Fig. S17A). We found that *D. virilis* Short Oskar is predicted to form the same dimerization interface observed in homodimers of *D. melanogaster* Short Oskar (Fig. S17B). Furthermore, a heterodimer forming through interaction at the LOTUS domain is also predicted between *D. melanogaster* and *D. virilis* Short Oskar (Fig. S17C). These predictions are consistent with the hypothesis that *D. melanogaster* and *D. virilis* may directly interact in the trans-species transgenic *D. melanogaster* lines studied herein.

Unlike the predicted homodimers, the heterodimer also exhibits moderately high confidence interactions between the OSK domains of *D. melanogaster* Oskar and *D. virilis* Oskar proteins (Fig. S17C). These OSK-OSK interactions are also apparent in higher-order predicted oligomeric structures containing both *D. melanogaster* and *D. virilis* full length Oskar (Fig. S17C). Further, when both Oskar orthologs are present, *D. melanogaster* Oskar is

bioRxiv preprint doi: https://doi.org/10.1101/2025.08.02.668269; this version posted November 10, 2026. The copyright holder for this preprint (which was not certified by peer review) is the author/funder, who has granted bioRxiv a license to display the preprint in perpetuity. It is made available under a CC-BY 4.0 International license.

consistently predicted to heterodimerize with *D. virilis* rather than forming homodimers (Fig. S17C). We speculate that the predicted OSK-OSK interactions between *D. melanogaster* and *D. virilis* Oskar might preclude interactions between *D. melanogaster* germ plasm mRNA and the *D. virilis* Oskar and chimeric Oskars studied here. AlphaFold3 [49] predicts structures of *D. melanogaster* Oskar proteins with the *D. melanogaster nanos* 3'UTR that suggest multiple weak potential interactions between Oskar and the mRNA (Fig. S17D). Similar interactions are also predicted between *D. virilis* Oskar and the *D. melanogaster nanos* 3'UTR (Fig. S17E). However, these predicted interactions are lost in structures that include both *D. melanogaster* and *D. virilis* Oskar proteins with the *D. melanogaster nanos* 3'UTR. Instead, weak interactions appear between the OSK domains of *D. virilis* and *D. melanogaster* Oskar (Fig. S17F). These predictions further support the hypothesis that the dominant-negative effect of *D. virilis* Oskar in *D. melanogaster* arises through detrimental direct interactions with *D. melanogaster* Oskar. Future empirical tests of this hypothesis may provide new insights into the nature and functional significance of Oskar dimerization *in vivo*.

Evolution of oskar isoforms and the Long Oskar domain

One element of Oskar function that our experiments cannot speak to, is the relative amounts of the Long and Short isoforms of Oskar. To date, the mechanisms that regulate the stoichiometry of these Oskar isoforms in *D. melanogaster*, and the dynamics and biological significance of the stoichiometry, remain unknown. The C-terminal HA-tagged design of our chimeric transgenes means we are unable to distinguish between chimeric Long and Short isoforms in our transgenic lines. It is possible that alteration of these ratios for one or both of endogenous or chimeric Oskars, contributes to the trans-species incompatibility that we explore

bioRxiv preprint doi: https://doi.org/10.1101/2025.08.02.668269; this version posted November 10, 2026. The copyright holder for this preprint (which was not certified by peer review) is the author/funder, who has granted bioRxiv a license to display the preprint in perpetuity. It is made available under a CC-BY 4.0 International license.

here. We also note that the polyclonal antibody we raised against *D. virilis* Oskar cannot distinguish between the two isoforms. Consequently, we cannot comment on whether the *D. virilis* Long isoform, or chimeras containing the *D. virilis* Long Oskar domain, are localized cortically and/or to endosomes, as is the case for *D. melanogaster* Long Oskar [36–38,100].

However, some evidence suggests that *oskar* mRNAs and proteins from these two fly species do not have identical subcellular behaviors. We observed that *D. virilis* Oskar protein is more prone to localize closer to the embryonic cortex, than *D. melanogaster* Oskar, both in the endogenous *D. virilis* context and in the trans-species transgenic one. In addition, we (this study) and others [42] have observed that *D. virilis oskar* gene products may be less strongly restricted to the posterior at certain stages than *D. melanogaster* Oskar, both in the trans-species context of the *D. melanogaster* embryo (protein in Fig. 6A, mRNA in Webster and colleagues' Figure 3 and described as "data not shown" in their Figure 4 [42]) and in the endogenous context of the *D. virilis* oocyte (mRNA in Webster and colleagues' Figure 2[42]). Similarly, transcripts of the *oskar* homologs of the jewel wasp *Nasonia vitripennis* and the ant *Messor pergandi* are also localized to the posterior of developing oocytes at early stages of oogenesis, but appear somewhat more diffuse than in *D. melanogaster* (Lynch and colleagues' Figures 3 and 8 [101]). These hymenopteran *oskar* sequences lack a Long Oskar domain [101], showing that despite its important role in germ plasm anchoring in *D. melanogaster*, this domain can be dispensable for functional germ plasm assembly in other species.. This could mean that the anchoring function demonstrated for the *D. melanogaster* Long Oskar domain is species-specific, and an evolutionary innovation relative to Oskar's conserved germ plasm assembly role. Consistent with this hypothesis, we previously provided evidence that the wasp example is not an isolated case: the Long Oskar domain itself is entirely absent from Oskar proteins in most insects, and evolved

bioRxiv preprint doi: https://doi.org/10.1101/2025.08.02.668269; this version posted November 10, 2026. The copyright holder for this preprint (which was not certified by peer review) is the author/funder, who has granted bioRxiv a license to display the preprint in perpetuity. It is made available under a CC-BY 4.0 International license.

only approximately 70 million years ago, around the time of divergence of the lineage leading to the Pinpunculidae (the big-headed flies) [20]. This also indicates that evolving the Long Oskar domain is not what allowed *oskar*, which likely originally played a role in somatic development [20,102,103], to evolve its germ line role, since at least some *oskar* orthologs without the Long Oskar domain can still assemble germ plasm.

Evolution-inspired analysis of protein structure-function relationships

Functional characterization of classical *oskar* alleles generated with random mutagenesis offered the first insights into the biological processes regulated by Oskar [87,104]. More recently, targeted mutagenesis has been used to determine the functional significance of specific regions of the Oskar protein, identifying residues that might be important for interaction with Vasa [27] or mRNA [25,26]. However, designing such targeted experiments inherently relies on assumptions about which residues might be good candidates to test. Here, we leveraged the naturally occurring sequence divergence associated with the functional incompatibility of *D. virilis* Oskar in *D. melanogaster* to identify functionally significant regions of Oskar *in vivo.* By taking advantage of species-specific sequence variations, we were able to evaluate functionally significant portions of Oskar in an unbiased manner. This type of approach has offered insight into other structure-function relationships. For instance, the pea aphid (*Acyrthosiphon pisum*) homolog of Vasa fails to localize to the germ plasm when expressed in *D. melanogaster* [105]. By generating a series of chimeras swapping domains between *D. melanogaster* and *A. pisum* Vasa, researchers demonstrated that specific residues within the C-terminal HELICc domain of Vasa are required for posterior localization *in vivo* [105]. Going forward, our work on Oskar may provide a foundation for targeted screens, for instance within the OSK domain, to identify specific

bioRxiv preprint doi: https://doi.org/10.1101/2025.08.02.668269; this version posted November 10, 2026. The copyright holder for this preprint (which was not certified by peer review) is the author/funder, who has granted bioRxiv a license to display the preprint in perpetuity. It is made available under a CC-BY 4.0 International license.

779 residues important for pole cell formation. This approach provides a powerful framework for
780 dissecting the molecular evolution of developmental genes and identifying functionally
781 significant residues in rapidly evolving proteins.

bioRxiv preprint doi: https://doi.org/10.1101/2025.08.02.668269; this version posted November 10, 2026. The copyright holder for this preprint (which was not certified by peer review) is the author/funder, who has granted bioRxiv a license to display the preprint in perpetuity. It is made available under a CC-BY 4.0 International license.

Acknowledgements

We thank members of the Extavour Lab for helpful discussions, particularly Chandrashekar Kuyyamudi for assistance with image analysis. We also thank several Extavour lab members for assistance with experiments required for revision of the manuscript: Tarun Kumar for fly crosses and maintenance; Chandrashekar Kuyyamudi for embryo collection, staining, and imaging; Macy Ingersoll for dissections and embryo collection; and Evelyn Schwager, Damien Markus, Yu Shirai, Suhrid Ghosh, Daniella Haber and Petra Kovacikova for embryo collection. We thank Mariana Wolfner and members of her lab for assistance with Western Blots. This study was supported by NIH award # 1R01GM143611, funds from Harvard University, and from the Howard Hughes Medical Institute awarded to CGE. Additional support was provided by the NSF-Simons Center for Mathematical and Statistical Analysis of Biology at Harvard (award number #1764269), the Harvard Quantitative Biology Initiative, a Boehringer Ingelheim Fonds Ph.D. fellowship awarded to A.R., and a Herchel Smith Graduate Fellowship awarded to ELR.

Author Contributions

CGE, JRS, and ELR conceived and designed the project. ELR and JRS performed the experiments. AR provided custom scripts for image analysis. CGE supervised the project and acquired funding. ELR and CGE wrote the manuscript. All authors reviewed and edited the manuscript.

Competing interests

The authors declare no competing interests.

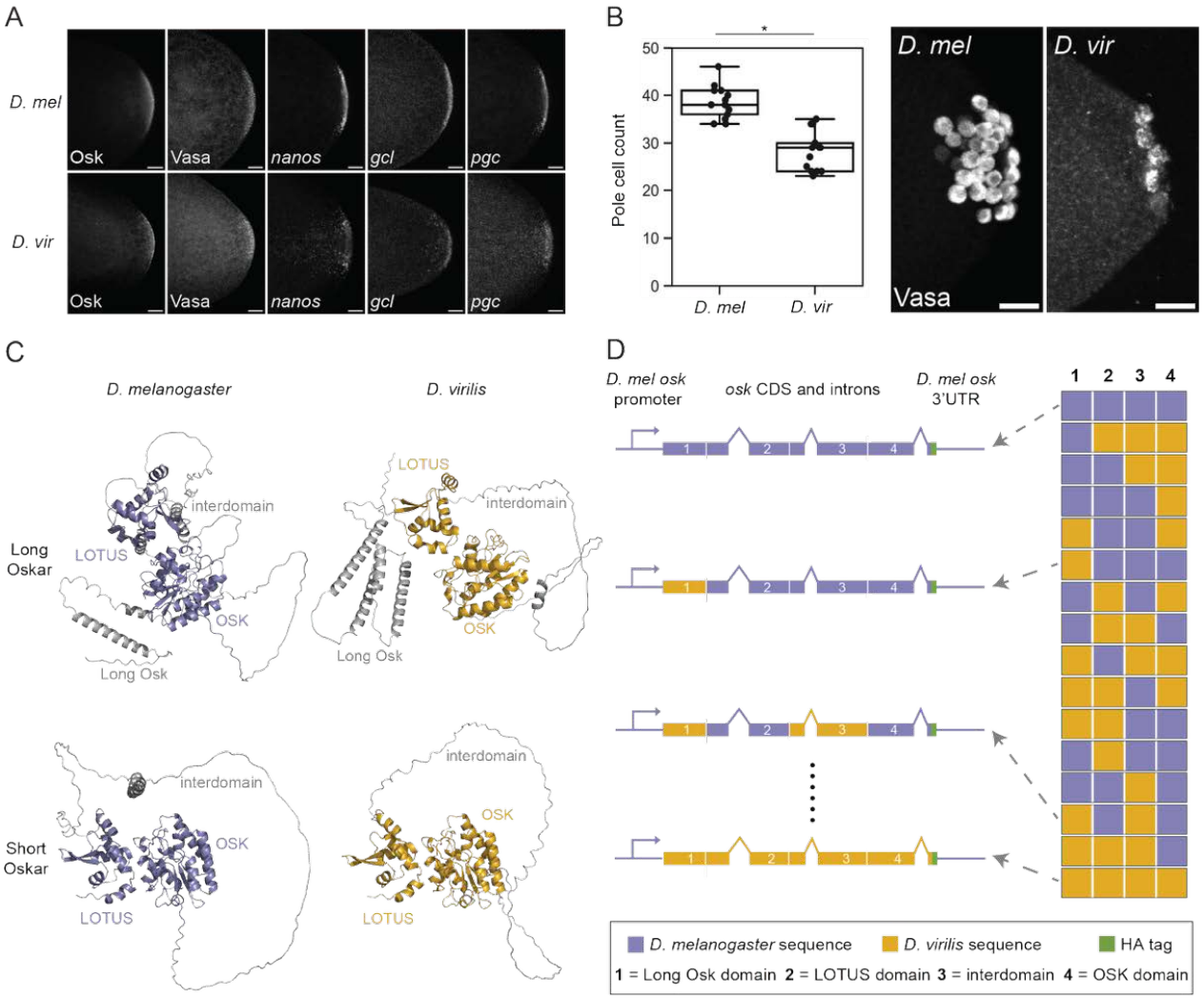


Figure 1. *D. virilis* exhibits posterior localization of several germ plasm molecules, including Oskar, which shares a similar domain architecture with *D. melanogaster* Oskar. A) Posterior poles of *D. melanogaster* (*D. mel*, top row) and *D. virilis* (*D. vir*, bottom row) stage 2 embryos with Oskar, Vasa, *nanos*, *germ cell-less* (*gcl*), and *polar granule component* (*pgc*) labeled. **B)** Pole cell counts for *D. virilis* and *D. melanogaster* stage 5 embryos. Asterisk designates significance (p-value < 0.01, estimated from the distribution of difference of means between sample and control from 100,000 simulated samples). n = 13 embryos for each species. **B')** *D. melanogaster* and *D. virilis* stage 5 embryos with germ cells labeled with anti-*D. melanogaster* Vasa antibody. All micrographs are maximum intensity projections of 20 optical sections (step size = 0.5 μm) oriented with posterior to the right and scale bars = 20 μm. **C)** AlphaFold3 [49] structural predictions of Long and Short Oskar isoform orthologs from *D. melanogaster* and *D. virilis* with the Long Osk, LOTUS, interdomain, and OSK domains labeled. **D)** Schematic of *D. melanogaster–D. virilis oskar* chimeric constructs. *D. melanogaster* (purple) and *D. virilis* (gold) genomic DNA sequences encoding the four domains shown in (**C**) were fused in frame in all possible combinations. The *D. melanogaster oskar* promoter, 5'UTR, and 3'UTR were used for all constructs. An HA tag (green) was added to the C-terminus of all sequences. The rightmost portion of the schematic represents the 16 different chimeras generated for this experiment.

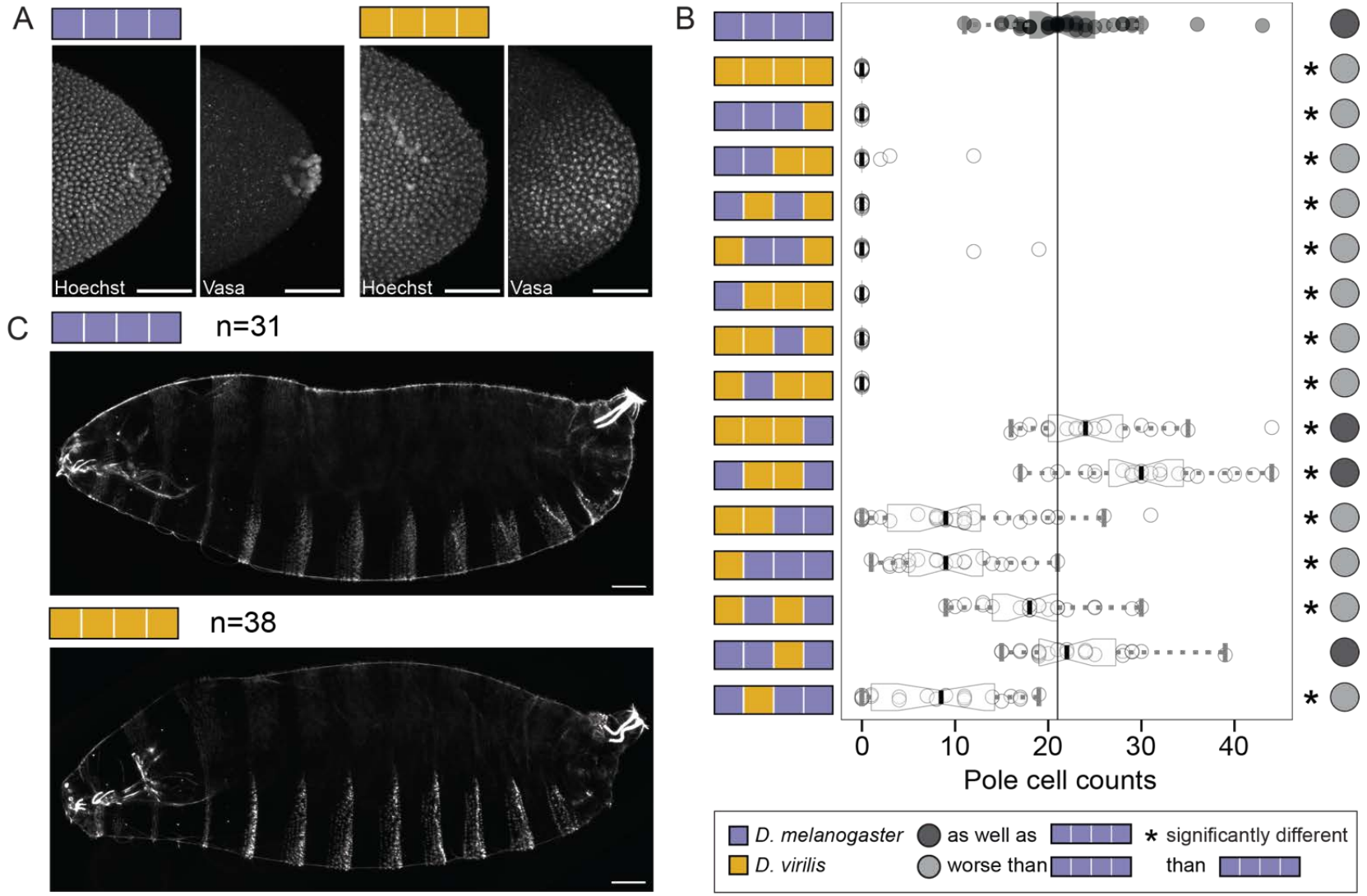


Figure 2. *D. virilis* Oskar and chimeras with the *D. virilis* OSK domain fail to rescue pole cell formation but rescue embryonic patterning defects. A) Posterior poles of stage 5 embryos from *D. melanogaster* mothers expressing *D. melanogaster* (purple, left) or *D. virilis oskar* (gold, right) in an *oskar* null background. Embryos are stained with a nuclear marker (Hoechst) and anti-*D. melanogaster* Vasa antibody. Micrographs are maximum intensity projections of 60 optical sections (step size = 1 μm) and scale bars = 50 μm. **B)** Pole cell counts in stage 5 embryos expressing chimeric *oskar*. Distribution for embryos from flies expressing the *D. melanogaster oskar* chimera (positive control) is in black with the median marked with a black line. Significant difference from positive control distribution (p-value < 0.05, estimated from the distribution of difference of means between sample and control from 100,000 simulated samples) indicated by asterisk. Circles to the right of the plots indicate data interpretation as follows: dark gray = specifies pole cells as well as *D. melanogaster oskar*; light gray = specifies pole cells worse than *D. melanogaster oskar*. Sample sizes ≥15 for each genotype; see Table S2. **C)** Cuticles of first instar larval progeny of mothers expressing *D. melanogaster* (purple, left) and *D. virilis oskar* (gold, right) exhibit wild-type patterning. Micrographs are projections of 15 optical sections (step size = 1.47 μm). Scale bars = 50 μm. Posterior is to the right in all micrographs.

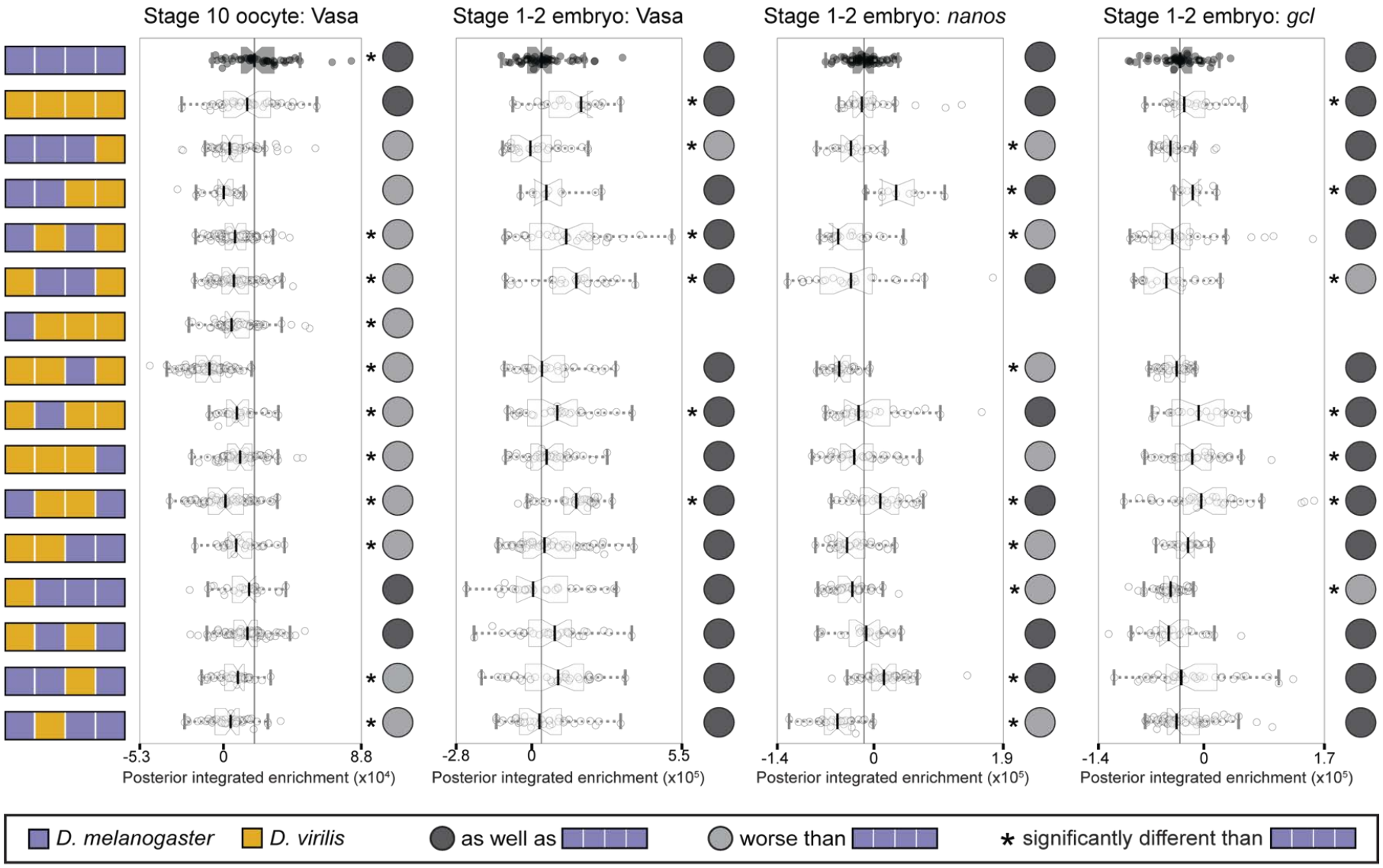


Figure 3. *D. melanogaster–D. virilis oskar* chimeras effectively recruit Vasa protein but not germ plasm mRNAs in *D. melanogaster oskar* null embryos. Posterior integrated enrichment of Vasa, *nanos*, and *gcl* in stage 10 oocytes and stage 1–2 embryos from *D. melanogaster* mothers expressing chimeric Oskar proteins. For the chimeric genotype with the Long Osk domain from *D. melanogaster* and the other three domains from *D. virilis*, sufficient posterior HA enrichment was found in oocytes to pass our threshold for analysis of germ plasm enrichment, but no embryos had sufficient enrichment to be included in the analysis. Distribution for eggs from flies expressing D. *melanogaster oskar* (positive control) is in black with the median marked with a black line. Significant difference from positive control distribution (p-value < 0.05, estimated from the distribution of difference of means between sample and control from 100,000 simulated samples) indicated by asterisk. Circles to the right of the plots indicate data interpretation as follows: dark gray = enriches the germ plasm molecule at least as well as *D. melanogaster oskar*; light gray = enriches the germ plasm molecule worse than *D. melanogaster oskar*. Sample sizes ≥9 for each condition; see Table S3.

bioRxiv preprint doi: https://doi.org/10.1101/2025.08.02.668269; this version posted November 10, 2026. The copyright holder for this preprint (which was not certified by peer review) is the author/funder, who has granted bioRxiv a license to display the preprint in perpetuity. It is made available under a CC-BY 4.0 International license.

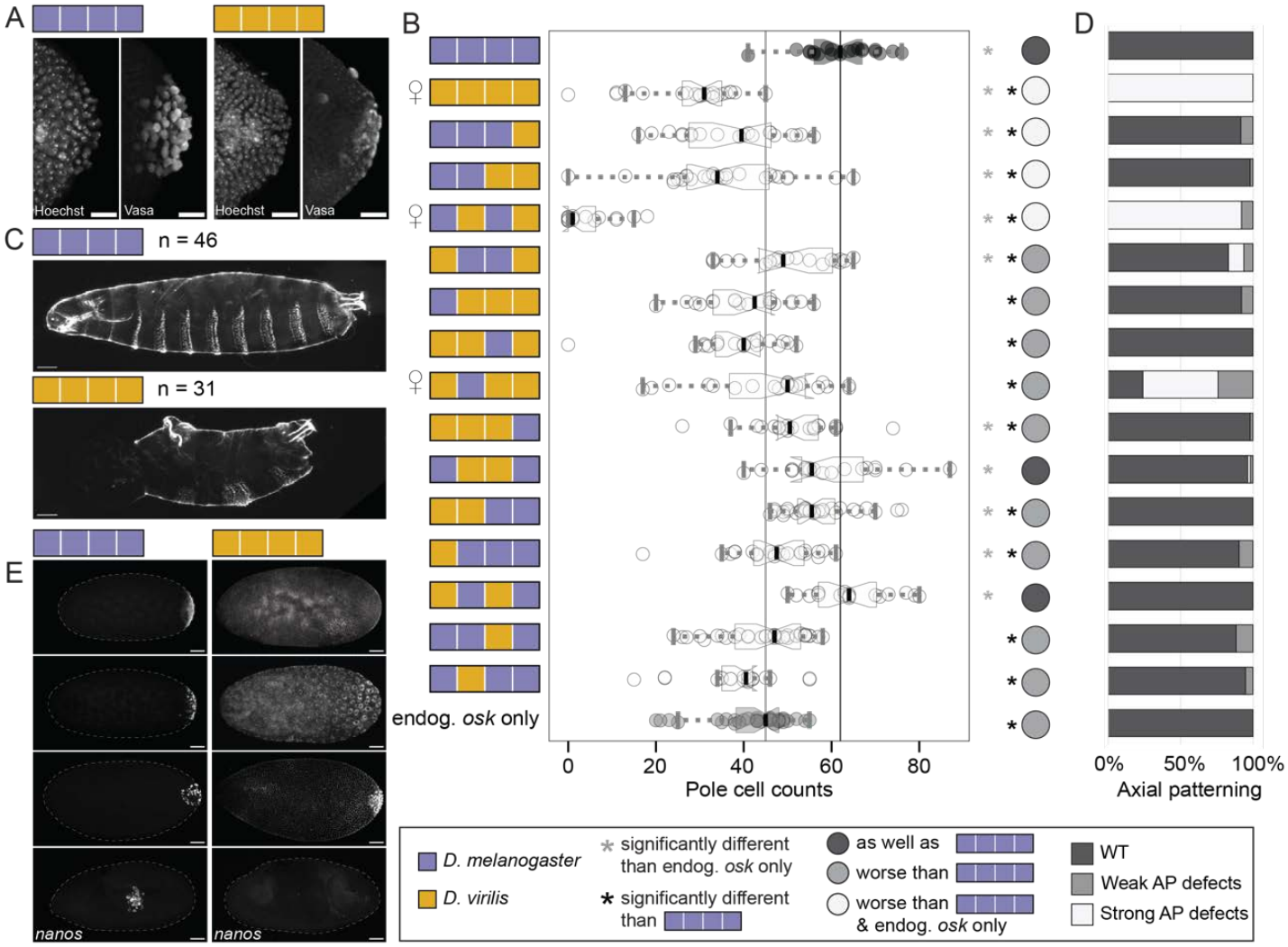


Figure 4. *D. virilis* Oskar and several Oskar chimeras disrupt axial patterning and impair germ cell formation in the presence of endogenous *oskar*. A) Stage 5 embryos from *D. melanogaster* mothers *expressing D. melanogaster* (purple, left) or *D. virilis oskar* (gold, right). Pole cells are marked by anti-*D. melanogaster* Vasa antibody and nuclei are marked with Hoechst. Micrographs are maximum intensity projections of 60 optical sections (step size = 1 μm) and scale bars = 20 μm. **B)** Pole cell counts in stage 5 embryos expressing chimeric *oskar*. Distribution from flies expressing only endogenous *oskar* (endog. *osk* only, negative control) is in gray with the median marked with a gray line. Distribution from flies expressing *D. melanogaster oskar* (positive control) is in black with the median marked with a black line. Significant difference from positive and negative control distributions (p-value < 0.05, estimated from the distribution of difference of means between sample and control from 100,000 simulated samples) indicated by black or gray asterisks respectively. Circles to the right of the plots indicate data interpretation as follows: dark gray = specifies pole cells as well as *D. melanogaster oskar*; light gray = specifies pole cells worse than *D. melanogaster oskar*; white = specifies pole cells worse than both *D. melanogaster oskar* and endogenous *oskar* alone. Sample sizes ≥20 for each genotype; see Table S4. Mirror of Venus symbol to the left of the plot indicates chimeric genotypes that exhibited dominant female sterility. **C)** Cuticles of embryos/first instar larval progeny of *D. melanogaster* mothers expressing *D. melanogaster oskar* (left) have wild-type anterior patterning, while the cuticles of *D. melanogaster* animals whose mothers expressed *D. virilis oskar* (right) are bicaudal. Micrographs are projections of 15 optical sections (step size = 1.47 μm) and scale bars = 50 μm. **D)** Frequency of defects in anterior-posterior (AP) patterning in progeny from mothers expressing each chimeric Oskar protein. Dark gray (WT) = wild-type AP patterning; light gray = weak AP defects: some duplication of posterior segments in the anterior but not completely bicaudal; white = strong AP defects: bicaudal or complete mirror image duplications of the posterior. Sample sizes ≥31 for each genotype; see Table S4. **E**) Representative examples of the range of *nanos* localization patterns observed in wild-type *D. melanogaster* embryos expressing either *D. melanogaster* (left) or *D. virilis oskar* (right). Micrographs are displayed with increasingly advanced stages of embryogenesis going top to bottom. Dotted lines outline the outer edge of embryos. Micrographs are maximum intensity projections of 30 optical sections (step size = 2 μm) and scale bars = 50 μm. Posterior is to the right in all micrographs.

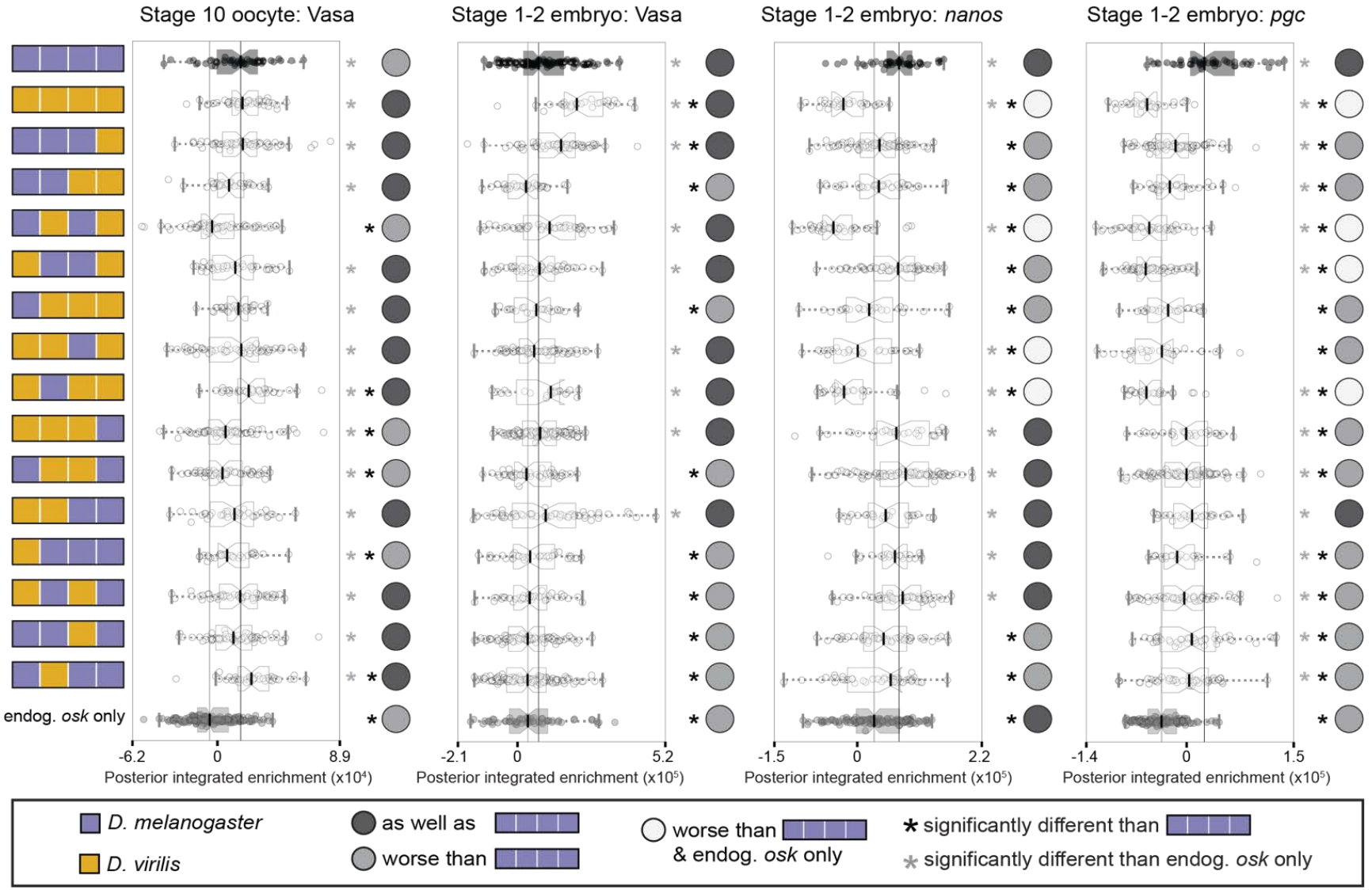


Figure 5. *D. melanogaster–D. virilis oskar* chimeras recruit Vasa protein but have dominant-negative effects on germ plasm mRNA localization in the presence of endogenous Oskar. Distributions of posterior integrated enrichment for Vasa, *nanos*, and *pgc* in stage 10 oocytes and stage 1–2 embryos from *D. melanogaster* mothers expressing chimeric *oskar*. Distribution from flies expressing *D. melanogaster oskar* (positive control) is in black with the median marked with a black line. Distribution from flies expressing only endogenous *oskar* (endog. *osk* only, negative control) is in gray with the median marked with a gray line. Significant difference from positive and negative control distributions (p-value < 0.05, estimated from the distribution of difference of means between sample and control from 100,000 simulated samples) indicated by black or gray asterisks respectively. Circles to the right of the plots indicate data interpretation as follows: dark gray = enriches the germ plasm molecule at least as well as *D. melanogaster oskar*; light gray = enriches the germ plasm molecule worse than *D. melanogaster oskar*; white = enriches Vasa worse than both *D. melanogaster oskar* and endogenous *oskar* alone. Sample sizes ≥16 for each condition; see Table S5.

bioRxiv preprint doi: https://doi.org/10.1101/2025.08.02.668269; this version posted November 10, 2026. The copyright holder for this preprint (which was not certified by peer review) is the author/funder, who has granted bioRxiv a license to display the preprint in perpetuity. It is made available under a CC-BY 4.0 International license.

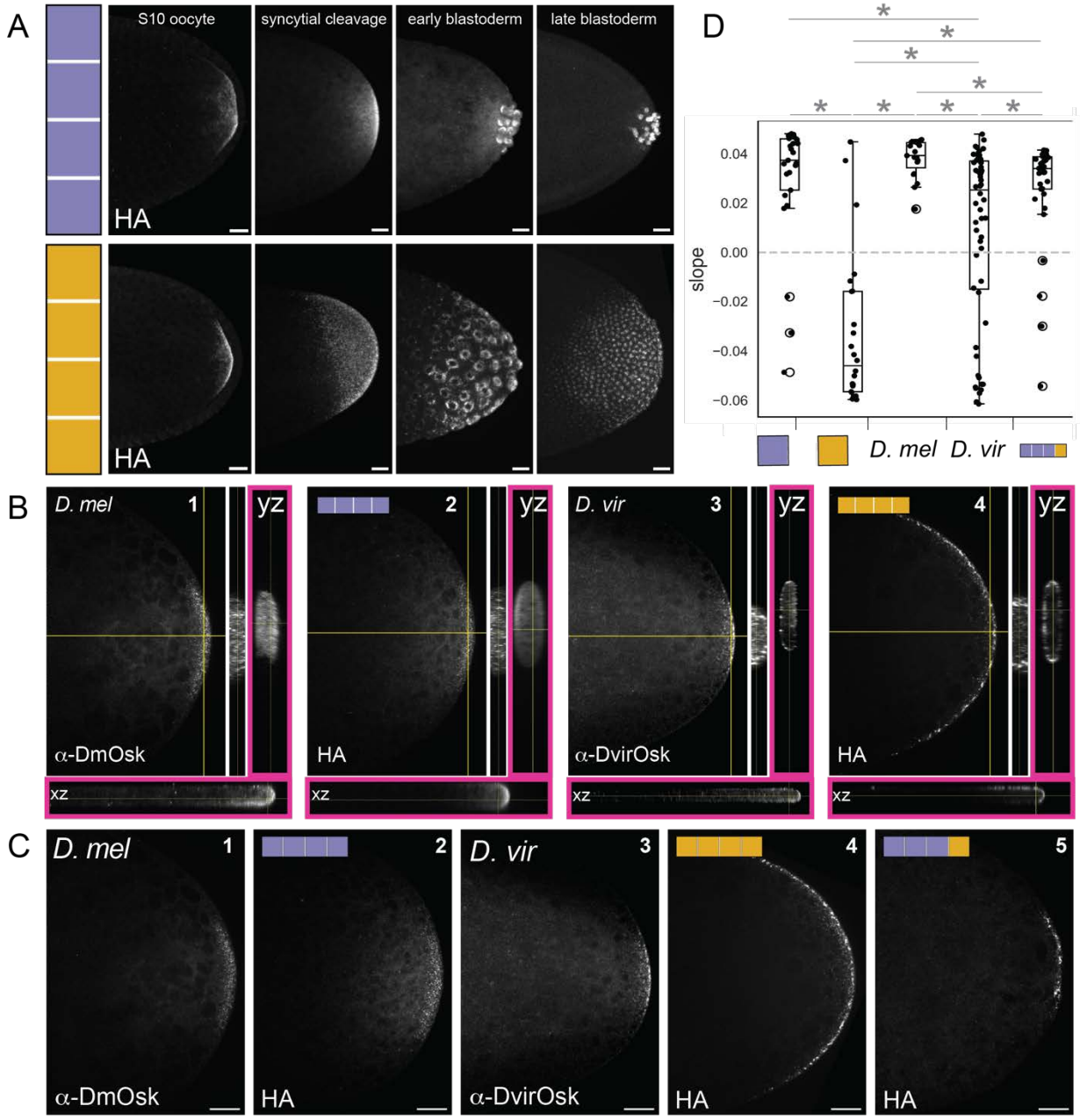


Figure 6. The OSK domain contributes to regulating species-specific granule size and localization. A) Oocytes and embryos from *D. melanogaster* mothers expressing *D. melanogaster* (purple, top row) or *D. virilis oskar* (gold, bottom row). Images are oriented with posterior to the right and are shown in order of increasing developmental time going left to right. Anti-HA antibody staining marks the localization of Oskar protein. Micrographs are maximum intensity projections of 30 optical sections (step size = 2 μm) and scale bars = 20 μm. **B)** Cleavage stage embryos of wild-type *D. melanogaster* (1: Oregon R) and *D. virilis* (3) stained with species-specific anti-Oskar antibodies, and *D. melanogaster* embryos from mothers expressing *D. melanogaster oskar* (2) or *D. virilis oskar* (4) stained with anti-HA antibody. Orthogonal views in the yz and xz orientations flank each image. Main images and orthogonal projections immediately to the right were captured with a 60x objective; orthogonal views bounded in pink were captured with a 20x objective, included here to more clearly visualize the distinct cortical localization of *D. virilis* and *D. melanogaster* Oskar proteins. **C)** Posterior pole of cleavage stage embryos from Oregon R (1), wild-type *D. virilis* (4), *D. melanogaster* expressing *D. melanogaster oskar* (2), *D. melanogaster* expressing *D. virilis oskar* (4), and *D. melanogaster* (bottom right) expressing *D. melanogaster oskar* with the OSK domain swapped with *D. virilis* sequence (5). *D. melanogaster* and *D. virilis* embryos are stained with species-specific Oskar antibodies and transgenic animals are stained for HA. Micrographs are single optical sections and scale bars = 20 μm. Posterior is to the right in all micrographs. **D)** Plot of the slopes for lines of best fit that were drawn for curves of the fluorescent signal intensity when eroding yz projections of HA signal in embryos (see Fig. S13). Positive slope indicates more signal towards the middle of the embryo than the edges, and negative slope indicates more signal at the edges of the embryo. Significant

bioRxiv preprint doi: https://doi.org/10.1101/2025.08.02.668269; this version posted November 10, 2026. The copyright holder for this preprint (which was not certified by peer review) is the author/funder, who has granted bioRxiv a license to display the preprint in perpetuity. It is made available under a CC-BY 4.0 International license.

888 difference in distributions (p-value < 0.05, estimated from the distribution of difference of means between sample and control from
889 100,000 simulated samples) indicated by asterisk; n.s. = not significant.

bioRxiv preprint doi: https://doi.org/10.1101/2025.08.02.668269; this version posted November 10, 2026. The copyright holder for this preprint (which was not certified by peer review) is the author/funder, who has granted bioRxiv a license to display the preprint in perpetuity. It is made available under a CC-BY 4.0 International license.

Methods

Generation of chimeric oskar *constructs*

We removed the UAS, promoter, and *k10* 3'UTR elements from pVALIUM22 [51-53] via round-the-world polymerase chain reaction (RTW-PCR), leaving the *gypsy* insulator elements. We inserted a 6,577 kb ApaI–XhoI *D. melanogaster* genomic digest fragment corresponding to the genomic *oskar* locus (GenBank Acc. No. AE014297, region 8932758-8939335; gift from Dr. Anne Ephrussi, European Molecular Biology Laboratory, Heidelberg, Germany) into this linearized and modified pVALIUM22 via Gibson assembly. This genomic locus has previously been shown to provide wild-type *oskar* function in a loss-of-function background [34]. We introduced a C-terminal hemagglutinin (HA) epitope tag (TACCCATACGATGTTCCGGATTACGCT, encoding YPYDVPDA) via RTW-PCR, generating the plasmid pVAL22-Dm1234-HA. A clone of the *D. virilis osk* genomic locus [42] (GenBank Acc. No. L22556; obtained from Dr. Paul Macdonald, University of Texas at Austin, Texas, U.S.A.) served as the template for fragment amplification.

To generate various combinations of *D. melanogaster* and *D. virilis osk* fragments, we applied RTW-PCR to pVAL22-Dm1234-HA to delete a specific region, PCR to amplify the corresponding region from the *D. virilis osk* genomic locus clone, and Gibson assembly to insert the *D. virilis osk* fragment into the truncated pVAL22-Dm1234-HA plasmid. This strategy was applied to four specific regions in pVAL22- Dm1234-HA, corresponding to the Long Osk, LOTUS, interdomain, and OSK domains (Fig. 1D), which led to the creation of 16 total constructs. All transgenic constructs possess the *D. melanogaster oskar* 5'UTR and 3'UTR sequences.

bioRxiv preprint doi: https://doi.org/10.1101/2025.08.02.668269; this version posted November 10, 2026. The copyright holder for this preprint (which was not certified by peer review) is the author/funder, who has granted bioRxiv a license to display the preprint in perpetuity. It is made available under a CC-BY 4.0 International license.

Drosophila stocks

We prepared plasmid midi preps containing each *oskar* chimeric construct (Qiagen HiSpeed Plasmid Midi Kit) and sent them to BestGene (Chino Hills, CA, USA) for injection into the attP40 line (*y[1] w[67c23]; P{CaryP}attP40*). We crossed P_0 adults to *y[1] v[1]* to screen for transformants based on *vermillion* rescue, balanced constructs over *CyO,* and introduced the recessive marker *scute* to distinguish transgenic lines from wild-type animals (*y[1] sc[*] v[1]; chimeric-osk/CyO.*) Heterozygotes for the transgene were used in experiments testing the effects of one copy of chimeric *oskar* expression in a background with endogenous *oskar*. We used *y[1] sc[*] v[1]; +/CyO* animals as a negative control in these experiments (referred to as "endogenous *oskar*" in the text).

For rescue experiments, we generated animals expressing the chimeric *oskar* constructs in the *oskar* RNA null allele background *y[1] sc[*] v[1]; chimeric-osk/CyO; TI{w[+mC]=TI}osk[0.EGFP]* (*oskar* allele obtained from Bloomington *Drosophila* Stock Center 67407), which contains a 3xP3-EGFP-tubulin 3'UTR cassette inserted 26 nucleotides upstream of the *oskar* transcriptional start site that leads to failure to transcribe *oskar* [55] (*/TM3*). Animals heterozygous for the chimeric *oskar* construct and homozygous for *osk[0.EGFP]* were used in experiments testing the effect of one copy of chimeric *oskar* expression in an *oskar* null background.

For experiments with wild-type animals, we used the *D. melanogaster* strain *Oregon R* (Bloomington *Drosophila* Stock Center 5) and *D. virilis* (gift from Rainbow Transgenics, Camarillo, CA, USA).

All flies were reared at 25°C at 60% humidity with standard fly food and yeast as previously described [106].

bioRxiv preprint doi: https://doi.org/10.1101/2025.08.02.668269; this version posted November 10, 2026. The copyright holder for this preprint (which was not certified by peer review) is the author/funder, who has granted bioRxiv a license to display the preprint in perpetuity. It is made available under a CC-BY 4.0 International license.

937

938 *Immunofluorescence and in situ hybridization*

939 For antibody staining experiments in oocytes, we dissected ovaries from 3–5 day old
940 females in 1xPBS (phosphate buffered saline), fixed for 20 minutes in 4% PFA
941 (paraformaldehyde) in 1xPBS, and washed with 1xPBS. We permeabilized tissue twice for five
942 minutes in 1xPBT (1xPBS + 0.2% Tween-20), once for two hours in 1xPBTT (1xPBT + 1%
943 Triton X- 100), and once more for five minutes in 1xPBT. We blocked for two hours in 1xPBT +
944 1% BSA (bovine serum albumin, Millipore Sigma) and incubated with primary antibody
945 overnight at 4°C (see list of antibodies and concentrations in Table S12 and Key Resources
946 Table). The following day, we washed three times for one hour in 1xPBT + 1% BSA and
947 blocked for one hour in 1xPBT + 1% BSA + 2% NGS (normal goat serum, Jackson
948 ImmunoResearch). We mixed secondary antibody solution in 1xPBST + 1% BSA + 4% NGS
949 and incubated overnight at 4°C. The following day, we washed five times for 15 minutes in
950 1xPBT, mounted samples in Vectashield (Vector Laboratories), and stored slides at –20°C until
951 imaging.

952 For antibody staining experiments in embryos, we collected embryos on apple juice
953 plates (18 g agar + 20 g sucrose + 200 mL apple juice + 600 mL Milli-Q water) for one hour
954 (stage 1–2 embryos) or two hours plus two hours incubation at 25°C (stage 5 embryos). We
955 dechorionated embryos for one minute in 100% bleach (Chlorox), washed with distilled water,
956 and fixed for 20 minutes in 1:1 heptane:4% PFA in 1xPBS on a horizontal rotating shaker. We
957 devitellinized by manual shaking in 1:1 heptane:methanol and washed with 100% methanol (note
958 that for experiments with phalloidin staining, we used 80% ethanol in place of methanol). We
959 gradually stepped embryos out of methanol (or ethanol) into 1xPBS and permeabilized/blocked

bioRxiv preprint doi: https://doi.org/10.1101/2025.08.02.668269; this version posted November 10, 2026. The copyright holder for this preprint (which was not certified by peer review) is the author/funder, who has granted bioRxiv a license to display the preprint in perpetuity. It is made available under a CC-BY 4.0 International license.

960 embryos in 1xPBT + 1 mg/mL BSA (1xPBS + 0.2% Triton X-100) three times for 30 minutes.
961 We incubated embryos in primary antibody overnight at 4°C. The following day, we washed
962 three times for one hour in 1xPBT + 1 mg/mL BSA and blocked two times for one hour in
963 1xPBT + 1mg/mL BSA + 5% NGS. We incubated in secondary antibody solution overnight at
964 4°C. The following day, we washed five times for 15 minutes in 1xPBT, mounted samples in
965 Vectashield, and stored slides at -20°C until imaging.

966 For fluorescence *in situ* hybridization (FISH) experiments, we obtained hybridization
967 chain reaction (HCR) probes and amplifiers from Molecular Instruments (Los Angeles, CA,
968 USA; see Table S13 for list). We dechorionated and devitellinized stage 1–2 embryos as
969 described above. For FISH experiments (in wild-type *D. melanogaster* and *D. virilis* tissues), we
970 used the HCR RNA-FISH protocol for whole-mount fruit fly embryos from Molecular
971 Instruments. For experiments combining HCR FISH with HA antibody staining (in chimeric
972 *oskar* tissues), we gradually stepped embryos out of methanol in 1xPBS and permeabilized twice
973 for five minutes in 1xPBT (1xPBS + 0.2% Tween-20), once for one hour in 1xPBTT (1xPBT +
974 1% Triton X-100), and once for five minutes in 1xPBT. We blocked twice for one hour in
975 1xPBT + 5% NGS and incubated in primary antibody overnight at 4°C. The following day, we
976 washed four times for 30 minutes in 1xPBT and incubated in 2° antibody in 1xPBT + 5% NGS
977 for three hours at room temperature. We washed five times for five minutes in 1xPBT and five
978 times for five minutes in 5xSSCT (5xSSC (saline-sodium citrate) + 0.1% Triton X-100). We
979 post-fixed in 4% formaldehyde (Millipore Sigma) and washed four times for five minutes in
980 5xSSCT. We incubated at 37°C for two hours in probe hybridization buffer (Molecular
981 Instruments) and then added 16 nM of probe to incubate overnight at 37°C. The following day,
982 we washed four times for 30 minutes at 37°C in probe wash buffer (Molecular Instruments) and

bioRxiv preprint doi: https://doi.org/10.1101/2025.08.02.668269; this version posted November 10, 2026. The copyright holder for this preprint (which was not certified by peer review) is the author/funder, who has granted bioRxiv a license to display the preprint in perpetuity. It is made available under a CC-BY 4.0 International license.

then once for five minutes in 5xSSCT at room temperature. We incubated in amplification buffer (Molecular Instruments) for one hour and then added snap-cooled hairpins to incubate overnight at room temperature. The following day, we washed two times for five minutes and two times for 30 minutes in 5xSSCT. We incubated for one hour in Hoechst 33342 (Sigma Aldrich, 10 mg/mL stock solution) and then washed five times for five minutes in SSCT. We mounted samples in Vectashield and stored slides at -20°C before imaging.

Antibody generation and validation

We generated a polyclonal antibody, chicken anti-*D. virilis* Oskar, using AbClonal (Woburn, MA, USA) custom antibody services. AbClonal synthesized the gene sequence of a partial protein antigen target (*Drosophila virilis* Oskar, UniProt ID: Q24741, M161-R260) and cloned it into an expression vector. They purified this protein and injected it into two chickens for immunization. Total IgY was precipitated and purified from 10 egg yolks of immunized chickens.

We validated antibodies with Western Blots using adult Oregon R ovary protein lysates generated from 30 pairs of ovaries squished in RIPA (radioimmunoprecipitation assay) buffer with protein amount estimated using a Pierce Detergent Compatible Bradford Assay (ThermoFisher Scientific) (Fig. S18A–B). We ran an SDS-PAGE gel with lysates mixed and boiled with 5% beta-mercaptoethanol and 5xPierce Lane Marker Non-Reducing Sample Buffer (ThermoFisher Scientific). We also loaded Precision Plus Dual Color (Bio-Rad, chemiluminescent blots). We conducted semi-dry transfer using a Bio-Rad Trans-Blot Turbo Transfer System (Bio-Rad) and the Trans-Blot Turbo RTA PVDF Transfer Kit (Bio-Rad).

bioRxiv preprint doi: https://doi.org/10.1101/2025.08.02.668269; this version posted November 10, 2026. The copyright holder for this preprint (which was not certified by peer review) is the author/funder, who has granted bioRxiv a license to display the preprint in perpetuity. It is made available under a CC-BY 4.0 International license.

We washed membranes once for five minutes in 1xTBS-T (1xTBS (Tris-buffered saline) + 0.1% Tween-20) and blocked for one hour in 1xTBST + 5% milk (Carnation Instant Nonfat Dry Milk). We washed twice for one minute, once for 15 minutes, and twice for five minutes in 1xTBST. We incubated membranes overnight at 4°C in 1:500 primary antibody in 1xTBST + 5% BSA + 0.03% sodium azide. The following day, we washed three times for ten minutes in 1xTSBT, incubated in 1:5000 anti-chicken HRP secondary antibody (ThermoFisher Scientific) in 1xTBST + 5% milk at room temperature, and washed three times for ten minutes in TBST. For detection, we used the SuperSignal West Pico PLUS Chemiluminescent Substrate (ThermoFisher Scientific). We imaged using a CCD camera on a Sapphire Biomolecular Imager.

Larval cuticle preparations

We collected embryos for three hours on apple juice plates and incubated plates for 18 hours at 25°C. We dechorionated embryos/larvae for one minute in 100% bleach, washed with distilled water, and devitellinized by shaking in 1:1 heptane:methanol for five minutes. We removed the heptane and shook in 100% methanol for three minutes. We then washed once in methanol for three minutes, twice in 1xPBT (1xPBS + 0.1% Triton X-100) for three minutes, and once in 1xPBT for five minutes on a horizontal rotating shaker. We mounted samples in 3:1 lactic acid (Fisher Scientific):Milli-Q water, and we incubated slides at 65°C overnight. We stored slides at room temperature until imaging.

Image acquisition and analysis

For germ plasm molecule enrichment experiments, we used a Nikon CSU-W1 and Plan Apo λ 20x/0.75 air objective to capture image stacks (60 µm total, 2 µm step size). We used Fiji

bioRxiv preprint doi: https://doi.org/10.1101/2025.08.02.668269; this version posted November 10, 2026. The copyright holder for this preprint (which was not certified by peer review) is the author/funder, who has granted bioRxiv a license to display the preprint in perpetuity. It is made available under a CC-BY 4.0 International license.

to generate sum intensity projections of all stacks and masks of the tissue of interest within each projection. We used a previously described [26] Python script to calculate the relative signal enrichment for each pixel (z-score) in a projection, interpolate the relative signal enrichment along the anteroposterior axis, integrate the values for the 15% posterior-most positions, and plot the integrated posterior enrichment values. To ensure that we only tested for enrichment of germ plasm at the posterior in samples where the chimeric Oskar was localized at the posterior, we filtered our dataset to include only samples where the mean HA signal enrichment for the 15% posterior-most positions was greater than the mean plus three times the standard deviation of the HA signal enrichment observed in the genetic negative control for the experiments in the background with endogenous *oskar*. For the *oskar* RNA null experiments, we could not have a genetic negative control since *oskar* RNA null animals do not create late-stage oocytes or embryos [54], so we filtered for mean HA enrichment greater than the mean plus three times the standard deviation of signal in tissues of the same genotype with no primary antibody. We statistically compared each chimeric genotype's distribution of integrated posterior enrichment values to those of the controls by bootstrapping, estimating p-values from the distribution of mean differences between sample and control from 100,000 simulated samples.

To supplement this analysis, we also measured colocalization of HA and each germ plasm molecule of interest as previously described [26]. We found the Pearson correlation for the signal intensity between HA and another germ plasm molecule for the pixels in the 15% posterior-most end of the embryo with HA intensity values 2 standard deviations over the mean. We statistically compared distributions of Pearson correlation coefficients by bootstrapping, estimating p-values from the distribution of mean differences between sample and control from 100,000 simulated samples.

bioRxiv preprint doi: https://doi.org/10.1101/2025.08.02.668269; this version posted November 10, 2026. The copyright holder for this preprint (which was not certified by peer review) is the author/funder, who has granted bioRxiv a license to display the preprint in perpetuity. It is made available under a CC-BY 4.0 International license.

For the chimeric genotype with the Long Osk domain from *D. melanogaster* and the other three domains from *D. virilis*, sufficient posterior HA enrichment was found in oocytes to pass our threshold for analysis of germ plasm enrichment, but no embryos had sufficient enrichment to be included in the analysis (Fig. 3). We note that despite these low HA expression levels, sufficient *nanos* mRNA must be recruited for successful abdominal patterning, as we observed larval progeny of mothers expressing this chimera (data not shown).

For germ cell counting experiments, we used a Nikon CSU-W1 and Plan Apo λ 20x/0.75 air objective to capture image stacks (60 µm total, 1 µm step size). We used phalloidin staining to track the progress of cellularization and precisely stage embryos at the end of embryonic stage 5. We counted germ cells using the Fiji cell counter [107].

For axial patterning experiments, we used an EC Plan-Neofluar 20x/0.50 M27 on a Zeiss AxioImager Z1 and dark-field microscopy to capture image stacks (15 optical sections with a 1.47 µm step size). We used Helicon Focus (version 8.2.2) to render representative images with extended depth of field. We scored each cuticle patterning phenotype as “wild-type” (showing wild-type anterior-posterior (AP) patterning), “strong AP defects” (completely bicaudal, complete mirror image duplications of the posterior), or “partial AP defects” (some duplication of posterior segments in the anterior but not completely bicaudal). We calculated the Jensen–Shannon Divergence (JSD) for the distribution of “WT”, “strong anterior defects”, and “partial anterior defects” phenotypes in each chimeric background compared to the distribution of these phenotypes in the negative control (endogenous *oskar* only) and positive control (all *D. melanogaster oskar* sequence). A score of 0 indicates the distributions are identical, while a score of 1 indicates they are completely different.

bioRxiv preprint doi: https://doi.org/10.1101/2025.08.02.668269; this version posted November 10, 2026. The copyright holder for this preprint (which was not certified by peer review) is the author/funder, who has granted bioRxiv a license to display the preprint in perpetuity. It is made available under a CC-BY 4.0 International license.

For evaluation of the radial distribution of HA signal intensity in embryos, we analyzed images using a custom Python script. We rotated image stacks with the posterior of the embryo at the right, and used Cellpose [108] to segment the area containing the embryo (cyto3 model, diameter set to 1000). We cropped the image stacks and then rescaled in the z-dimension to account for differences in pixel dimensions. We computed the mean intensity along the yz axis to generate a 2D image and applied Otsu's threshold [109] within the masked area. We then eroded over 20 iterations and computed the mean intensity within the eroded region with each iteration. We normalized each intensity profile and then fitted a straight line to each normalized profile. We plotted the slopes of these fitted lines and compared the distributions for *D. virilis* and *D. melanogaster* with statistical analysis by bootstrapping, estimating p-values from the distribution of mean differences between each pair of genotypes from 100,000 simulated samples. See Fig. S13C for an overview of this image analysis workflow.

GPSite Analysis

Protein sequences for *D. melanogaster* and *D. virilis* Oskar, along with those of the chimeras, were input into the GPSite web server (https://bio-web1.nscc-gz.cn/app/GPSite) [84], and the output data were visualized with plots generated in Python. To generate the aligned line scores shown in Fig. S14, the *D. melanogaster* and *D. virilis* Oskar protein sequences were aligned with EMBOSS Needle [110].

bioRxiv preprint doi: https://doi.org/10.1101/2025.08.02.668269; this version posted November 10, 2026. The copyright holder for this preprint (which was not certified by peer review) is the author/funder, who has granted bioRxiv a license to display the preprint in perpetuity. It is made available under a CC-BY 4.0 International license.

1093 **Key Resources Table**
1094

	SOURCE	IDENTIFIER
Antibodies		
Rabbit polyclonal anti-Vasa	Laboratory of Akira Nakamura, Kumamoto University, Japan	N/A
Mouse monoclonal anti-HA	AbClonal	Cat# AE008
Chicken polyclonal anti-Vasa	Extavour Lab [26]	N/A
Chicken polyclonal anti-Oskar (virilis)	This paper	N/A
Mouse monoclonal anti-ATP5A (15H4C4)	Abcam	Cat# ab14748
Rat monoclonal anti-HA (3F10)	Millipore Sigma	Cat# 11867423001
Rabbit polyclonal anti-Oskar	Laboratory of Anne Ephrussi, European Molecular Biology Laboratory, Germany	N/A
Guinea pig polyclonal anti-Smaug	Laboratory of Howard Lipshitz, University of Toronto, Canada	N/A
Rabbit polyclonal anti-Par-1	Laboratory of Daniel St. Johnston, University of Cambridge, UK	N/A
Rabbit polyclonal anti-Nanos	Laboratory of Akira Nakmura, Kumamoto University, Japan	N/A
Rabbit polyclonal anti-GFP, conjugated to Alexa Fluor 488	ThermoFisher Scientific	Cat# A-21311
Alexa Fluor 488 AffiniPure goat anti-rabbit IgG (H+L) secondary antibody	Jackson ImmunoResearch Laboratories	Cat# 111-545-144
Alexa Fluor 647 goat anti-mouse IgG (H+L) highly cross-adsorbed secondary antibody	ThermoFisher Scientific	Cat# A-21236
Alexa Fluor 568 goat anti-chicken IgY (H+L) secondary antibody	ThermoFisher Scientific	Cat# A-11041
Alexa Fluor 488 goat anti-mouse IgG (H+L) highly cross-adsorbed secondary antibody	ThermoFisher Scientific	Cat# A-11029
Alexa Fluor 647 goat anti-rat IgG (H+L) highly cross-adsorbed secondary antibody	ThermoFisher Scientific	Cat# A-21247
Alexa Fluor 647 donkey anti-rabbit IgG (H+L) highly cross-adsorbed secondary antibody	ThermoFisher Scientific	Cat# A-31573
Alexa Fluor 568 goat anti-mouse IgG (H+L) highly cross-adsorbed secondary antibody	ThermoFisher Scientific	Cat# A-11004
Alexa Fluor 568 goat anti-rabbit IgG (H+L) cross-adsorbed secondary antibody	ThermoFisher Scientific	Cat# A-11011

bioRxiv preprint doi: https://doi.org/10.1101/2025.08.02.668269; this version posted November 10, 2026. The copyright holder for this preprint (which was not certified by peer review) is the author/funder, who has granted bioRxiv a license to display the preprint in perpetuity. It is made available under a CC-BY 4.0 International license.

Alexa Fluor 647 goat anti-chicken IgY (H+L) secondary antibody	ThermoFisher Scientific	Cat# A-21449
Alexa Fluor 568 goat anti-rat IgY (H+L) secondary antibody	ThermoFisher Scientific	Cat# A-11077
Alexa Fluor 488 goat anti-rat IgY (H+L) secondary antibody	ThermoFisher Scientific	Cat# A-11006
Cy5 donkey anti-guinea pig IgG (H+L) secondary antibody	ThermoFisher Scientific	Cat # A-17648
HRP goat anti-chicken IgY (H+L) secondary antibody	ThermoFisher Scientific	Cat# A-16054
Hoechst 33342	Sigma-Aldrich	Cat# B2261-25MG
Alexa Fluor 488 phalloidin	Invitrogen	Cat# A-12379
TRITC phalloidin	Invitrogen	Cat# R415
D. melanogaster oskar HCR probe, amp B1 (v3.0)	Molecular Instruments	N/A
D. melanogaster nanos HCR probe, amp B5 (v3.0)	Molecular Instruments	N/A
D. melanogaster germ cell-less HCR probe, amp B3 (v3.0)	Molecular Instruments	N/A
D. melanogaster polar granule component HCR probe, amp B4 (v3.0)	Molecular Instruments	N/A
D. melanogaster oskar 3'UTR HCR probe, amp B5 (v3.0)	Molecular Instruments	N/A
D. virilis oskar HCR probe, amp B1 (v3.0)	Molecular Instruments	N/A
D. virilis nanos HCR probe, amp B5 (v3.0)	Molecular Instruments	N/A
D. virilis germ cell-less HCR probe, amp B3 (v3.0)	Molecular Instruments	N/A
D. virilis polar granule component HCR probe, amp B4 (v3.0)	Molecular Instruments	N/A
HCR amplifier B1 488 (v3.0)	Molecular Instruments	N/A
HCR amplifier B5 555 (v3.0)	Molecular Instruments	N/A
HCR amplifier B3 594 (v3.0)	Molecular Instruments	N/A
HCR amplifier B4 647 (v3.0)	Molecular Instruments	N/A
Chemicals, peptides, and recombinant proteins		
Chlorox Germicidal Bleach	Chlorox	Cat# 67619-32
Heptane	Sigma-Aldrich	Cat# 32287
Methanol	Sigma-Aldrich	Cat# 646377
Ethanol	Sigma-Aldrich	Cat# E7023
Paraformaldehyde, powder, 95%	Sigma-Aldrich	Cat# 158127
Lactic acid, 90% solution in water	Fisher Scientific	Cat# AC189872500
2-mercaptoethanol, Omnipur	Avantor	Cat# EM-6050
Formaldehyde solution	Sigma-Aldrich	Cat# 252549

bioRxiv preprint doi: https://doi.org/10.1101/2025.08.02.668269; this version posted November 10, 2026. The copyright holder for this preprint (which was not certified by peer review) is the author/funder, who has granted bioRxiv a license to display the preprint in perpetuity. It is made available under a CC-BY 4.0 International license.

5x Pierce Lane Marker Non-Reducing Sample Buffer	Thermo Scientific	Cat# 39001
Precision Plus Protein Dual Color Standards	Bio-Rad	Cat# 1610394
SuperSignal West Pico PLUS Chemiluminescent Substrate	Thermo Scientific	Cat# 34580
Sodium azide	Sigma-Aldrich	Cat# S2002
Drosophila virilis Oskar, (UniProt ID: Q24741, M161-R260 aa)	This paper	N/A
Critical commercial assays		
HiSpeed Plasmid Kit	Qiagen	Cat# 12643
QIAprep Spin Miniprep Kit	Qiagen	Cat# 27104
Pierce Detergent Compatible Bradford Assay Kit	Thermo Scientific	Cat# 23246
Trans-Blot Turbo RTA Mini 0.2 µm PVDF Transfer Kit	Bio-Rad	Cat# 1704272
Deposited data		
Code for analyzing radial distribution of HA signal	This paper	https://github.com/erivard/dmdv_osk_chimera.git
Sequences of *D. melanogaster–D. virilis oskar* chimeras	This paper	https://github.com/erivard/dmdv_osk_chimera.git
Experimental models: Organisms/strains		
y[1] sc v[1]; P{y[+] v[+]=(Dm1234-HA)attP40/CyO*	This paper	N/A
y[1] sc v[1]; P{y[+] v[+]=(Dv1234-HA)attP40/CyO*	This paper	N/A
y[1] sc v[1]; P{y[+] v[+]=(Dm123Dv4-HA)attP40/CyO*	This paper	N/A
y[1] sc v[1]; P{y[+] v[+]=(Dm12Dv34-HA)attP40/CyO*	This paper	N/A
y[1] sc v[1]; P{y[+] v[+]=(Dm13Dv24-HA)attP40/CyO*	This paper	N/A
y[1] sc v[1]; P{y[+] v[+]=(Dm23Dv14-HA)attP40/CyO*	This paper	N/A
y[1] sc v[1]; P{y[+] v[+]=(Dm1Dv234-HA)attP40/CyO*	This paper	N/A
y[1] sc v[1]; P{y[+] v[+]=(Dm3Dv124-HA)attP40/CyO*	This paper	N/A
y[1] sc v[1]; P{y[+] v[+]=(Dm2Dv134-HA)attP40/CyO*	This paper	N/A
y[1] sc v[1]; P{y[+] v[+]=(Dm4Dv123-HA)attP40/CyO*	This paper	N/A
y[1] sc v[1]; P{y[+] v[+]=(Dm14Dv23-HA)attP40/CyO*	This paper	N/A
y[1] sc v[1]; P{y[+] v[+]=(Dm34Dv12-HA)attP40/CyO*	This paper	N/A
y[1] sc v[1]; P{y[+] v[+]=(Dm234Dv1-HA)attP40/CyO*	This paper	N/A
y[1] sc v[1]; P{y[+] v[+]=(Dm24Dv13-HA)attP40/CyO*	This paper	N/A

bioRxiv preprint doi: https://doi.org/10.1101/2025.08.02.668269; this version posted November 10, 2026. The copyright holder for this preprint (which was not certified by peer review) is the author/funder, who has granted bioRxiv a license to display the preprint in perpetuity. It is made available under a CC-BY 4.0 International license.

y[1] sc v[1]; P{y[+] v[+]=(Dm124Dv3-HA)attP40/CyO*	This paper	N/A
y[1] sc v[1]; P{y[+] v[+]=(Dm134Dv2-HA)attP40/CyO*	This paper	N/A
y[1] sc v[1]; P{y[+] v[+]=(Dm1234-HA)attP40/CyO; osk[0.EGFP]/TM3 Sb[1]*	This paper	N/A
y[1] sc v[1]; P{y[+] v[+]=(Dv1234-HA)attP40/CyO; osk[0.EGFP]/TM3 Sb[1]*	This paper	N/A
y[1] sc v[1]; P{y[+] v[+]=(Dm123Dv4-HA)attP40/CyO; osk[0.EGFP]/TM3 Sb[1]*	This paper	N/A
y[1] sc v[1]; P{y[+] v[+]=(Dm12Dv34-HA)attP40/CyO; osk[0.EGFP]/TM3 Sb[1]*	This paper	N/A
y[1] sc v[1]; P{y[+] v[+]=(Dm13Dv24-HA)attP40/CyO; osk[0.EGFP]/TM3 Sb[1]*	This paper	N/A
y[1] sc v[1]; P{y[+] v[+]=(Dm23Dv14-HA)attP40/CyO; osk[0.EGFP]/TM3 Sb[1]*	This paper	N/A
y[1] sc v[1]; P{y[+] v[+]=(Dm1Dv234-HA)attP40/CyO; osk[0.EGFP]/TM3 Sb[1]*	This paper	N/A
y[1] sc v[1]; P{y[+] v[+]=(Dm3Dv124-HA)attP40/CyO; osk[0.EGFP]/TM3 Sb[1]*	This paper	N/A
y[1] sc v[1]; P{y[+] v[+]=(Dm2Dv134-HA)attP40/CyO; osk[0.EGFP]/TM3 Sb[1]*	This paper	N/A
y[1] sc v[1]; P{y[+] v[+]=(Dm4Dv123-HA)attP40/CyO; osk[0.EGFP]/TM3 Sb[1]*	This paper	N/A
y[1] sc v[1]; P{y[+] v[+]=(Dm14Dv23-HA)attP40/CyO; osk[0.EGFP]/TM3 Sb[1]*	This paper	N/A
y[1] sc v[1]; P{y[+] v[+]=(Dm34Dv12-HA)attP40/CyO; osk[0.EGFP]/TM3 Sb[1]*	This paper	N/A
y[1] sc v[1]; P{y[+] v[+]=(Dm234Dv1-HA)attP40/CyO; osk[0.EGFP]/TM3 Sb[1]*	This paper	N/A
y[1] sc v[1]; P{y[+] v[+]=(Dm24Dv13-HA)attP40/CyO; osk[0.EGFP]/TM3 Sb[1]*	This paper	N/A
y[1] sc v[1]; P{y[+] v[+]=(Dm124Dv3-HA)attP40/CyO; osk[0.EGFP]/TM3 Sb[1]*	This paper	N/A
y[1] sc v[1]; P{y[+] v[+]=(Dm134Dv2-HA)attP40/CyO; osk[0.EGFP]/TM3 Sb[1]*	This paper	N/A
w[1118]; Kr[If-1]/CyO; TI{w[+mC]=TI}osk[0.EGFP]/TM3, Ser[1]	Bloomington Drosophila Stock Center	BDSC 67407
vas[PH165]/CyO; Dr/TM3	Laboratory of Paul Lasko, McGill University, Canada	N/A
Df(2L)b87e25/CyO	Bloomington Drosophila Stock Center	BDSC 3138
Sco/CyO; osk-GFP[KI]/TM6B	Laboratory of Graydon Gonsalvez, Augusta University, USA	

bioRxiv preprint doi: https://doi.org/10.1101/2025.08.02.668269; this version posted November 10, 2026. The copyright holder for this preprint (which was not certified by peer review) is the author/funder, who has granted bioRxiv a license to display the preprint in perpetuity. It is made available under a CC-BY 4.0 International license.

D. melanogaster (*Oregon R*)	Laboratory of Cassandra Extavour	N/A
D. virilis	Gift from Rainbow Transgenics	N/A
Oligonucleotides		
Primers for cloning chimeras, see Table S14	This paper	N/A
Recombinant DNA		
pVAL22_Dm1234-HA	This paper	N/A
pVAL22_Dv1234-HA	This paper	N/A
pVAL22_Dm123Dv4-HA	This paper	N/A
pVAL22_Dm12Dv34-HA	This paper	N/A
pVAL22_Dm13Dv24-HA	This paper	N/A
pVAL22_Dm23Dv14-HA	This paper	N/A
pVAL22_Dm1Dv234-HA	This paper	N/A
pVAL22_Dm3Dv124-HA	This paper	N/A
pVAL22_Dm2Dv134-HA	This paper	N/A
pVAL22_Dm4Dv123-HA	This paper	N/A
pVAL22_Dm14Dv23-HA	This paper	N/A
pVAL22_Dm34Dv12-HA	This paper	N/A
pVAL22_Dm234Dv1-HA	This paper	N/A
pVAL22_Dm24Dv13-HA	This paper	N/A
pVAL22_Dm124Dv3-HA	This paper	N/A
pVAL22_Dm134Dv2-HA	This paper	N/A
pVALIUM22	Drosophila Genomics Resource Center	Cat# 1468
D. melanogaster oskar genomic locus	Laboratory of Anne Ephrussi	GenBank Acc. No. AE014297
D. virilis oskar genomic locus	Laboratory of Paul Macdonald	GenBank Acc. No. L22556
Software and algorithms		
Fiji	Schindelin et al.[107]	https://imagej.net/software/fiji/
Anaconda Python Distribution	Anaconda	https://www.anaconda.com/
Helicon Focus (v. 8.2.2)	HeliconSoft Limited	https://www.heliconsoft.com/heliconsoft-products/helicon-focus/
AliView	Larsson[111]	https://ormbunkar.se/aliview/#DOWNLOAD
PyMOL	Schrödinger	https://www.pymol.org/
GPSite	Biomedical HPC+AI Platform	https://bio-web1.nscc-gz.cn/app/GPSite
Other		

bioRxiv preprint doi: https://doi.org/10.1101/2025.08.02.668269; this version posted November 10, 2026. The copyright holder for this preprint (which was not certified by peer review) is the author/funder, who has granted bioRxiv a license to display the preprint in perpetuity. It is made available under a CC-BY 4.0 International license.

Nikon CSU-W1 SoRA	Nikon	N/A
Zeiss AxioImager	Zeiss	N/A
Trans-Blot Turbo Transfer System	Bio-Rad	Cat# 1704150
Sapphire Biomolecular Imager	Azure	N/A

bioRxiv preprint doi: https://doi.org/10.1101/2025.08.02.668269; this version posted November 10, 2026. The copyright holder for this preprint (which was not certified by peer review) is the author/funder, who has granted bioRxiv a license to display the preprint in perpetuity. It is made available under a CC-BY 4.0 International license.

Data Availability

Further information and requests for resources and reagents should be directed to and will be fulfilled by the lead contact, Cassandra G. Extavour (extavour@oeb.harvard.edu).

Antibodies and fly strains developed for this study are available upon request. Source Data are provided with this paper in the associated file **dmdv_chim_rawdata.xlsx**.

Code Availability

Custom scripts used for data analysis are available at https://github.com/erivard/dmdv_osk_chimera.git (commit ID e92a908).

bioRxiv preprint doi: https://doi.org/10.1101/2025.08.02.668269; this version posted November 10, 2026. The copyright holder for this preprint (which was not certified by peer review) is the author/funder, who has granted bioRxiv a license to display the preprint in perpetuity. It is made available under a CC-BY 4.0 International license.

References

1. Veraksa, A., Campo, M. D. & McGinnis, W. Developmental Patterning Genes and Their Conserved Functions: From Model Organisms to Humans. *Mol. Genet. Metab.* **69**, 85–100 (2000).

2. Ponting, C. P. Biological function in the twilight zone of sequence conservation. *BMC Biol.* **15**, 71 (2017).

3. Sanetra, M., Begemann, G., Becker, M.-B. & Meyer, A. Conservation and co-option in developmental programmes: the importance of homology relationships. *Front Zool* **2**, 15 (2005).

4. Cutter, A. D., Garrett, R. H., Mark, S., Wang, W. & Sun, L. Molecular evolution across developmental time reveals rapid divergence in early embryogenesis. *Evol. Lett.* **3**, 359–373 (2019).

5. Lee, Y. C. G. *et al.* Rapid Evolution of Gained Essential Developmental Functions of a Young Gene via Interactions with Other Essential Genes. *Mol. Biol. Evol.* **36**, 2212–2226 (2019).

6. Ahuja, A. & Extavour, C. G. Patterns of molecular evolution of the germ line specification gene oskar suggest that a novel domain may contribute to functional divergence in Drosophila. *Dev. Genes Evol.* **224**, 65–77 (2014).

7. Whittle, C. A. & Extavour, C. G. Contrasting patterns of molecular evolution in metazoan germ line genes. *BMC Evol. Biol.* **19**, 53 (2019).

8. McGregor, A. P. *et al.* Morphological evolution through multiple cis-regulatory mutations at a single gene. *Nature* **448**, 587–90 (2007).

9. Reed, R. D. *et al.* optix drives the repeated convergent evolution of butterfly wing pattern mimicry. *Science* **333**, 1137–41 (2011).

10. Gompel, N., Prud'homme, B., Wittkopp, P. J., Kassner, V. A. & Carroll, S. B. Chance caught on the wing: cis-regulatory evolution and the origin of pigment patterns in Drosophila. *Nature* **433**, 481–7 (2005).

11. Méndez-González, I. D., Williams, T. M. & Rebeiz, M. Changes in locus wide repression underlie the evolution of Drosophila abdominal pigmentation. *PLOS Genet.* **19**, e1010722 (2023).

12. Hoekstra, H. E., Hirschmann, R. J., Bundey, R. A., Insel, P. A. & Crossland, J. P. A single amino acid mutation contributes to adaptive beach mouse color pattern. *Science* **313**, 101–4 (2006).

bioRxiv preprint doi: https://doi.org/10.1101/2025.08.02.668269; this version posted November 10, 2026. The copyright holder for this preprint (which was not certified by peer review) is the author/funder, who has granted bioRxiv a license to display the preprint in perpetuity. It is made available under a CC-BY 4.0 International license.

13. Ronshaugen, M., McGinnis, N. & McGinnis, W. Hox protein mutation and macroevolution of the insect body plan. *Nature* **415**, 914–7 (2002).

14. Protas, M. E. *et al.* Genetic analysis of cavefish reveals molecular convergence in the evolution of albinism. *Nat. Genet.* **38**, 107–11 (2006).

15. Kowarsch, A., Fuchs, A., Frishman, D. & Pagel, P. Correlated Mutations: A Hallmark of Phenotypic Amino Acid Substitutions. *PLoS Comput. Biol.* **6**, e1000923 (2010).

16. Guo, H. H., Choe, J. & Loeb, L. A. Protein tolerance to random amino acid change. *Proc. Natl. Acad. Sci.* **101**, 9205–9210 (2004).

17. Rey, C. *et al.* Detecting adaptive convergent amino acid evolution. *Philos. Trans. R. Soc. B* **374**, 20180234 (2019).

18. Ewen-Campen, B., Schwager, E. E. & Extavour, C. G. M. The molecular machinery of germ line specification. *Mol. Reprod. Dev.* **77**, 3–18 (2010).

19. Fierro-Constaín, L. *et al.* The Conservation of the Germline Multipotency Program, from Sponges to Vertebrates: A Stepping Stone to Understanding the Somatic and Germline Origins. *Genome Biol. Evol.* **9**, evw289 (2017).

20. Blondel, L., Besse, S., Rivard, E. L., Ylla, G. & Extavour, C. G. Evolution of a cytoplasmic determinant: Evidence for the biochemical basis of functional evolution of the novel germ line regulator Oskar. *Mol. Biol. Evol.* **38**, 5491–5513 (2021).

21. Ross, A. Insect Evolution: The Origin of Wings. *Curr. Biol.* **27**, R113–R115 (2017).

22. Ephrussi, A. & Lehmann, R. Induction of germ cell formation by oskar. *Nature* **358**, 387–392 (1992).

23. Kistler, K. E. *et al.* Phase transitioned nuclear Oskar promotes cell division of Drosophila primordial germ cells. *eLife* **7**, e37949 (2018).

24. Jeske, M. *et al.* The Crystal Structure of the Drosophila Germline Inducer Oskar Identifies Two Domains with Distinct Vasa Helicase- and RNA-Binding Activities. *Cell Rep.* **12**, 587–598 (2015).

25. Yang, N. *et al.* Structure of Drosophila Oskar reveals a novel RNA binding protein. *Proc. Natl. Acad. Sci.* **112**, 11541–11546 (2015).

26. Repouliou, A., Srouji, J. R., Rivard, E. L., Leschziner, A. E. & Extavour, C. G. The LOTUS domain of Oskar promotes localisation of both protein and mRNA components of Drosophila germ plasm. *bioRxiv* 2025.05.02.651258 (2025) doi:10.1101/2025.05.02.651258.

bioRxiv preprint doi: https://doi.org/10.1101/2025.08.02.668269; this version posted November 10, 2026. The copyright holder for this preprint (which was not certified by peer review) is the author/funder, who has granted bioRxiv a license to display the preprint in perpetuity. It is made available under a CC-BY 4.0 International license.

1169 27. Jeske, M., Müller, C. W. & Ephrussi, A. The LOTUS domain is a conserved DEAD-box
1170 RNA helicase regulator essential for the recruitment of Vasa to the germ plasm and nuage. *Genes*
1171 *Dev.* **31**, 939–952 (2017).

1172 28. Breitwieser, W., Markussen, F. H., Horstmann, H. & Ephrussi, A. Oskar protein interaction
1173 with Vasa represents an essential step in polar granule assembly. *Genes Dev.* **10**, 2179–2188
1174 (1996).

1175 29. Schüpbach, T. & Wieschaus, E. Maternal-effect mutations altering the anterior-posterior
1176 pattern of the Drosophila embryo. *Roux's Arch. Dev. Biol.* **195**, 302–317 (1986).

1177 30. Curnutte, H. A. *et al.* Proteins rather than mRNAs regulate nucleation and persistence of
1178 Oskar germ granules in Drosophila. *Cell Rep.* **42**, 112723 (2023).

1179 31. Kubíková, J., Ubartaitė, G., Metz, J. & Jeske, M. Structural basis for binding of Drosophila
1180 Smaug to the GPCR Smoothened and to the germline inducer Oskar. *Proc. Natl. Acad. Sci.* **120**,
1181 e2304385120 (2023).

1182 32. Suyama, R., Jenny, A., Curado, S., Berkel, W. P. & Ephrussi, A. The actin-binding protein
1183 Lasp promotes Oskar accumulation at the posterior pole of the Drosophila embryo. *Development*
1184 **136**, 95–105 (2009).

1185 33. Anne, J. Targeting and Anchoring Tudor in the Pole Plasm of the Drosophila Oocyte. *PLoS*
1186 *ONE* **5**, e14362 (2010).

1187 34. Markussen, F. H., Michon, A. M., Breitwieser, W. & Ephrussi, A. Translational control of
1188 oskar generates short OSK, the isoform that induces pole plasm assembly. *Dev Camb Engl* **121**,
1189 3723–32 (1995).

1190 35. Hurd, T. R. *et al.* Long Oskar Controls Mitochondrial Inheritance in Drosophila
1191 melanogaster. *Dev Cell* **39**, 560–571 (2016).

1192 36. Vanzo, N. F. & Ephrussi, A. Oskar anchoring restricts pole plasm formation to the posterior
1193 of the Drosophila oocyte. *Development* **129**, 3705–3714 (2002).

1194 37. Vanzo, N., Oprins, A., Xanthakis, D., Ephrussi, A. & Rabouille, C. Stimulation of
1195 Endocytosis and Actin Dynamics by Oskar Polarizes the Drosophila Oocyte. *Dev Cell* **12**, 543–
1196 555 (2007).

1197 38. Tanaka, T. & Nakamura, A. The endocytic pathway acts downstream of Oskar in Drosophila
1198 germ plasm assembly. *Development* **135**, 1107–1117 (2008).

1199 39. Chang, C.-W. *et al.* Anterior–posterior axis specification in Drosophila oocytes:
1200 identification of novel bicoid and oskar mRNA localization factors. *Genetics* **188**, 883–896
1201 (2011).

bioRxiv preprint doi: https://doi.org/10.1101/2025.08.02.668269; this version posted November 10, 2026. The copyright holder for this preprint (which was not certified by peer review) is the author/funder, who has granted bioRxiv a license to display the preprint in perpetuity. It is made available under a CC-BY 4.0 International license.

1202 40. Tanaka, T., Kato, Y., Matsuda, K., Hanyu-Nakamura, K. & Nakamura, A. Drosophila Mon2
1203 couples Oskar-induced endocytosis with actin remodeling for cortical anchorage of the germ
1204 plasm. *Development* **138**, 2523–2532 (2011).

1205 41. Jones, J. R. & Macdonald, P. M. Oskar controls morphology of polar granules and nuclear
1206 bodies in Drosophila. *Development* **134**, 233–236 (2007).

1207 42. Webster, P. J., Suen, J. & .Macdonald, P. M. Drosophila virilis oskar transgenes direct body
1208 patterning but not pole cell formation or maintenance of mRNA localization in D. melanogaster.
1209 *Development* **120**, 2027–2037 (1994).

1210 43. Russo, C. A. M., Mello, B., Frazão, A. & Voloch, C. M. Phylogenetic analysis and a time
1211 tree for a large drosophilid data set (Diptera: Drosophilidae). *Zoöl. J. Linn. Soc.* **169**, 765–775
1212 (2013).

1213 44. Doyle, D. A. *et al.* Germ Granule Evolution Provides Mechanistic Insight into Drosophila
1214 Germline Development. *Mol. Biol. Evol.* **40**, msad174 (2023).

1215 45. Gavis, E. R., Curtis, D. & Lehmann, R. Identification of cis-Acting Sequences That Control
1216 nanos RNA Localization. *Dev. Biol.* **176**, 36–50 (1996).

1217 46. Curtis, D., Apfeld, J. & Lehmann, R. nanos is an evolutionarily conserved organizer of
1218 anterior-posterior polarity. *Dev Camb Engl* **121**, 1899–910 (1995).

1219 47. Rangan, P. *et al.* Temporal and spatial control of germ-plasm RNAs. *Curr Biology Cb* **19**,
1220 72–7 (2008).

1221 48. Eagle, W. V. I., Yeboah-Kordieh, D. K., Niepielko, M. G. & Gavis, E. R. Distinct cis-acting
1222 elements mediate targeting and clustering of Drosophila polar granule mRNAs. *Development*
1223 **145**, dev.164657 (2018).

1224 49. Abramson, J. *et al.* Accurate structure prediction of biomolecular interactions with
1225 AlphaFold 3. *Nature* **630**, 493–500 (2024).

1226 50. Hachet, O. & Ephrussi, A. Splicing of oskar RNA in the nucleus is coupled to its cytoplasmic
1227 localization. *Nature* **428**, 959–963 (2004).

1228 51. Jambor, H., Brunel, C. & Ephrussi, A. Dimerization of oskar 3′ UTRs promotes hitchhiking
1229 for RNA localization in the Drosophila oocyte. *Rna* **17**, 2049–2057 (2011).

1230 52. Bose, M., Rankovic, B., Mahamid, J. & Ephrussi, A. An architectural role of specific RNA–
1231 RNA interactions in oskar granules. *Nat. Cell Biol.* **26**, 1934–1942 (2024).

1232 53. Kenny, A., Morgan, M. B., Mohr, S. & Macdonald, P. M. Knock down analysis reveals
1233 critical phases for specific oskar noncoding RNA functions during Drosophila oogenesis. *G3* **11**,
1234 jkab340 (2021).

bioRxiv preprint doi: https://doi.org/10.1101/2025.08.02.668269; this version posted November 10, 2026. The copyright holder for this preprint (which was not certified by peer review) is the author/funder, who has granted bioRxiv a license to display the preprint in perpetuity. It is made available under a CC-BY 4.0 International license.

54. Jenny, A. *et al.* A translation-independent role of oskar RNA in early Drosophila oogenesis. *Development* **133**, 2827–2833 (2006).

55. Gáspár, I., Sysoev, V., Komissarov, A. & Ephrussi, A. An RNA -binding atypical tropomyosin recruits kinesin-1 dynamically to oskar mRNP s. *EMBO J.* **36**, 319–333 (2017).

56. Lasko, P. F. & Ashburner, M. Posterior localization of vasa protein correlates with, but is not sufficient for, pole cell development. *Genes Dev.* **4**, 905–921 (1990).

57. Hay, B., Jan, L. Y. & Jan, Y. N. Localization of vasa, a component of Drosophila polar granules, in maternal-effect mutants that alter embryonic anteroposterior polarity. *Development* **109**, 425–433 (1990).

58. Robertson, S. E., Dockendorff, T. C., Leatherman, J. L., Faulkner, D. L. & Jongens, T. A. germ cell-less is required only during the establishment of the germ cell lineage of,Drosophila and has activities which are dependent and independent of its localization to the nuclear envelope. *Dev. Biol.* **215**, 288–297 (1999).

59. Lehmann, R. Germ Plasm Biogenesis - An Oskar-Centric Perspective. *Curr. Top. Dev. Biol.* **116**, 679–707 (2016).

60. Nüsslein-Volhard, C. Maternal effect mutations that alter the spatial coordinates of the embryo of Drosophila melanogaster. in 185–211 (Academic Press, New York, 1979).

61. Mohler, J. & Wieschaus, E. F. Bicaudal Mutations of Drosophila melanogaster: Alteration of Blastoderm Cell Fate. *Cold Spring Harb. Symp. Quant. Biol.* **50**, 105–111 (1985).

62. Nüsslein-Volhard, C. & Wieschaus, E. Mutations affecting segment number and polarity in Drosophila. *Nature* **287**, 795–801 (1980).

63. Bull, A. L. Bicaudal, a genetic factor which affects the polarity of the embryo in Drosophila melanogaster. *J Exp Zool* **161**, 221–241 (1966).

64. Mohler, J. & Wieschaus, E. F. Dominant maternal-effect mutations of Drosophila melanogaster causing the production of double-abdomen embryos. *Genetics* **112**, 803–22 (1986).

65. Nüsslein-Volhard, C. Genetic analysis of pattern-formation in the embryo of Drosophila melanogaster. *Wilhelm Roux's Arch. Dev. Biol.* **183**, 249–268 (1977).

66. Wang, C. & Lehmann, R. Nanos is the localized posterior determinant in Drosophila. *Cell* **66**, 637–647 (1991).

67. Zimyanin, V., Lowe, N. & Johnston, D. S. An Oskar-Dependent Positive Feedback Loop Maintains the Polarity of the Drosophila Oocyte. *Curr Biol* **17**, 353–359 (2007).

bioRxiv preprint doi: https://doi.org/10.1101/2025.08.02.668269; this version posted November 10, 2026. The copyright holder for this preprint (which was not certified by peer review) is the author/funder, who has granted bioRxiv a license to display the preprint in perpetuity. It is made available under a CC-BY 4.0 International license.

68. Dollar, G., Struckhoff, E., Michaud, J. & Cohen, R. S. Rab11 polarization of the Drosophila oocyte: a novel link between membrane trafficking, microtubule organization, and oskar mRNA localization and translation. *Development* **129**, 517–526 (2002).

69. Wu, Y. & Griffin, E. E. Chapter Eleven Regulation of Cell Polarity by PAR-1/MARK Kinase. *Curr. Top. Dev. Biol.* **123**, 365–397 (2017).

70. Doerflinger, H., Benton, R., Torres, I. L., Zwart, M. F. & Johnston, D. S. Drosophila Anterior-Posterior Polarity Requires Actin-Dependent PAR-1 Recruitment to the Oocyte Posterior. *Curr Biol* **16**, 1090–1095 (2006).

71. Tian, A.-G. & Deng, W.-M. Par-1 and Tau regulate the anterior–posterior gradient of microtubules in Drosophila oocytes. *Dev Biol* **327**, 458–464 (2009).

72. Shulman, J. M., Benton, R. & Johnston, D. S. The Drosophila Homolog of C. elegans PAR-1 Organizes the Oocyte Cytoskeleton and Directs oskar mRNA Localization to the Posterior Pole. *Cell* **101**, 377–388 (2000).

73. Doerflinger, H., Benton, R., Shulman, J. M. & Johnston, D. S. The role of PAR-1 in regulating the polarised microtubule cytoskeleton in the Drosophila follicular epithelium. *Development* **130**, 3965–3975 (2003).

74. Cox, D. N., Lu, B., Sun, T.-Q., Williams, L. T. & Jan, Y. N. Drosophila par-1 is required for oocyte differentiation and microtubule organization. *Curr Biol* **11**, 75–87 (2001).

75. Riechmann, V., Gutierrez, G. J., Filardo, P., Nebreda, A. R. & Ephrussi, A. Par-1 regulates stability of the posterior determinant Oskar by phosphorylation. *Nat Cell Biol* **4**, 337–342 (2002).

76. Vaccari, T. & Ephrussi, A. The Fusome and Microtubules Enrich Par-1 in the Oocyte, Where It Effects Polarization in Conjunction with Par-3, BicD, Egl, and Dynein. *Curr Biol* **12**, 1524–1528 (2002).

77. Eddy, E. M. Germ Plasm and the Differentiation of the Germ Cell Line. *International Review of Cytology* **43**, 229–280 (1975).

78. Hegner, R. W. *The Germ Cell Cycle in Animals*. (The Macmillan Company, New York, 1914).

79. Counce, S. J. Developmental morphology of polar granules in Drosophila. Including observations on pole cell behavior and distribution during embryogenesis. *J. Morphol.* **112**, 129–145 (1963).

80. Mahowald, A. P. Polar granules of Drosophila. II. Ultrastructural changes during early embryogenesis. *J. Exp. Zool.* **167**, 237–261 (1968).

bioRxiv preprint doi: https://doi.org/10.1101/2025.08.02.668269; this version posted November 10, 2026. The copyright holder for this preprint (which was not certified by peer review) is the author/funder, who has granted bioRxiv a license to display the preprint in perpetuity. It is made available under a CC-BY 4.0 International license.

1298 81. Mahowald, A. P. Polar granules of Drosophila. III. The continuity of polar granules during
1299 the life cycle of Drosophila. *J Exp Zool* **176**, 329–343 (1971).

1300 82. Mahowald, A. P. Polar granules of Drosophila. IV. Cytochemical studies showing loss of
1301 RNA from polar granules during early stages of embryogenesis. *J Exp Zool* **176**, 345–352
1302 (1971).

1303 83. Mahowald, A. P. Fine structure of pole cells and polar granules in Drosophila melanogaster.
1304 *J. Exp. Zool.* **151**, 201–215 (1962).

1305 84. Yuan, Q., Tian, C. & Yang, Y. Genome-scale annotation of protein binding sites via
1306 language model and geometric deep learning. *eLife* **13**, RP93695 (2024).

1307 85. Trcek, T. *et al.* Drosophila germ granules are structured and contain homotypic mRNA
1308 clusters. *Nat. Commun.* **6**, 7962 (2015).

1309 86. Chen, R., Stainier, W., Dufourt, J., Lagha, M. & Lehmann, R. Direct observation of
1310 translational activation by a ribonucleoprotein granule. *Nat. Cell Biol.* **26**, 1322–1335 (2024).

1311 87. Ephrussi, A., Dickinson, L. K. & Lehmann, R. oskar organizes the germ plasm and directs
1312 localization of the posterior determinant nanos. *Cell* **66**, 37–50 (1991).

1313 88. Irish, V., Lehmann, R. & Akam, M. The Drosophila posterior-group gene nanos functions by
1314 repressing hunchback activity. *Nature* **338**, 646–648 (1989).

1315 89. Lehmann, R. & Nüsslein-Volhard, C. The maternal gene nanos has a central role in posterior
1316 pattern formation of the Drosophila embryo. *Development* **112**, 679–691 (1991).

1317 90. Deshpande, G., Calhoun, G., Yanowitz, J. L. & Schedl, P. D. Novel Functions of nanos in
1318 Downregulating Mitosis and Transcription during the Development of the Drosophila Germline.
1319 *Cell* **99**, 271–281 (1999).

1320 91. Forbes, A. & Lehmann, R. Nanos and Pumilio have critical roles in the development and
1321 function of Drosophila germline stem cells. *Development* **125**, 679–690 (1998).

1322 92. Sato, K. *et al.* Maternal Nanos represses hid/skl-dependent apoptosis to maintain the germ
1323 line in Drosophila embryos. *Proc National Acad Sci* **104**, 7455–7460 (2007).

1324 93. Hayashi, Y., Hayashi, M. & Kobayashi, S. Nanos suppresses somatic cell fate in Drosophila
1325 germ line. *P Natl Acad Sci Usa* **101**, 10338–10342 (2004).

1326 94. Kilwein, M. D. *et al.* Formation of Drosophila germ cells requires spatial patterning of
1327 phospholipids. *Curr. Biol.* https://doi.org/10.1016/j.cub.2025.01.071 (2025)
1328 doi:10.1016/j.cub.2025.01.071.

bioRxiv preprint doi: https://doi.org/10.1101/2025.08.02.668269; this version posted November 10, 2026. The copyright holder for this preprint (which was not certified by peer review) is the author/funder, who has granted bioRxiv a license to display the preprint in perpetuity. It is made available under a CC-BY 4.0 International license.

95. Kilwein, M. D. *et al.* Dual control of PIP2 drives germline/soma segregation in Drosophila. *Proc. Natl. Acad. Sci.* **123**, e2604429123 (2026).

96. Lerit, D. A. & Gavis, E. R. Transport of germ plasm on astral microtubules directs germ cell development in Drosophila. *Curr. Biol.* **21**, 439–448 (2011).

97. Jongens, T. A., Ackerman, L. D., Swedlow, J. R., Jan, L. Y. & Jan, Y. N. Germ cell-less encodes a cell type-specific nuclear pore-associated protein and functions early in the germ-cell specification pathway of Drosophila. *Genes Dev.* **8**, 2123–2136 (1994).

98. Bonner, A. M. & Hawley, R. S. Functional Consequences of the Evolution of Matrimony, a Meiosis-Specific Inhibitor of Polo Kinase. *Mol. Biol. Evol.* **36**, 69–83 (2019).

99. Avila, S., Casero, M. C., Fernandez-Cantón, R. & Sastre, L. Transactivation domains are not functionally conserved between vertebrate and invertebrate serum response factors. *Eur. J. Biochem.* **269**, 3669–77 (2002).

100. Tanaka, T., Tani, N. & Nakamura, A. Receptor-mediated yolk uptake is required for oskar mRNA localization and cortical anchorage of germ plasm components in the Drosophila oocyte. *Plos Biol* **19**, e3001183 (2021).

101. Lynch, J. A. *et al.* The Phylogenetic Origin of oskar Coincided with the Origin of Maternally Provisioned Germ Plasm and Pole Cells at the Base of the Holometabola. *PLoS Genet.* **7**, e1002029 (2011).

102. Kulkarni, A. *et al.* oskar acts with the transcription factor Creb to regulate long-term memory in crickets. *Proc. Natl. Acad. Sci.* **120**, e2218506120 (2023).

103. Ewen-Campen, B., Srouji, J. R., Schwager, E. E. & Extavour, C. G. oskar Predates the Evolution of Germ Plasm in Insects. *Curr Biol* **22**, 2278–2283 (2012).

104. Lehmann, R. & Nüsslein-Volhard, C. Abdominal segmentation, pole cell formation, and embryonic polarity require the localized activity of oskar, a maternal gene in drosophila. *Cell* **47**, 141–152 (1986).

105. Wang, S.-C. *et al.* Germ plasm localisation of the HELICc of Vasa in Drosophila: analysis of domain sufficiency and amino acids critical for localisation. *Sci Rep-uk* **5**, 14703 (2015).

106. Sarikaya, D. P. *et al.* The roles of cell size and cell number in determining ovariole number in Drosophila. *Dev Biol* **363**, 279–289 (2012).

107. Schindelin, J. *et al.* Fiji: an open-source platform for biological-image analysis. *Nat. Methods* **9**, 676–82 (2012).

108. Stringer, C., Wang, T., Michaelos, M. & Pachitariu, M. Cellpose: a generalist algorithm for cellular segmentation. *Nat. Methods* **18**, 100–106 (2021).

bioRxiv preprint doi: https://doi.org/10.1101/2025.08.02.668269; this version posted November 10, 2026. The copyright holder for this preprint (which was not certified by peer review) is the author/funder, who has granted bioRxiv a license to display the preprint in perpetuity. It is made available under a CC-BY 4.0 International license.

109. Otsu, N. A threshold selection method from gray-level histograms. *IEEE Trans. Syst., Man, Cybern.* **9**, 62–66 (1979).

110. Rice, P., Longden, I. & Bleasby, A. EMBOSS: The European Molecular Biology Open Software Suite. *Trends Genet* **16**, 276–277 (2000).

111. Larsson, A. AliView: a fast and lightweight alignment viewer and editor for large datasets. *Bioinformatics* **30**, 3276–8 (2014).

Supplementary Material for

Protein sequence evolution underlies interspecies incompatibility of a cell fate determinant

Emily L. Rivard, John R. Srouji, Anastasia Repouliou, Cassandra G. Extavour

This document contains the following materials:

- Supplemental Figures S1 through S18
- Supplemental Tables S1 through S14
- Supplemental References

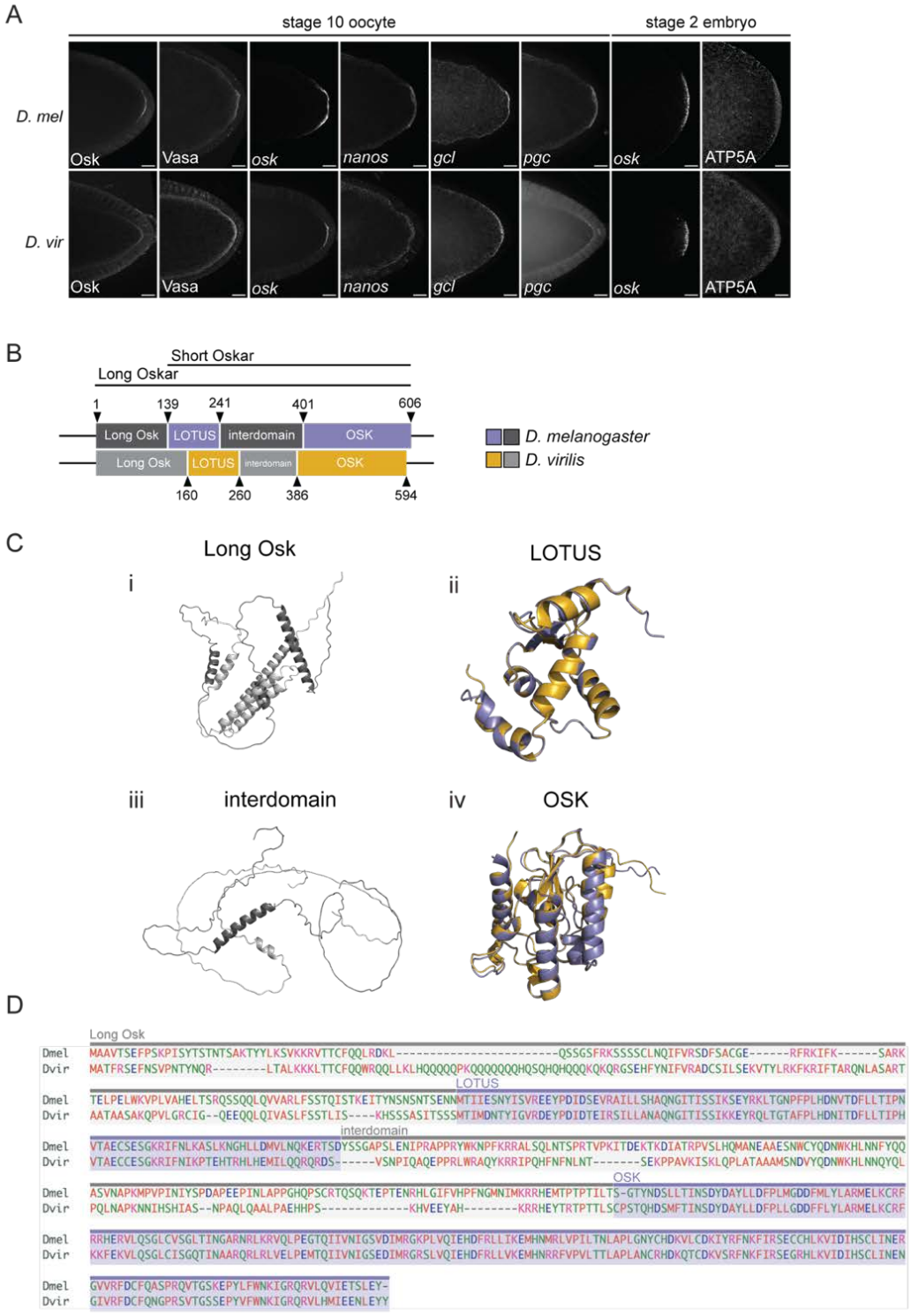


Figure S1. Comparison of germ plasm, Oskar structure and sequence between *D. melanogaster* and *D. virilis*. A) *D. melanogaster* (*D. mel*, top row) and *D. virilis* (*D. vir*, bottom row) stage 10 oocytes with Oskar, Vasa, *oskar*, *nanos*, *germ cell-less* (*gcl*), and *polar granule component* (*pgc*) labeled, and stage 2 embryos with *oskar* and mitochondria labeled (with anti-ATP5A antibody staining). All tissues are oriented with posterior to the right. Micrographs are maximum intensity projections of 20 optical sections (step size = 0.5 μm) and scale bars represent 20 μm. **B)** Schematic of *D. melanogaster* (top) and *D. virilis* (bottom) Oskar protein domain structures with amino acid residue number positions demarcating boundaries between domains. **C)** Individual *D. melanogaster* and *D. virilis* Oskar domain structural predictions generated with AlphaFold3 [1] and aligned in PyMOL (*D. melanogaster*: dark gray disordered regions, purple folded regions; *D. virilis*: light gray disordered regions, gold folded regions). **D)** Alignment of *D. melanogaster* and *D. virilis* Oskar protein sequences generated with MUSCLE. Domains shown in (**B**) are designated with colored background boxes.

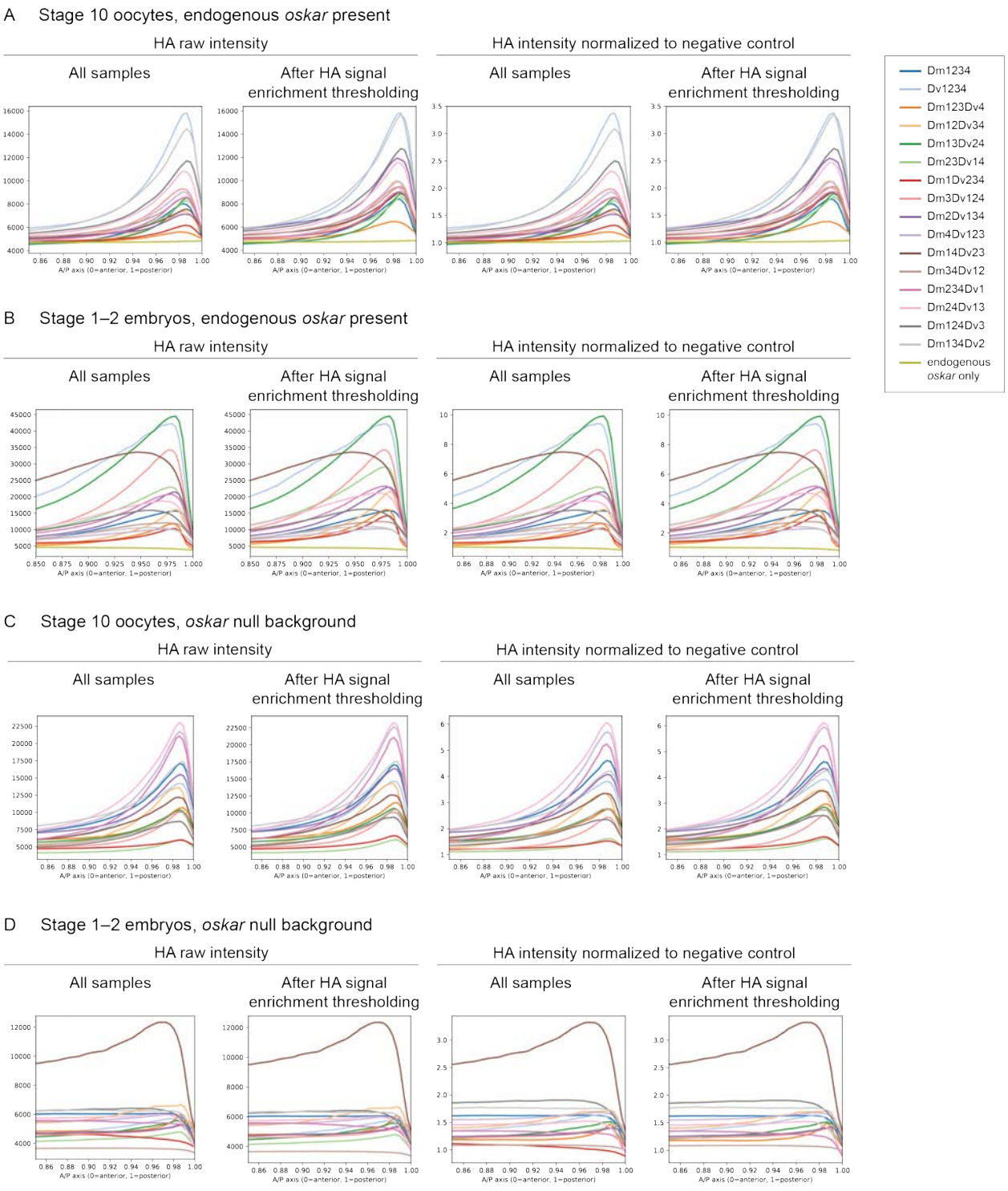
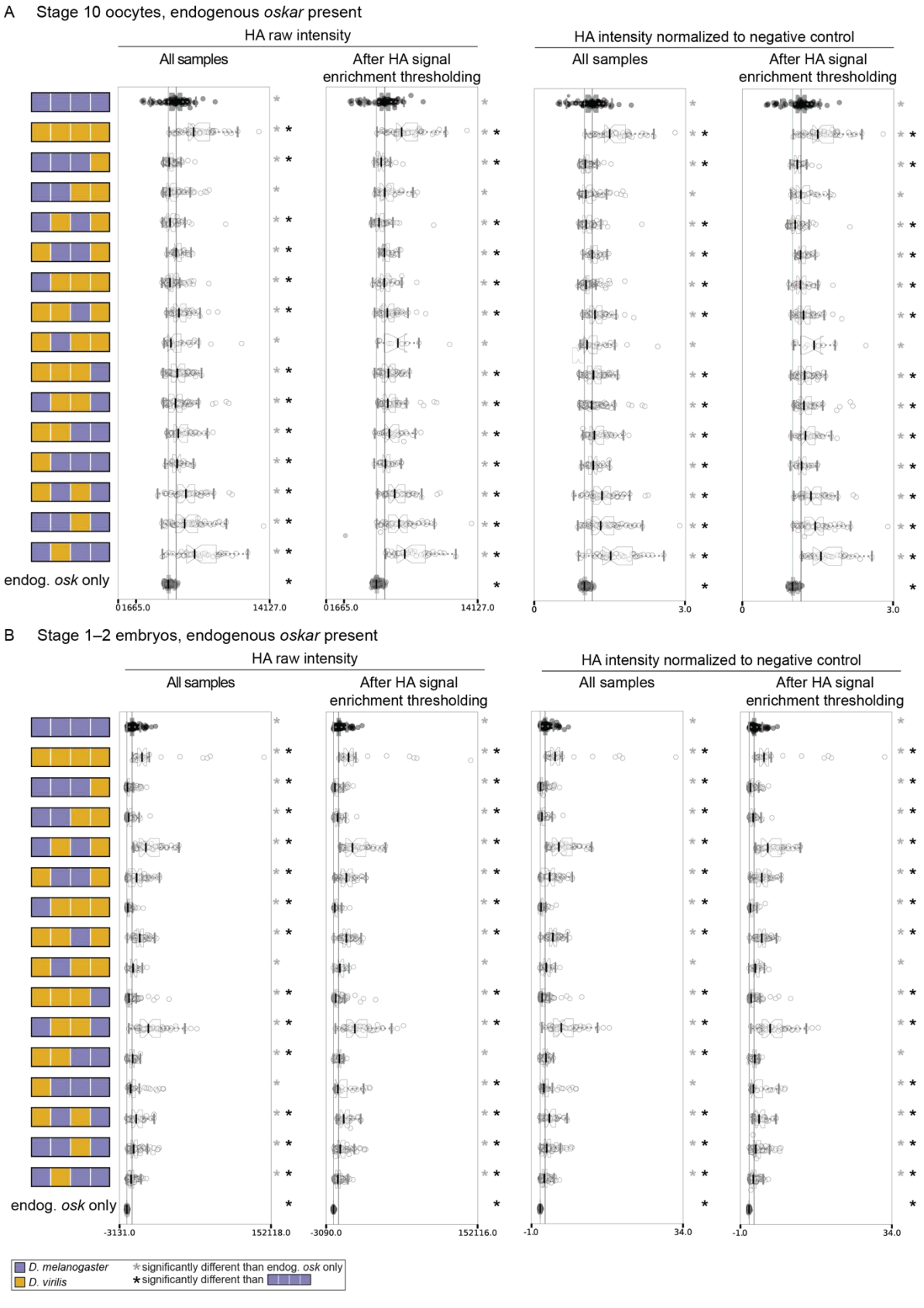


Figure S2. Line scans of posterior HA signal. A–D) Mean raw intensity (left) and intensity normalized to the average of negative control samples (right) are plotted for the posterior 15% of oocytes and embryos. Mean intensities are plotted for all samples that were included in the germ plasm enrichment analyses performed in this paper, based on thresholding for HA signal two standard deviations over the mean posterior signal for negative control samples. **A–B)** Negative control samples for normalization were samples expressing no transgene (endogenous *oskar* only). **C–D)** Negative control samples for normalization were embryos of the same genotype stained with no primary antibody. **A)** Stage 10 oocytes in a background with endogenous *oskar*. **B)** Stage 1–2 embryos in a background with endogenous *oskar*. **C)** Stage 10 oocytes in an *oskar* null background. **D)** Stage 1–2 embryos in an *oskar* null background.


A Stage 10 oocytes, endogenous oskar present
HA raw intensity
All samples
After HA signal enrichment thresholding
HA intensity normalized to negative control
All samples
After HA signal enrichment thresholding
endog. osk only
0
1665.0
14127.0
0
1665.0
14127.0
0
3.0
0
3.0
B Stage 1–2 embryos, endogenous oskar present
HA raw intensity
All samples
After HA signal enrichment thresholding
HA intensity normalized to negative control
All samples
After HA signal enrichment thresholding
endog. osk only
-3131.0
152118.0
-3090.0
152116.0
-1.0
34.0
-1.0
34.0
D. melanogaster
D. virilis
significantly different than endog. osk only
significantly different than

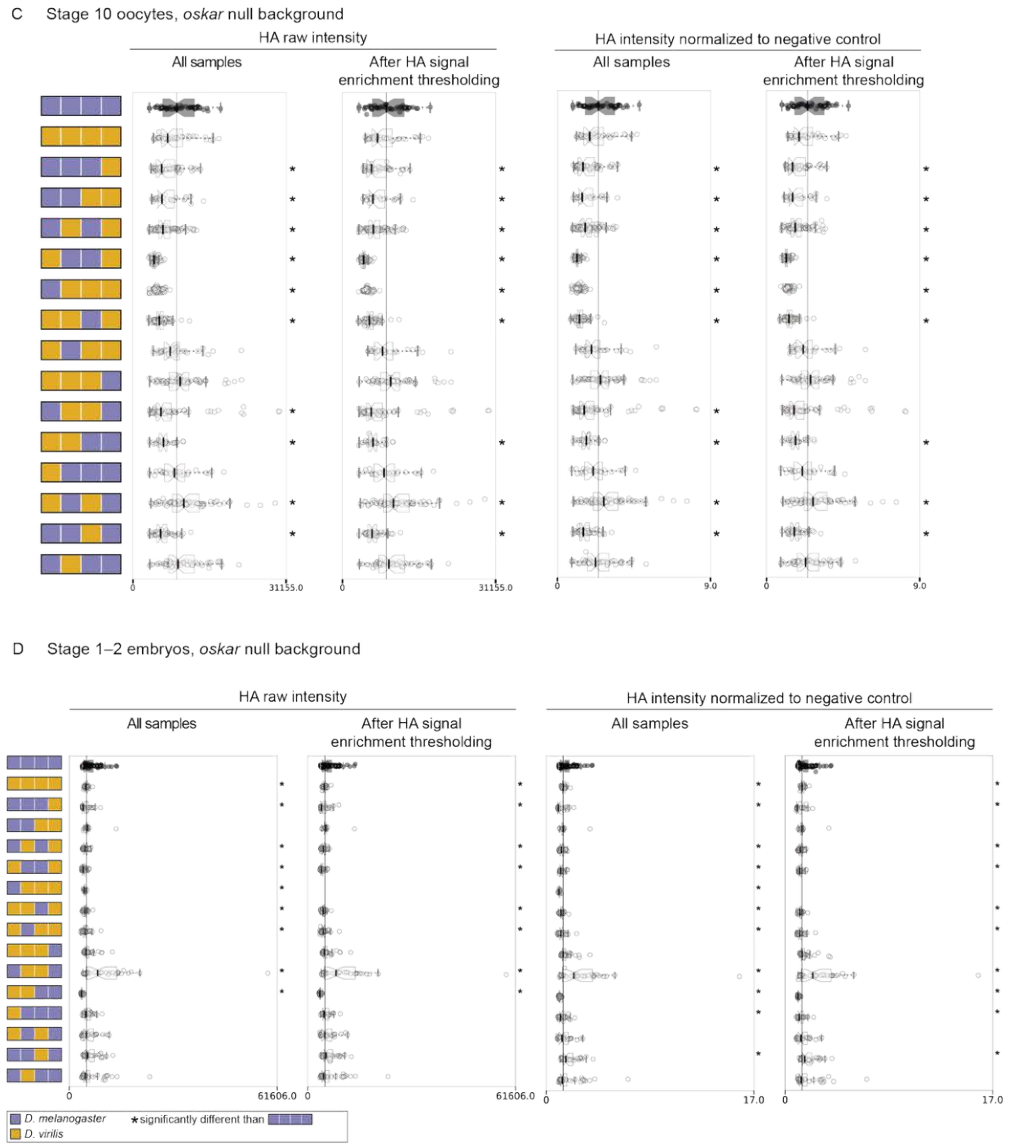


Figure S3. Box plot of integrated posterior HA signal. A–D) Integrated raw intensity (left) and intensity normalized to the average of negative control samples (right) are plotted for the posterior 15% of oocytes and embryos. Mean intensities are plotted for all samples that were included in the germ plasm enrichment analyses performed in this paper, included based on thresholding for HA signal two standard deviations over the mean posterior signal for negative control samples. **A–B)** Negative control samples for normalization were samples expressing no transgene (endogenous *oskar* only). **C–D)** Negative control samples for normalization were embryos of the same genotype stained with no primary antibody. **A)** Stage 10 oocytes in a background with endogenous *oskar*. **B)** Stage 1–2 embryos in a background with endogenous *oskar.* **C)** Stage 10 oocytes in an *oskar* null background. **D)** Stage 1–2 embryos in an *oskar* null background.

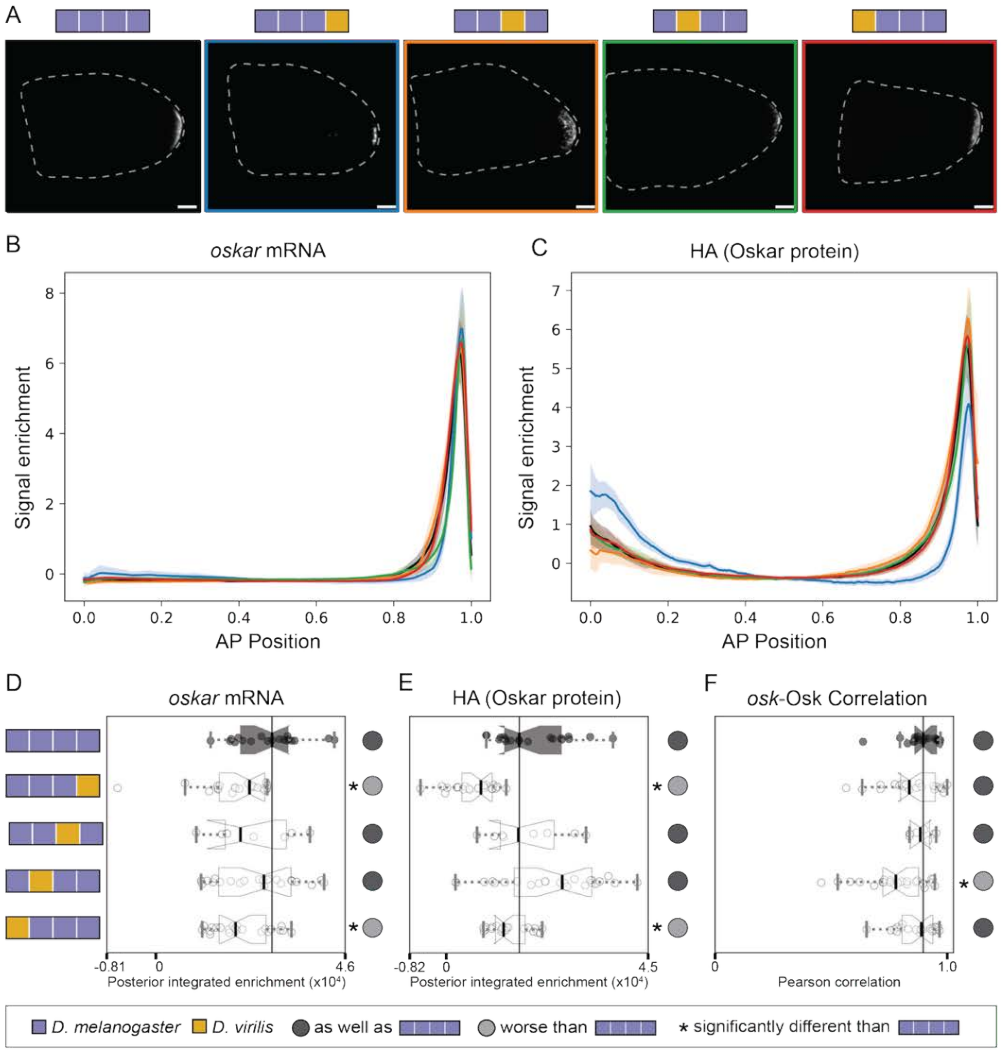
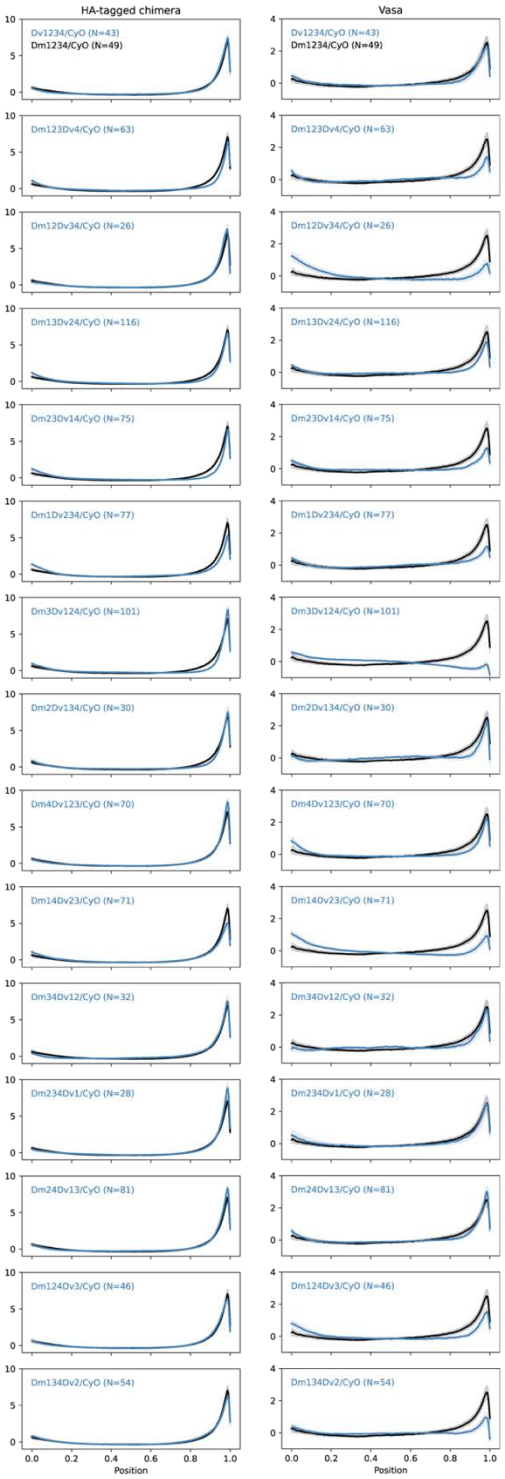


Figure S4. Chimeric *oskar* mRNA successfully localizes to the posterior during oogenesis. A) Representative images of oocytes from *D. melanogaster* mothers expressing chimeric Oskar sequences in an *oskar* RNA null background. HCR *in situ* hybridization marks the localization of the transgenic *oskar* mRNA. Images are oriented with posterior to the right. Micrographs are maximum intensity projections of 41 optical sections (step size = 1 μm) and scale bars = 20 μm. **B)** Line scans displaying *oskar* mRNA signal enrichment (z-score) across stage 10 oocytes. **C)** Line scans displaying HA (as a proxy for Oskar protein) signal enrichment (z-score) across stage 10 oocytes. For plots B) and C), on the X axis, 0 represents the anterior and 1 the posterior end of the oocyte. Mean (solid lines) and 95% confidence intervals (shaded regions) are shown. Line colors correspond to the chimeras shown in A). **D)** Posterior integrated enrichment of *oskar* mRNA in stage 10 oocytes from *D. melanogaster* mothers expressing chimeric Oskar proteins in an *oskar* RNA null background. **E)** Posterior integrated enrichment of HA (as a proxy for Oskar protein) in stage 10 oocytes from *D. melanogaster* mothers expressing chimeric Oskar proteins in an *oskar* RNA null background. **F)** Pearson correlation scores between intensities of the *oskar* mRNA and HA signals quantified in A) and B) respectively. For plots D-F), the distribution for eggs from flies expressing *D. melanogaster oskar* (positive control) is in black with the median marked with a black line. Significant difference from positive control distribution (p-value < 0.05, estimated from the distribution of difference of means between sample and control from 100,000 simulated samples) indicated by asterisk. Circles to the right of the plots indicate data interpretation as follows: dark gray = enriches the germ plasm molecule at least as well as *D. melanogaster oskar*; light gray = enriches the germ plasm molecule worse than *D. melanogaster oskar*. Sample sizes ≥8 for each condition; see Table S1.

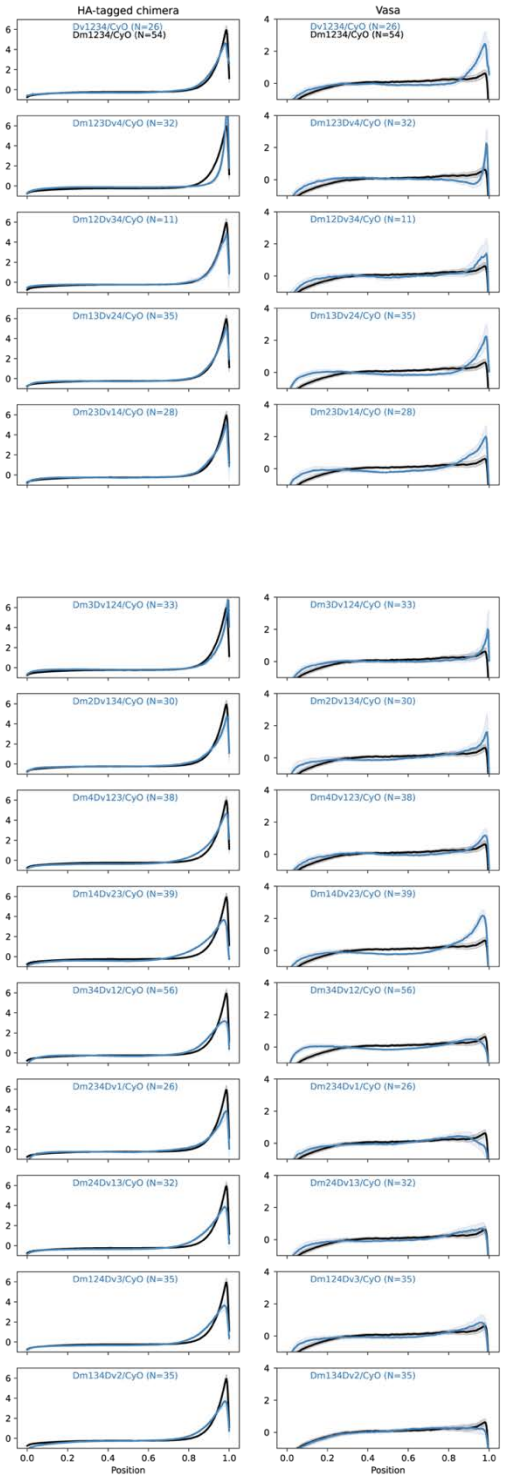
A

Stage 10 oocyte: Vasa
(null background)



B

Stage 1-2 embryo: Vasa
(null background)



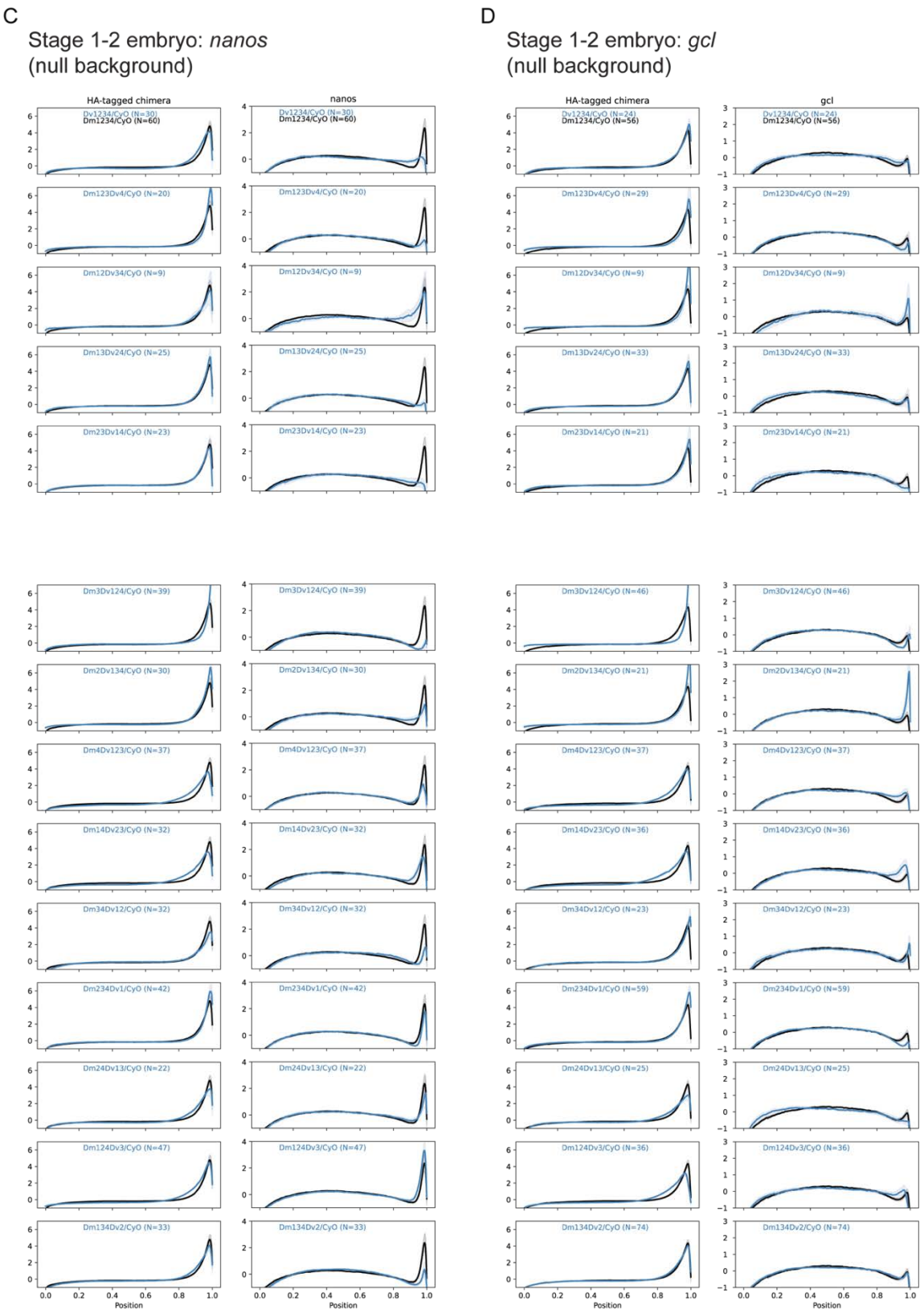
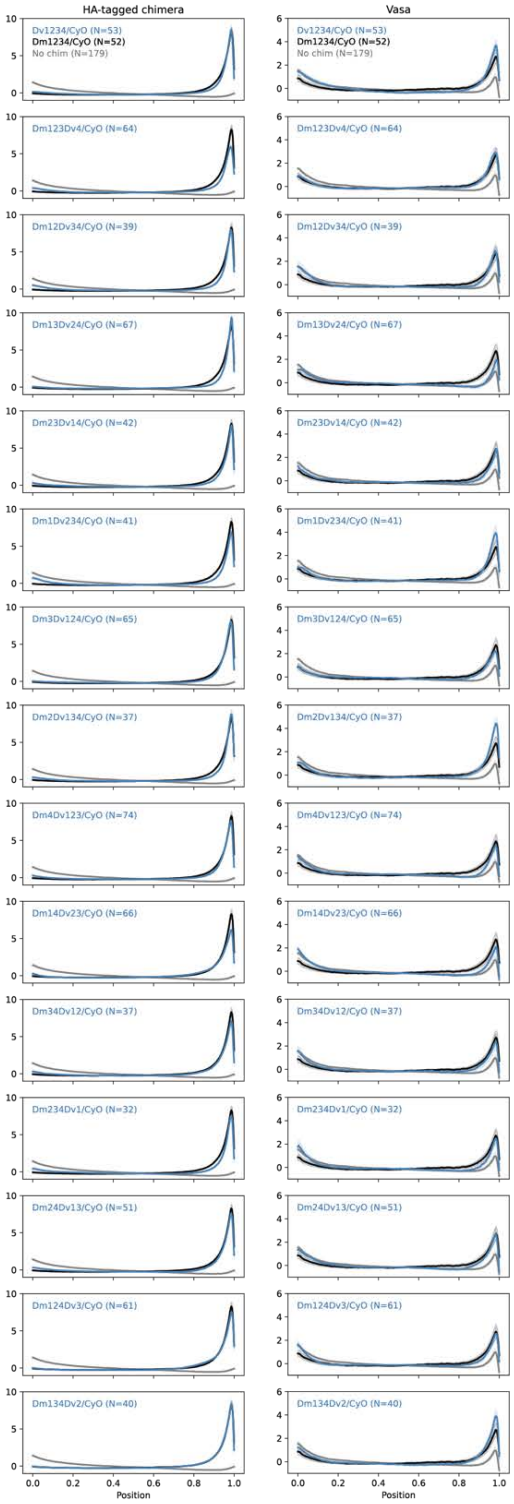


Figure S5. A, B) Vasa, **C)** *nanos,* and **D)** *gcl* signal enrichment (z-score) across stage 10 oocytes (A) and stage 1–2 embryos (B-D) in the *oskar* RNA null background *y[1] sc[*] v[1]; Kr[If-1]/CyO; TI{w[+mC]=TI}osk[0.EGFP]*. On the X axis, 0 designates the anterior and 1 the posterior. Mean (solid lines) and 95% confidence intervals (shaded regions) are shown. Black lines are measurements from positive control animals expressing the *D. melanogaster oskar* construct. Blue lines are measurements from each chimera genotype. Sample sizes for the measurements in each plot are noted in parentheses.

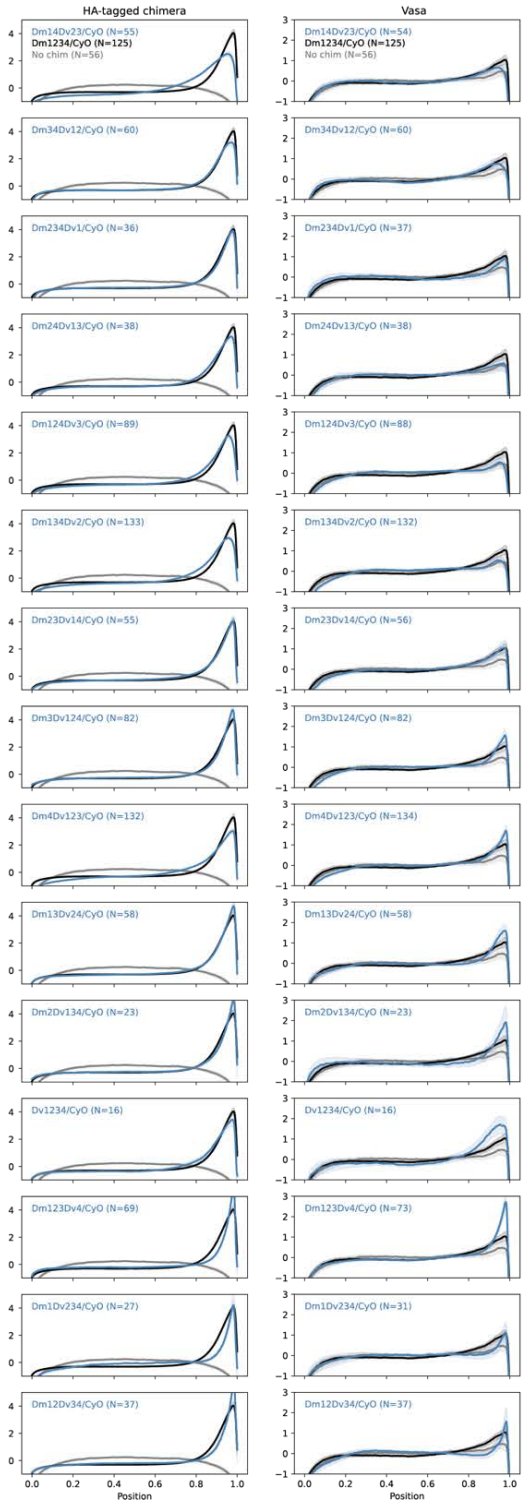
A

Stage 10 oocyte: Vasa
(endog. background)



B

Stage 1-2 embryo: Vasa
(endog. background)



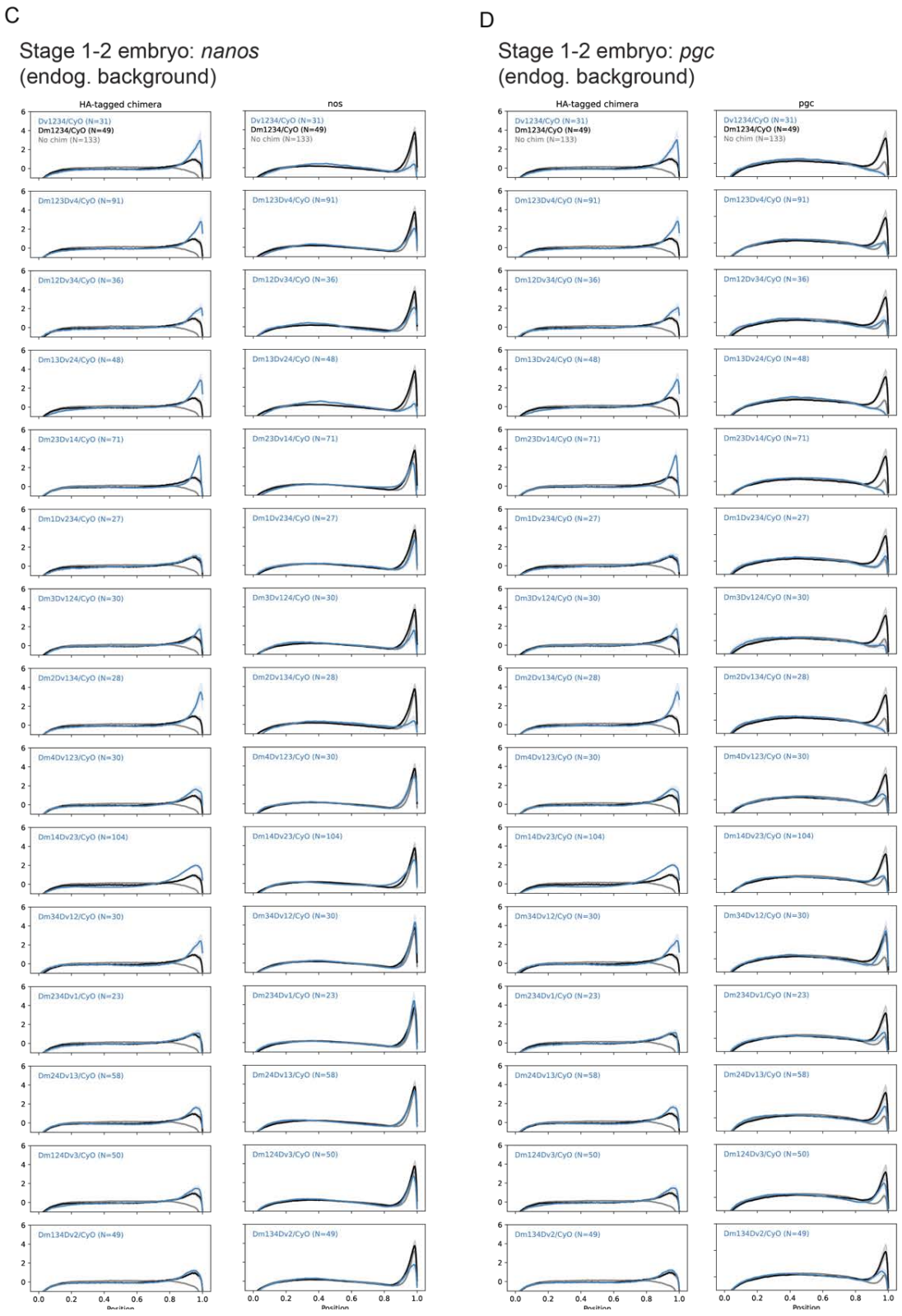


Figure S6. Vasa, *nanos,* and *pgc* signal enrichment (z-score) across stage 10 oocytes and stage 1–2 embryos for chimeras expressed in a background with endogenous *oskar*. On the X axis, 0 represents the anterior and 1 the posterior. Mean (solid lines) and 95% confidence intervals (shaded regions) are shown. Gray lines are measurements from flies not expressing a chimeric construct (only endogenous Oskar is expressed). Black lines are measurements from positive control animals expressing the *D. melanogaster oskar* construct. Blue lines are measurements from each chimera genotype. Sample sizes for the measurements in each plot are noted in parentheses.

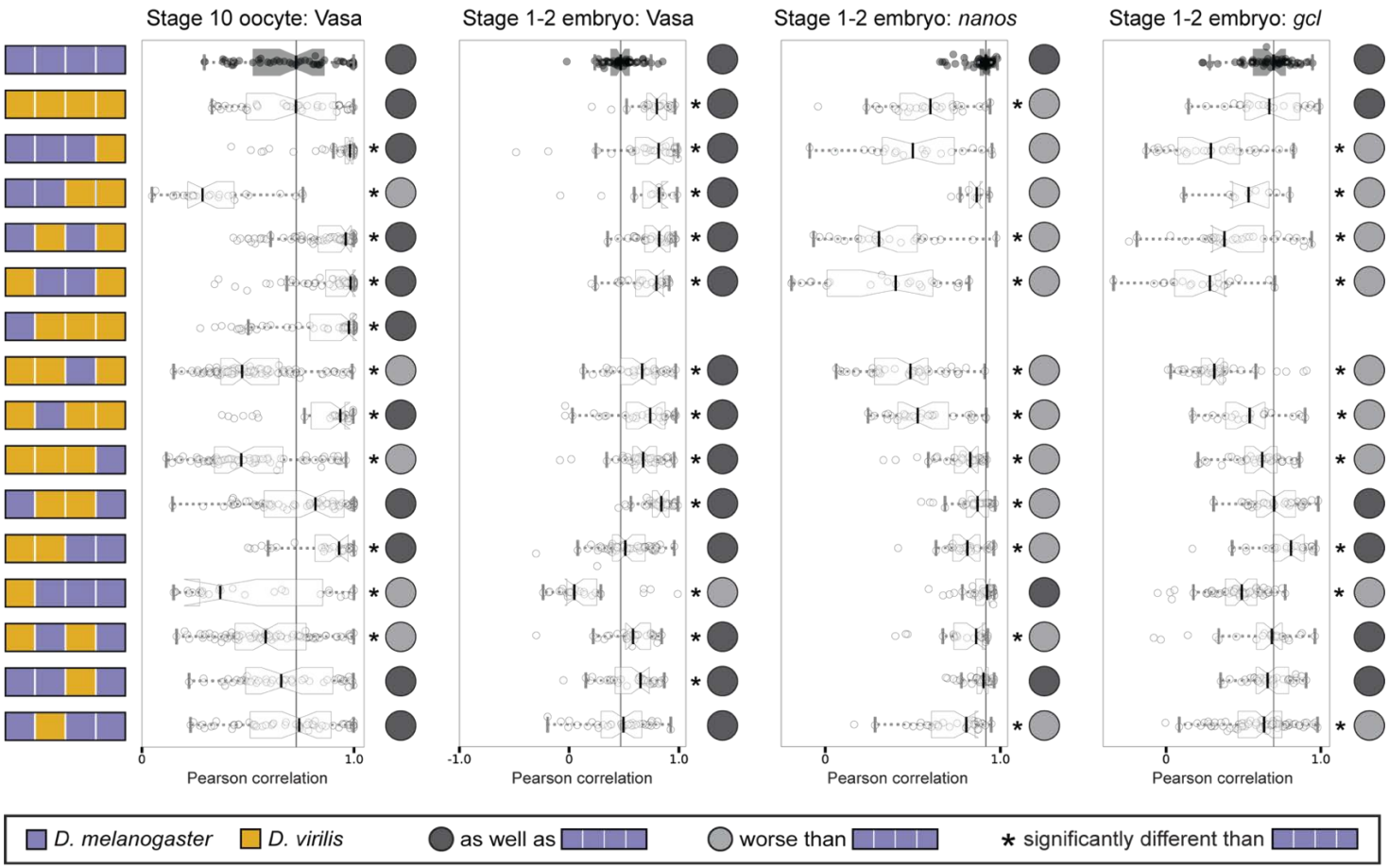


Figure S7. Pearson correlation scores between intensities of HA and Vasa, *nanos*, or *gcl* in stage 10 oocytes and stage 1–2 embryos from mothers expressing chimeric *oskar* in an *oskar* RNA null background (*y[1] sc[*] v[1]; Kr[If-1]/CyO; TI{w[+mC]=TI}osk[0.EGFP]).* For the chimeric genotype with the Long Osk domain from *D. melanogaster* and the other three domains from *D. virilis*, sufficient posterior HA enrichment was found in oocytes to pass our threshold for analysis of germ plasm enrichment, but no embryos had sufficient enrichment to be included in the analysis. Distribution for eggs laid by *D. melanogaster* mothers expressing the *D. melanogaster oskar* chimera (positive control) is in black with the median marked with a black line. Significant difference from positive control distribution (p-value < 0.05, estimated from the distribution of difference of means between sample and control from 100,000 simulated samples) indicated by asterisk. Circles to the right of the plots indicate data interpretation as follows: dark gray = chimera enriches the germ plasm molecule at least as well as *D. melanogaster oskar*; light gray = chimera enriches the germ plasm molecule worse than *D. melanogaster oskar*.

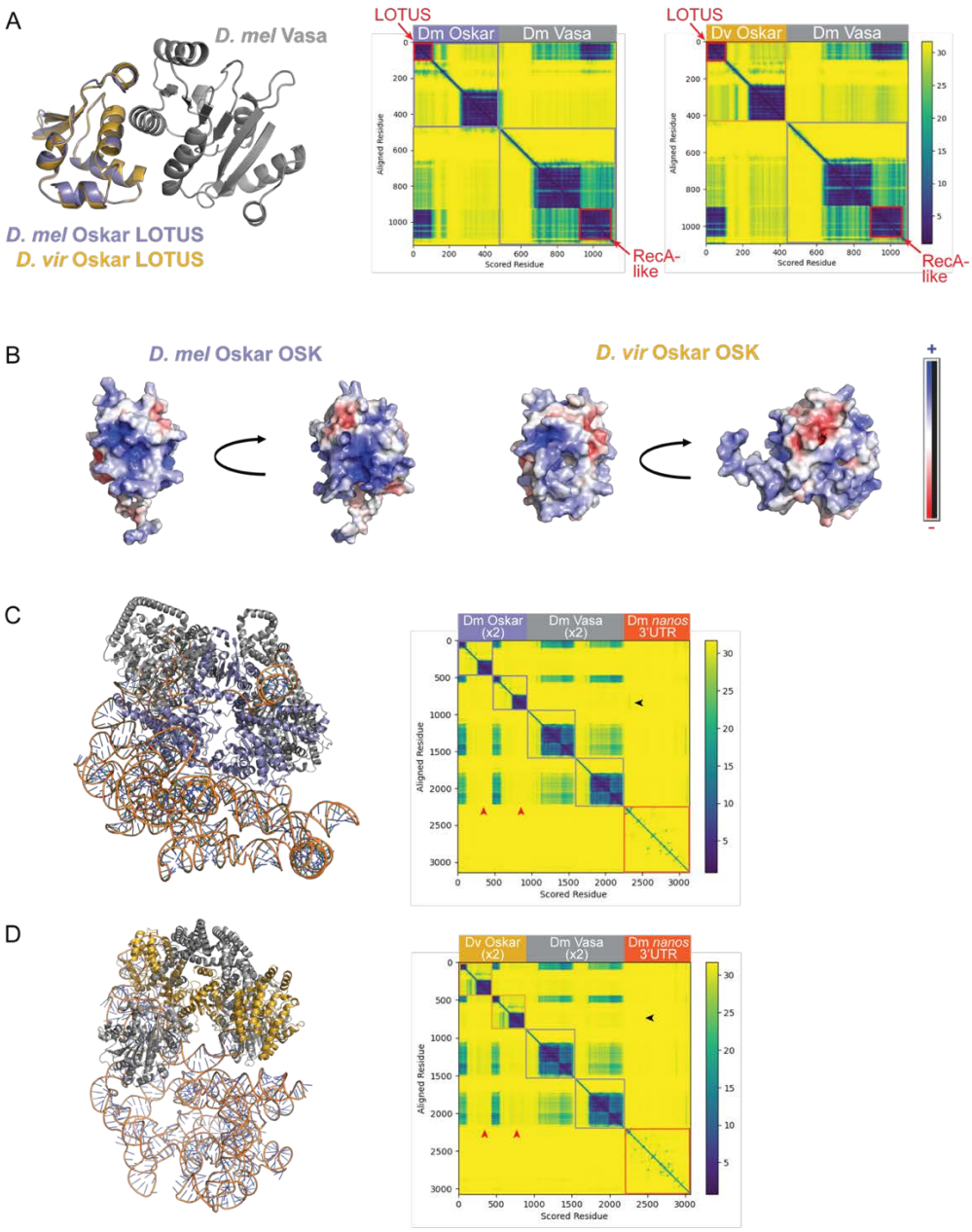


Figure S8. **A)** AlphaFold3 [1] predictions for *D. melanogaster* (purple) and *D. virilis* Short Oskar interactions with *D. melanogaster* Vasa (gray). The LOTUS domains of *D. melanogaster* and *D. virilis* Oskar, as well as *D. melanogaster* Vasa, are shown in structural predictions on the left. On the right, predicted aligned error plots reflect the confidence in the relative placement of residues in the predicted structure. Blue regions mark areas with low error and therefore higher confidence. Colored boxes designate the boundaries between the different proteins in each prediction. **B)** Electrostatic maps for AlphaFold3 predictions of the OSK domain from *D. melanogaster* (left) and *D. virilis* (right) Oskar protein. Blue indicates more positive and red indicates more negative surface charge. **C, D)** Structural predictions and accompanying predicted aligned error plots for two copies of *D. melanogaster* (C) and *D. virilis* (D) Short Oskar in complex with two copies of *D. melanogaster* Vasa and the *D. melanogaster nanos* 3'UTR. Red arrowheads mark where the *D. virilis* Oskar OSK domain has moderate predicted confidence of interaction with Vasa while *D. melanogaster* Oskar does not.

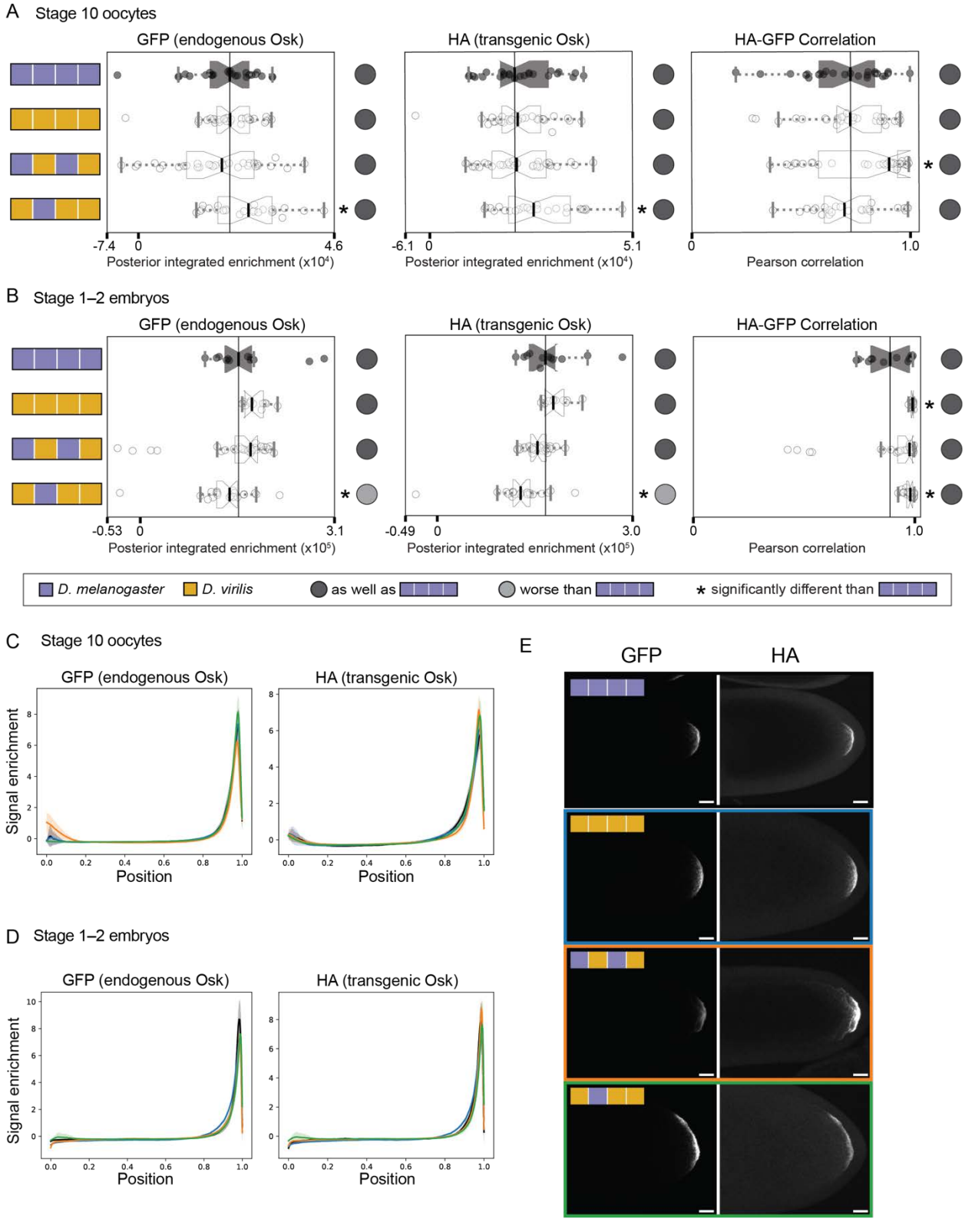
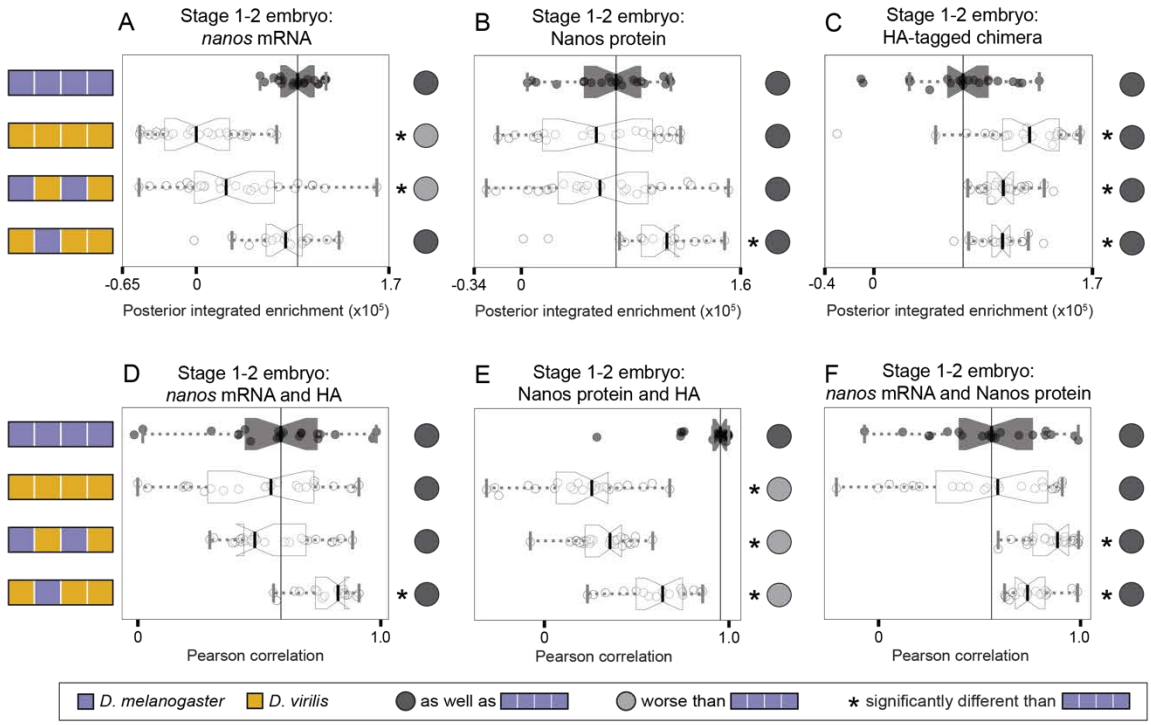
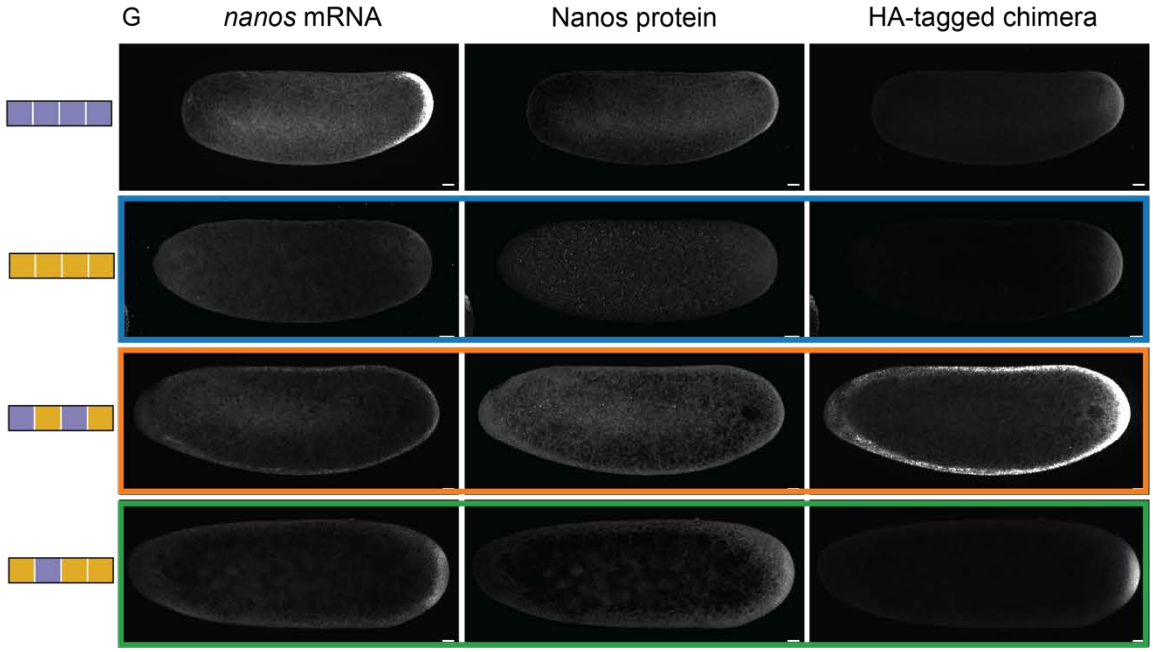
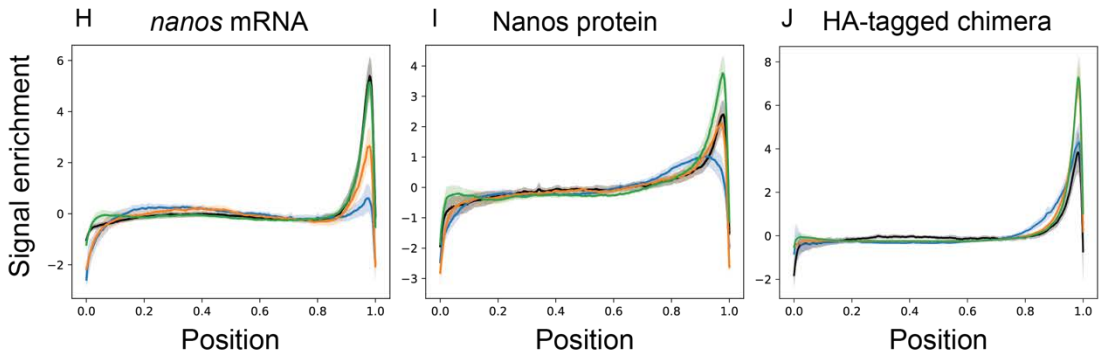

A Stage 10 oocytes
GFP (endogenous Osk)
HA (transgenic Osk)
HA-GFP Correlation
-7.4 0 4.6
Posterior integrated enrichment (x10⁴)
-6.1 0 5.1
Posterior integrated enrichment (x10⁴)
0 1.0
Pearson correlation
B Stage 1–2 embryos
GFP (endogenous Osk)
HA (transgenic Osk)
HA-GFP Correlation
-0.53 0 3.1
Posterior integrated enrichment (x10⁵)
-0.49 0 3.0
Posterior integrated enrichment (x10⁵)
0 1.0
Pearson correlation
D. melanogaster
D. virilis
as well as
worse than
* significantly different than
C Stage 10 oocytes
GFP (endogenous Osk)
HA (transgenic Osk)
Signal enrichment
Position
Position
D Stage 1–2 embryos
GFP (endogenous Osk)
HA (transgenic Osk)
Signal enrichment
Position
Position
E
GFP
HA

Figure S9 (previous page). Chimeric Oskar co-localizes with endogenous Oskar. A–B) Posterior integrated enrichment (left and middle plots) of GFP (endogenous Oskar) and HA (transgenic Oskar) in stage 10 oocytes **(A)** and stage 1–2 embryos **(B)** from *D. melanogaster* mothers expressing chimeric Oskar proteins in a background with endogenous Oskar labeled with GFP. Rightmost plot displays Pearson correlation scores between intensities of HA and GFP signal. For all plots, the distribution for eggs from flies expressing *D. melanogaster oskar* (positive control) is in black with the median marked with a black line. Significant difference from positive control distribution (p-value < 0.05, estimated from the distribution of difference of means between sample and control from 100,000 simulated samples) indicated by asterisk. Circles to the right of the plots indicate data interpretation as follows: dark gray = enriches the germ plasm molecule at least as well as *D. melanogaster oskar*; light gray = enriches the germ plasm molecule worse than *D. melanogaster oskar*. Sample sizes ≥12 for each condition; see Table S6. **C–D)** Line scans displaying GFP and HA signal enrichment (z-score) across stage 10 oocytes **(C)** and stage 1–2 embryos **(D)**. On the X axis, 0 represents the anterior and 1 the posterior. Mean (solid lines) and 95% confidence intervals (shaded regions) are shown. E) Representative images of oocytes from *D. melanogaster* mothers expressing chimeric Oskar sequences in a background with endogenous Oskar labeled with GFP. Anti-HA antibody staining marks the localization of transgenic Oskar and anti-GFP antibody staining marks the localization of endogenous Oskar protein. Images are oriented with posterior to the right. Micrographs are maximum intensity projections of 41 optical sections (step size = 1 μm) and scale bars = 20 μm.


A
Stage 1-2 embryo:
nanos mRNA
B
Stage 1-2 embryo:
Nanos protein
C
Stage 1-2 embryo:
HA-tagged chimera
-0.65
0
1.7
-0.34
0
1.6
-0.4
0
1.7
Posterior integrated enrichment (x10⁵)
D
Stage 1-2 embryo:
nanos mRNA and HA
E
Stage 1-2 embryo:
Nanos protein and HA
F
Stage 1-2 embryo:
nanos mRNA and Nanos protein
0
1.0
Pearson correlation
D. melanogaster
D. virilis
as well as
worse than
* significantly different than


G
nanos mRNA
Nanos protein
HA-tagged chimera


H
nanos mRNA
I
Nanos protein
J
HA-tagged chimera
Signal enrichment
Position
Position
Position

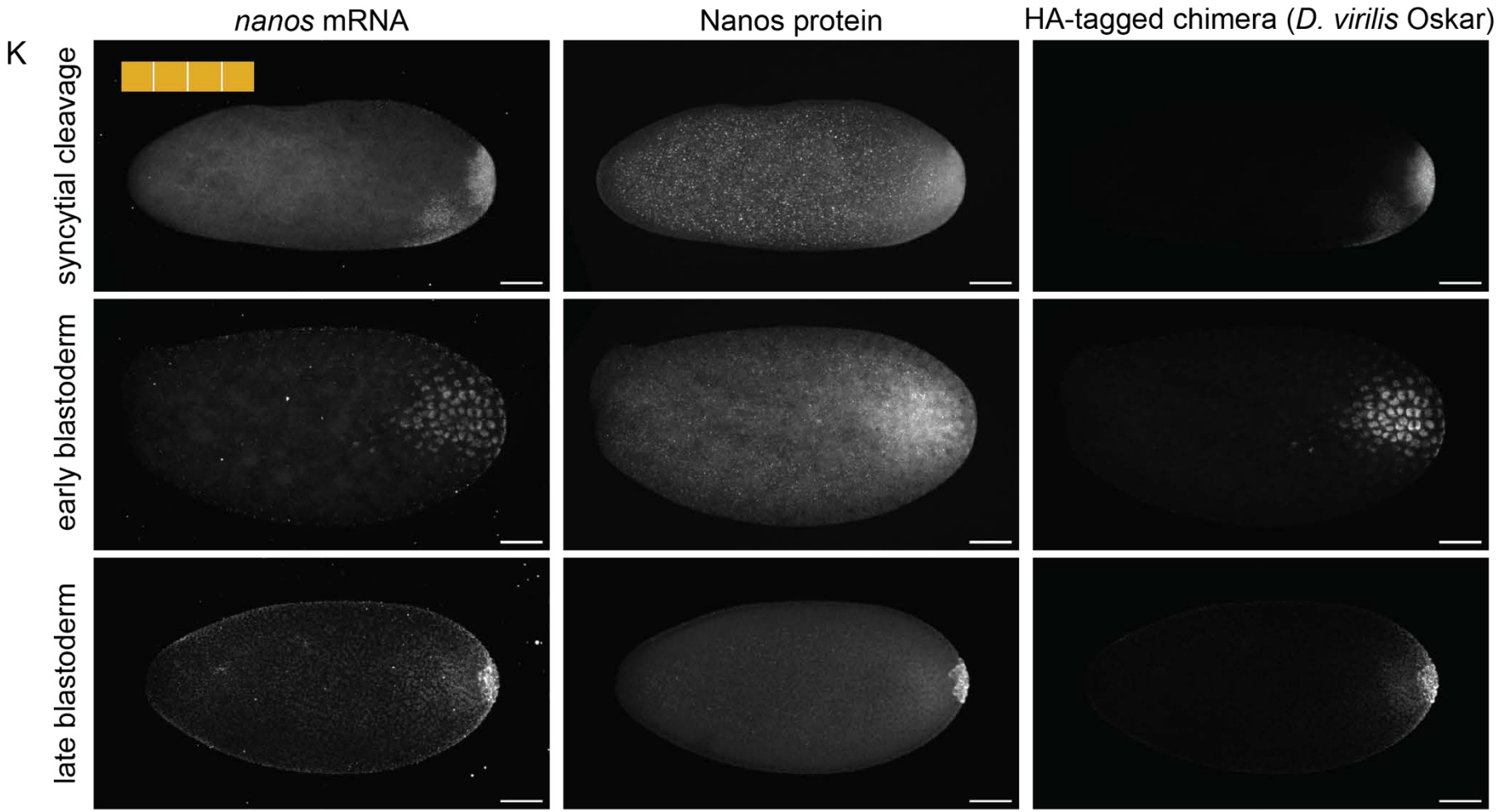

K
nanos mRNA
Nanos protein
HA-tagged chimera (D. virilis Oskar)
syncytial cleavage
early blastoderm
late blastoderm

Figure S10 (previous pages). Quantification of the relationships between chimeric Oskar proteins, *nanos* mRNA and Nanos protein. A) Posterior integrated enrichment of *nanos* mRNA. **B)** Posterior integrated enrichment of Nanos protein. **C)** Posterior integrated enrichment of HA-tagged chimeric Oskar protein. A-C) were quantified in stage 1–2 embryos from *D. melanogaster* mothers expressing chimeric Oskar proteins in a background with endogenous *oskar* present. **D)** Pearson correlation scores between intensities of HA and *nanos* mRNA signal. **E)** Pearson correlation scores between intensities of HA and Nanos protein signal. **F)** Pearson correlation scores between intensities of *nanos* mRNA and Nanos protein signal. All correlation scores are calculated for pixels in the 15% posterior-most end of the embryo with HA intensity values two standard deviations over the mean. For both integrated enrichment and correlation plots, the distribution for eggs from flies expressing D*. melanogaster oskar* (positive control) is in black with the median marked with a black line. Significant difference from positive control distribution (p-value < 0.05, estimated from the distribution of difference of means between sample and control from 100,000 simulated samples) indicated by asterisk. Circles to the right of the plots indicate data interpretation as follows: dark gray = enriches the germ plasm molecule at least as well as *D. melanogaster oskar*; light gray = enriches the germ plasm molecule worse than *D. melanogaster oskar*. Sample sizes ≥17 for each condition; see Table S7. **G)** Representative images of embryos from *D. melanogaster* mothers expressing chimeric Oskar sequences in a background with endogenous *oskar* present and stained with anti-Nanos antibody, *nanos* HCR *in situ* probes, and anti-HA to mark the chimeric Oskar proteins. Images are oriented with posterior to the right. Micrographs are maximum intensity projections of 41 optical sections (step size = 1 μm) and scale bars = 20 μm. **H)** Line scans displaying *nanos* mRNA, **I)** Nanos protein, and **J)** HA-tagged chimeric Oskar protein signal enrichment (Y axis; z-score) across stage 1–2 embryos. On the X axes, 0 represents the anterior and 1 the posterior. Mean (solid lines) and 95% confidence intervals (shaded regions) are shown. **K)** Representative images of embryos at distinct early stages from *D. melanogaster* mothers expressing *D. virilis* Oskar in a background with endogenous *oskar* present and stained with anti-Nanos antibody, *nanos* HCR *in situ* probes, and anti-HA to mark the *D. virilis* Oskar protein. Images are oriented with posterior to the right. Micrographs are maximum intensity projections of 30 optical sections (step size = 2 μm). Scale bars = 50 μm.

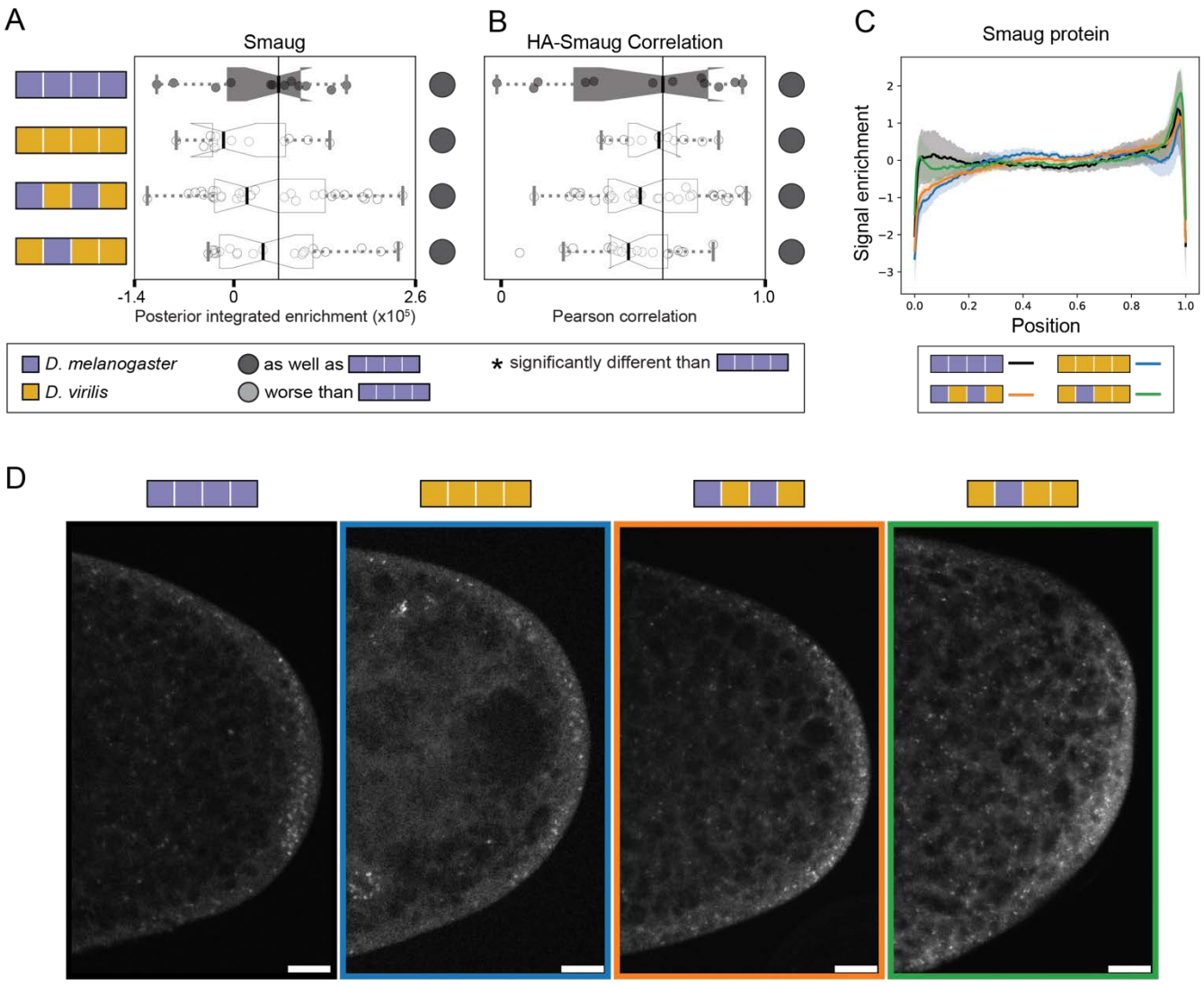


Figure S11. Smaug remains localized to the germ plasm when expressing chimeric *oskar* proteins containing the *D. virilis* OSK domain in a background with endogenous *oskar*. A) Posterior integrated enrichment of Smaug and HA in stage 1–2 embryos from *D. melanogaster* mothers expressing chimeric Oskar proteins in a background with endogenous *oskar* present. **B)** Pearson correlation scores between intensities of HA and Smaug signal. For both plots, the distribution for eggs from flies expressing D. *melanogaster oskar* (positive control) is in black with the median marked with a black line. Significant difference from positive control distribution (p-value < 0.05, estimated from the distribution of difference of means between sample and control from 100,000 simulated samples) indicated by asterisk. Circles to the right of the plots indicate data interpretation as follows: dark gray = enriches the germ plasm molecule at least as well as *D. melanogaster oskar*; light gray = enriches the germ plasm molecule worse than *D. melanogaster oskar*. Sample sizes ≥12 for each condition; see Table S8. **C)** Line scans displaying Smaug signal enrichment (z-score) across stage 2 embryos. On the X axis, 0 represents the anterior and 1 is the posterior. Mean (solid lines) and 95% confidence intervals (shaded regions) are shown. **D)** Representative images of embryos from *D. melanogaster* mothers expressing chimeric Oskar sequences in a background with endogenous *oskar* present and stained with anti-Smaug antibody (white). Images are oriented with posterior to the right. Micrographs are single optical sections and scale bars = 20 μm.

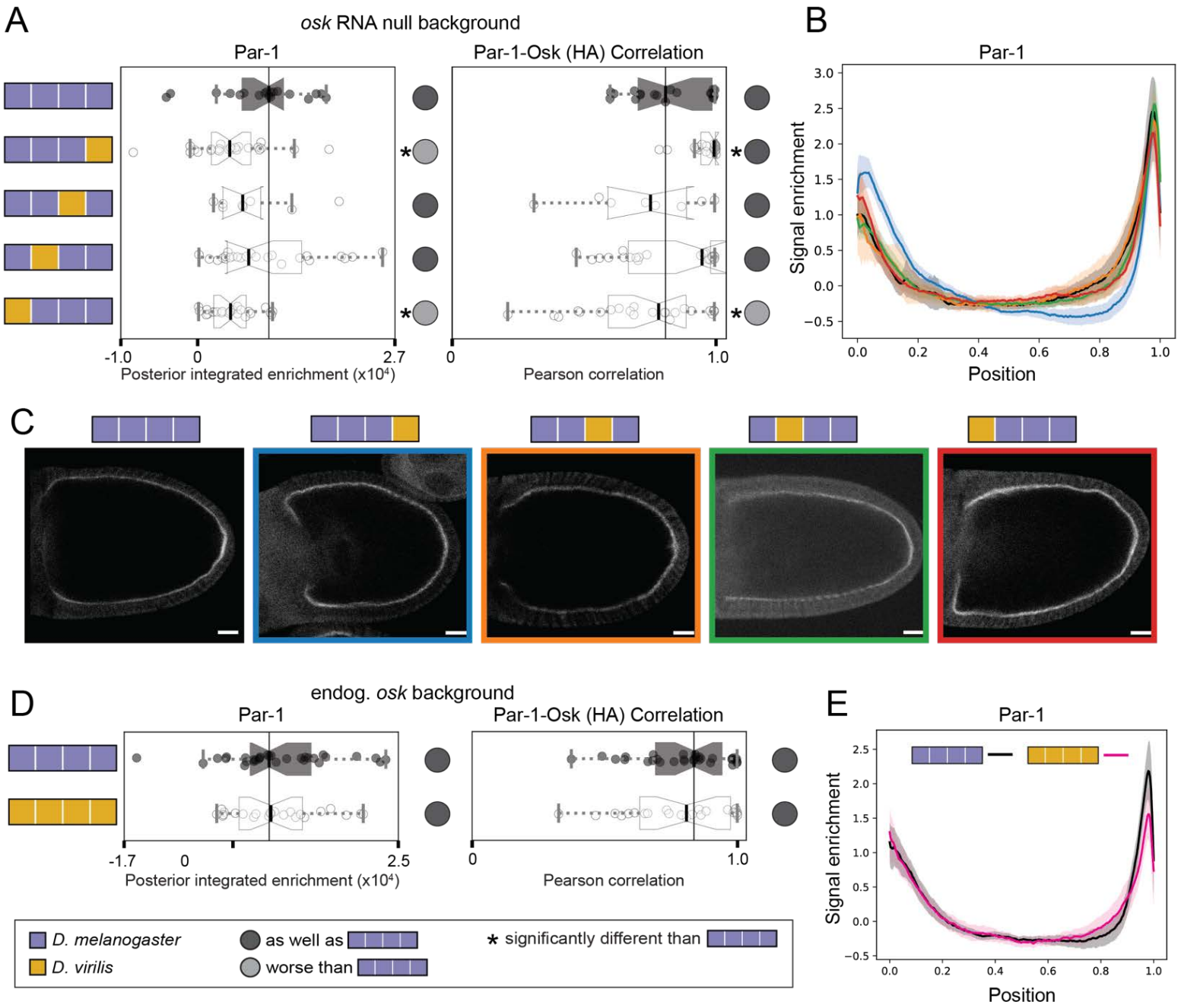

A
osk RNA null background
Par-1
Par-1-Osk (HA) Correlation
-1.0
0
2.7
Posterior integrated enrichment (x10⁴)
0
1.0
Pearson correlation
B
Par-1
Signal enrichment
Position
C
D
endog. osk background
Par-1
Par-1-Osk (HA) Correlation
-1.7
0
2.5
Posterior integrated enrichment (x10⁴)
0
1.0
Pearson correlation
D. melanogaster
D. virilis
as well as
worse than
* significantly different than
E
Par-1
Signal enrichment
Position

Figure S12 (previous page). Par-1 exhibits some variation in posterior enrichment in stage 10 oocytes for chimeras expressed in an *oskar* RNA null background. A) Posterior integrated enrichment (left) of Par-1 protein in stage 10 oocytes from *D. melanogaster* mothers expressing chimeric Oskar proteins in an *oskar* RNA null background. The plot on the right displays Pearson correlation scores between intensities of HA and Par-1 signal. For both plots, the distribution for eggs from flies expressing D. *melanogaster oskar* (positive control) is in black with the median marked with a black line. Significant difference from positive control distribution (p-value < 0.05, estimated from the distribution of difference of means between sample and control from 100,000 simulated samples) indicated by asterisk. Circles to the right of the plots indicate data interpretation as follows: dark gray = enriches the germ plasm molecule at least as well as *D. melanogaster oskar*; light gray = enriches the germ plasm molecule worse than *D. melanogaster oskar*. Sample sizes ≥8 for each condition; see Table S9. **B)** Line scans displaying Par-1 signal enrichment (z-score) across *oskar* RNA null stage 10 oocytes. On the X axis, 0 represents the anterior and 1 the posterior. Mean (solid lines) and 95% confidence intervals (shaded regions) are shown. **C)** Representative images of oocytes from *D. melanogaster* mothers expressing chimeric Oskar sequences in an *oskar* RNA null background. Anti-Par1 antibody staining (white) marks its localization. Images are oriented with posterior to the right. Micrographs depict single optical sections and scale bars = 20 μm. **D)** Posterior integrated enrichment (left) of Par-1 protein in stage 10 oocytes from *D. melanogaster* mothers expressing chimeric Oskar proteins in a background with endogenous *oskar* present. The plot on the right displays Pearson correlation scores between intensities of HA and Par-1 signal. For both plots, the distribution for eggs from flies expressing D. *melanogaster oskar* (positive control) is in black with the median marked with a black line. Significant difference from positive control distribution (p-value < 0.05, estimated from the distribution of difference of means between sample and control from 100,000 simulated samples) indicated by asterisk. Circles to the right of the plots designate the same interpretations described above. Sample sizes ≥23 for each condition; see Table S10. **E)** Line scans displaying Par-1 signal enrichment (z-score) across stage 10 oocytes in a background with endogenous *oskar* present. On the X axis, 0 represents the anterior and 1 the posterior. Mean (solid lines) and 95% confidence intervals (shaded regions) are shown.

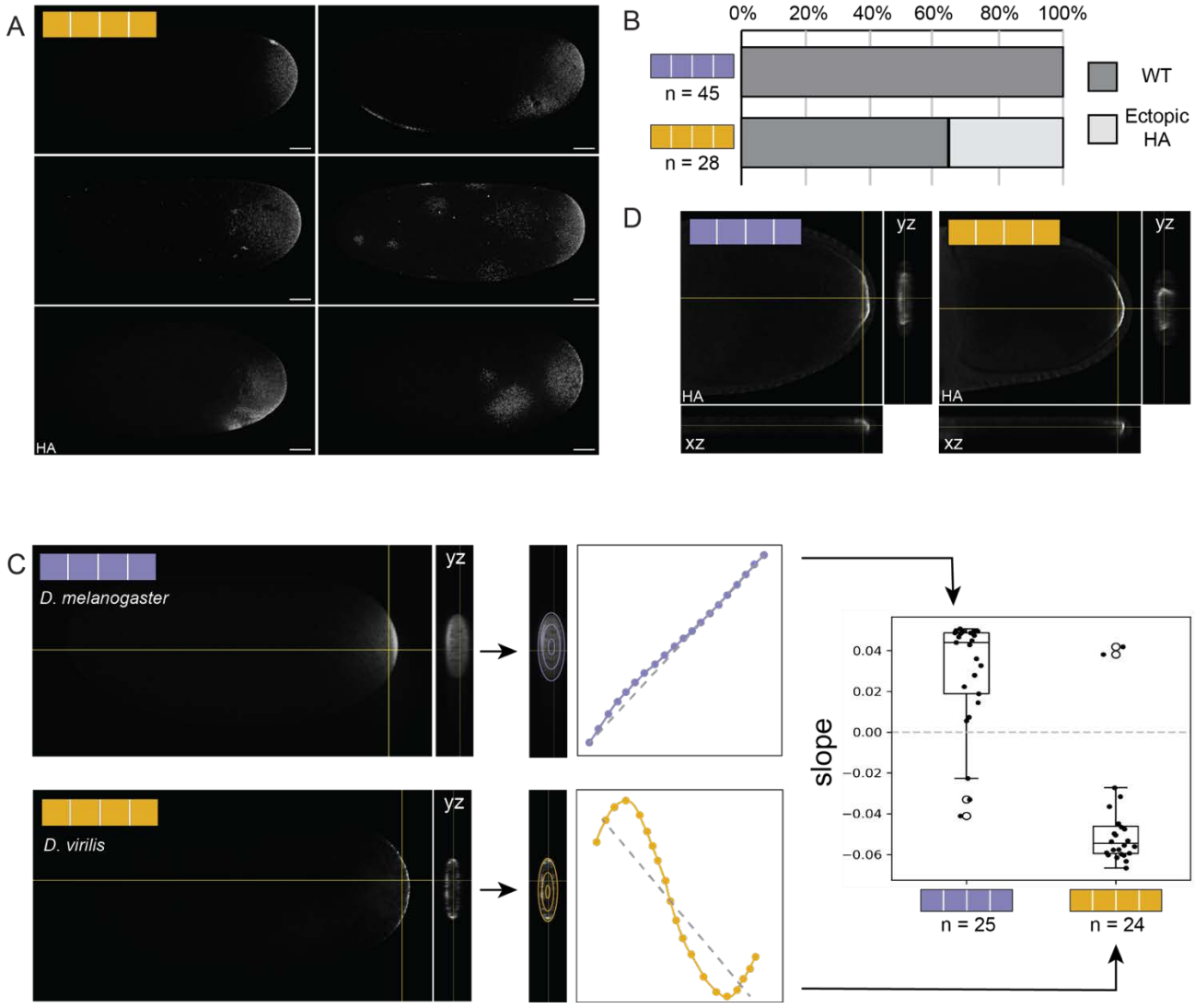


Figure S13. A) Cleavage stage embryos from *D. melanogaster* mothers expressing *D. virilis* Oskar exhibiting representative *D. virilis* Oskar localization patterns seen with anti-HA antibody stains. Micrographs are maximum intensity projections of 30 optical sections (step size = 2 μm), scale bars represent 50 μm and posterior is to the right. **B)** Frequency of ectopic patches of HA appearing away from the posterior pole in embryos from mothers expressing either *D. melanogaster* (left) or *D. virilis* (right) *oskar*. **C)** Schematic demonstrating how the plot in Fig. 6C was made. The yz projections from image stacks of anti-HA-stained embryos were eroded and fluorescent signal intensity measured 20 times. We drew a line of best fit for the curve of fluorescent signal intensity and plotted the slope of this line. **D)** Stage 10 oocytes from mothers expressing *D. melanogaster oskar* and *D. virilis oskar* stained with anti-HA antibody. Orthogonal views in the yz and xz orientations flank each image.

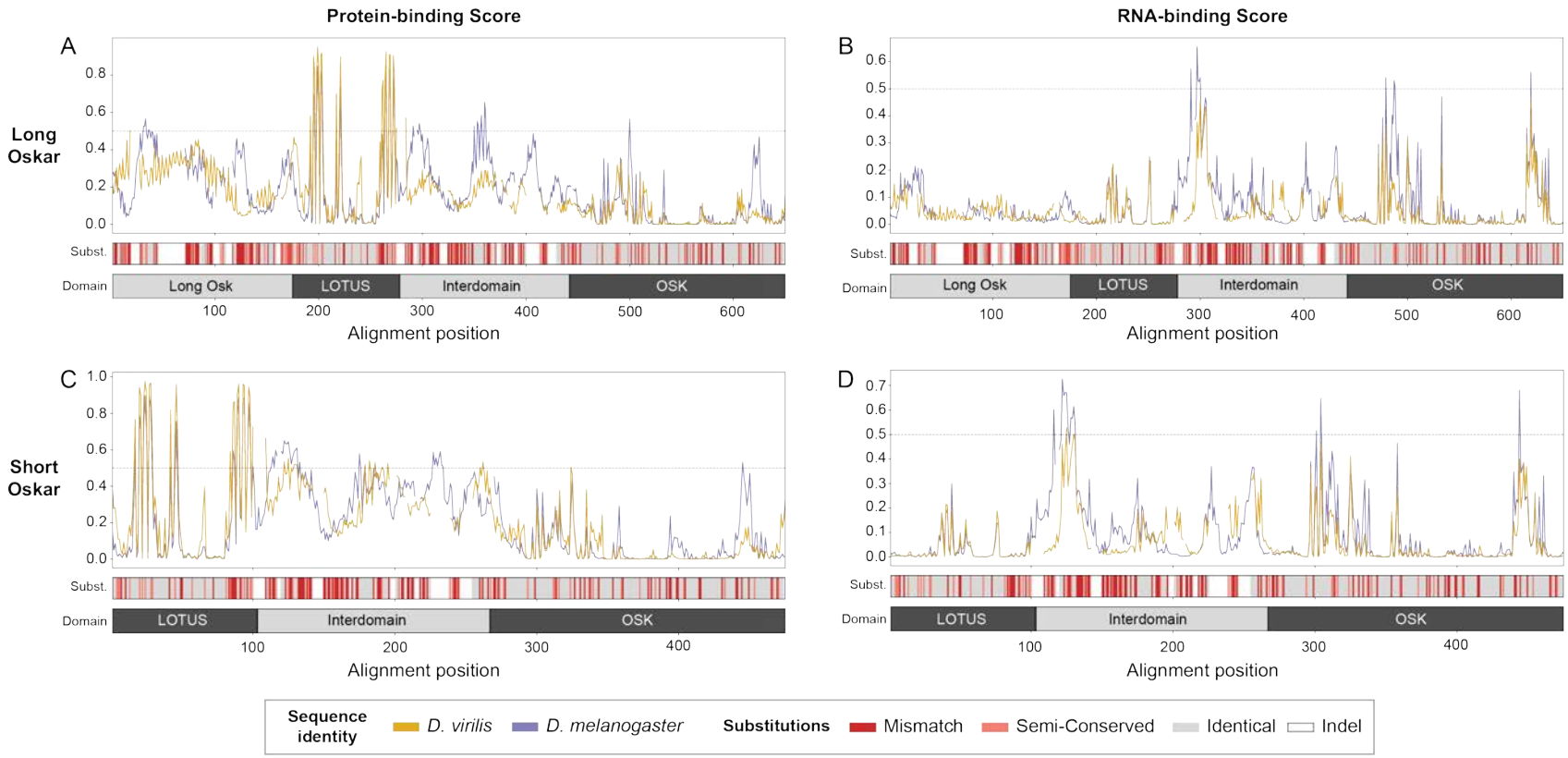


Figure S14. **A)** Line scans exhibiting the GPSite protein-binding score by residue for *D. melanogaster* (purple) and *D. virilis* (gold) Long Oskar sequences. **B)** Line scans exhibiting the GPSite RNA-binding score by residue for *D. melanogaster* (purple) and *D. virilis* (gold) Long Oskar sequences. **C)** Line scans exhibiting the GPSite protein-binding score by residue for *D. melanogaster* (purple) and *D. virilis* (gold) Short Oskar sequences. **D)** Line scans exhibiting the GPSite RNA-binding score by residue for *D. melanogaster* (purple) and *D. virilis* (gold) Short Oskar sequences. For all analyses, sequences were aligned using EMBOSS Needle [2]. A dotted line is drawn at 0.5. The bar below the line scans (Subst.) indicates where residues are identical between the orthologs in the alignment (gray), semi-conservative substitutions with shared biochemical properties (pink), and not conserved (red), while white indicates insertions/deletions. The four domains of Long Oskar (A, B), or the three domains of Short Oskar (C, D) are demarcated in the gray bar at the bottom of the figure (Domain).

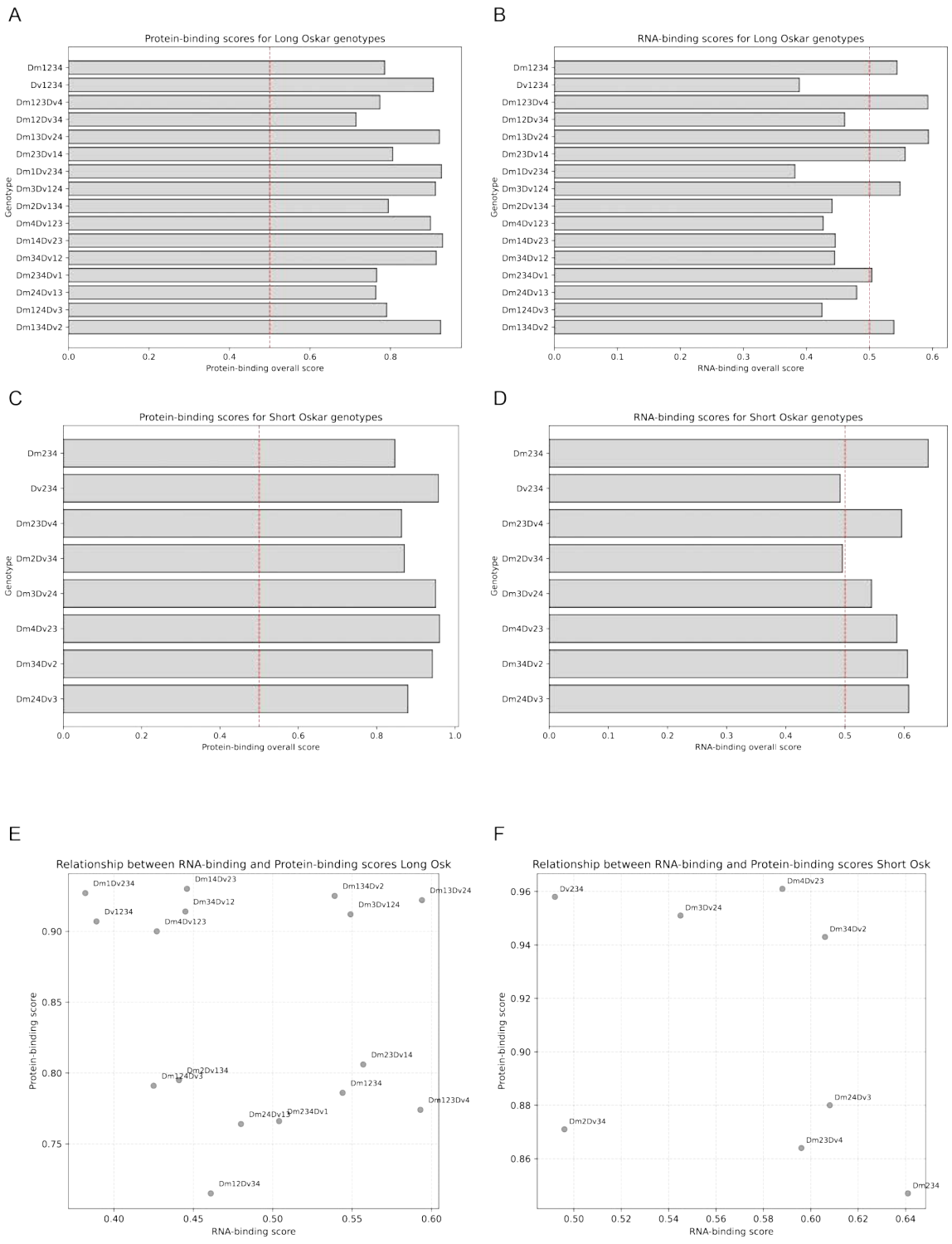


Figure S15. A) Overall protein-binding scores for Long Oskar chimeric proteins. **B)** Overall RNA-binding scores for Long Oskar chimeric proteins. **C)** Overall protein-binding scores for Short Oskar chimeric proteins. **D)** Overall RNA-binding scores for Short Oskar chimeric proteins. For A) through D), scores were generated using GPsite, and a red dotted line is drawn at 0.5. **E)** Scatter plot showing the correlation between predicted RNA-binding and protein-binding scores for Long Oskar chimeric proteins. **F)** Scatter plot showing the correlation between predicted RNA-binding and protein-binding scores for Short Oskar chimeric proteins. For E) and F), RNA-binding score is on the x-axis and protein-binding score is on the y-axis.

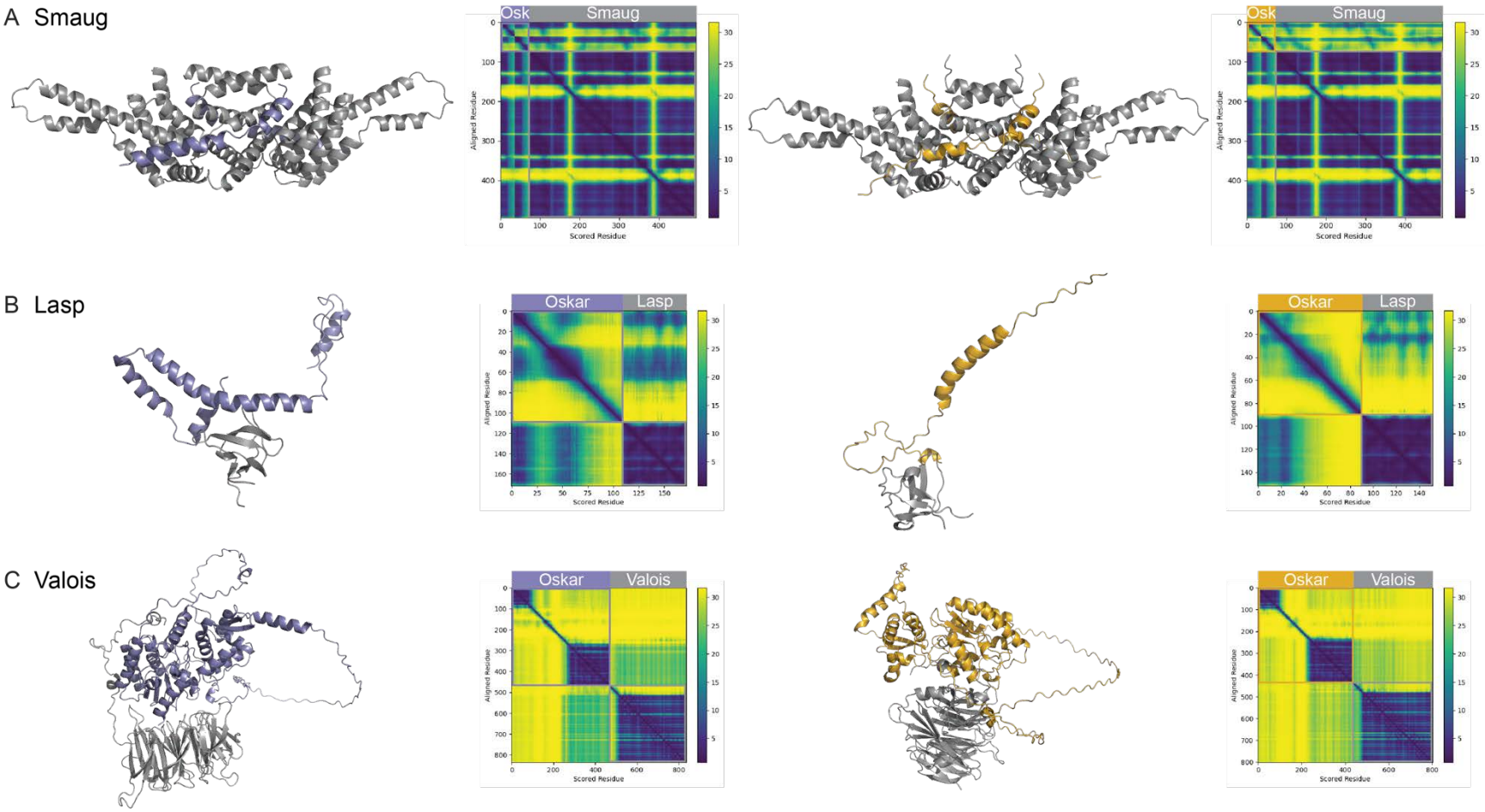
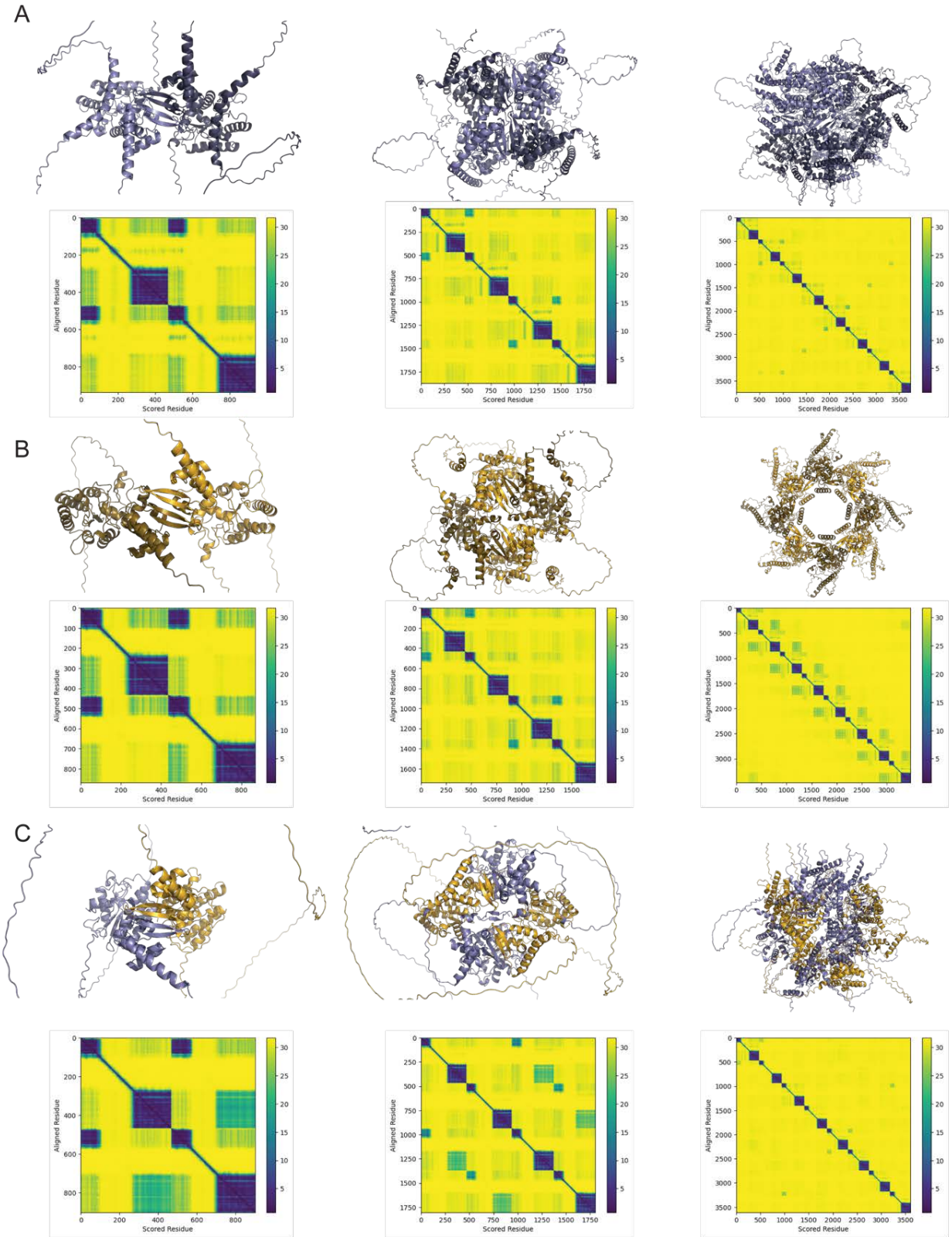


Figure S16. AlphaFold3 structural predictions and accompanying predicted aligned error plots for *D. melanogaster* Short Oskar (left) and *D. virilis* Short Oskar (right) with *D. melanogaster* Smaug (**A**), Lasp (**B**), and Valois (**C**). Only portions of Smaug [3], Lasp [4], and Valois [5] suggested by previous structural or *in vitro* assays to interact with Oskar, along with the corresponding portion of Oskar in this interaction, were used in the structural prediction.


A
B
C
Aligned Residue
Scored Residue

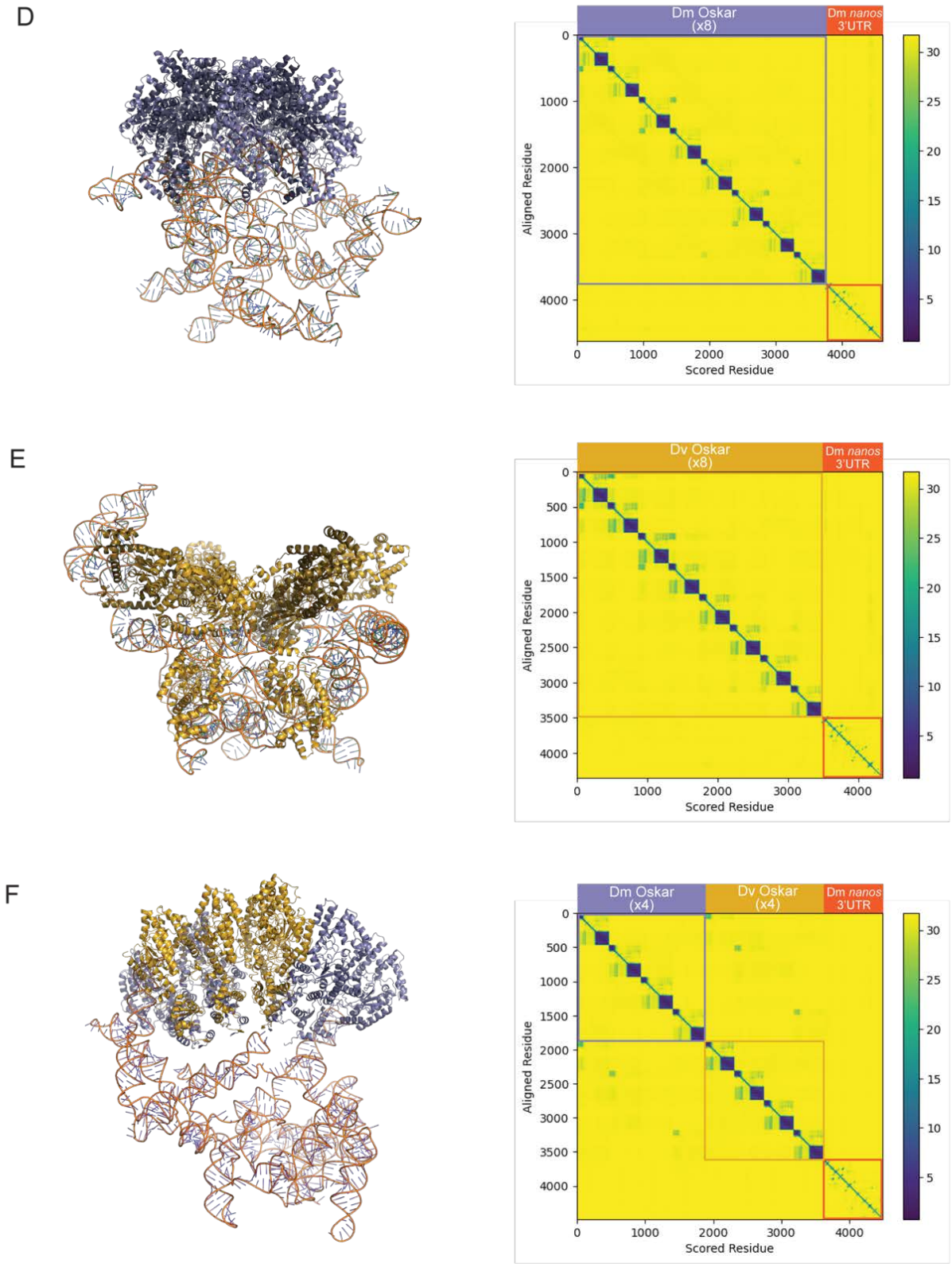


Figure S17. A–C) AlphaFold3 structural predictions and accompanying predicted aligned error plots for one (left column), two (middle column) or four (right column) monomers of each of *D. melanogaster* Short Oskar (**A**), *D. virilis* Short Oskar (**B**), both *D. melanogaster* and *D. virilis* Short Oskar (**C**). **D–F)** AlphaFold3 structural predictions and predicted aligned error plots for eight copies of *D. melanogaster* (**D**) *D. virilis* (**E**), and *D. melanogaster* and *D. virilis* Short Oskar (**F**) with *D. melanogaster nanos* 3'UTR.

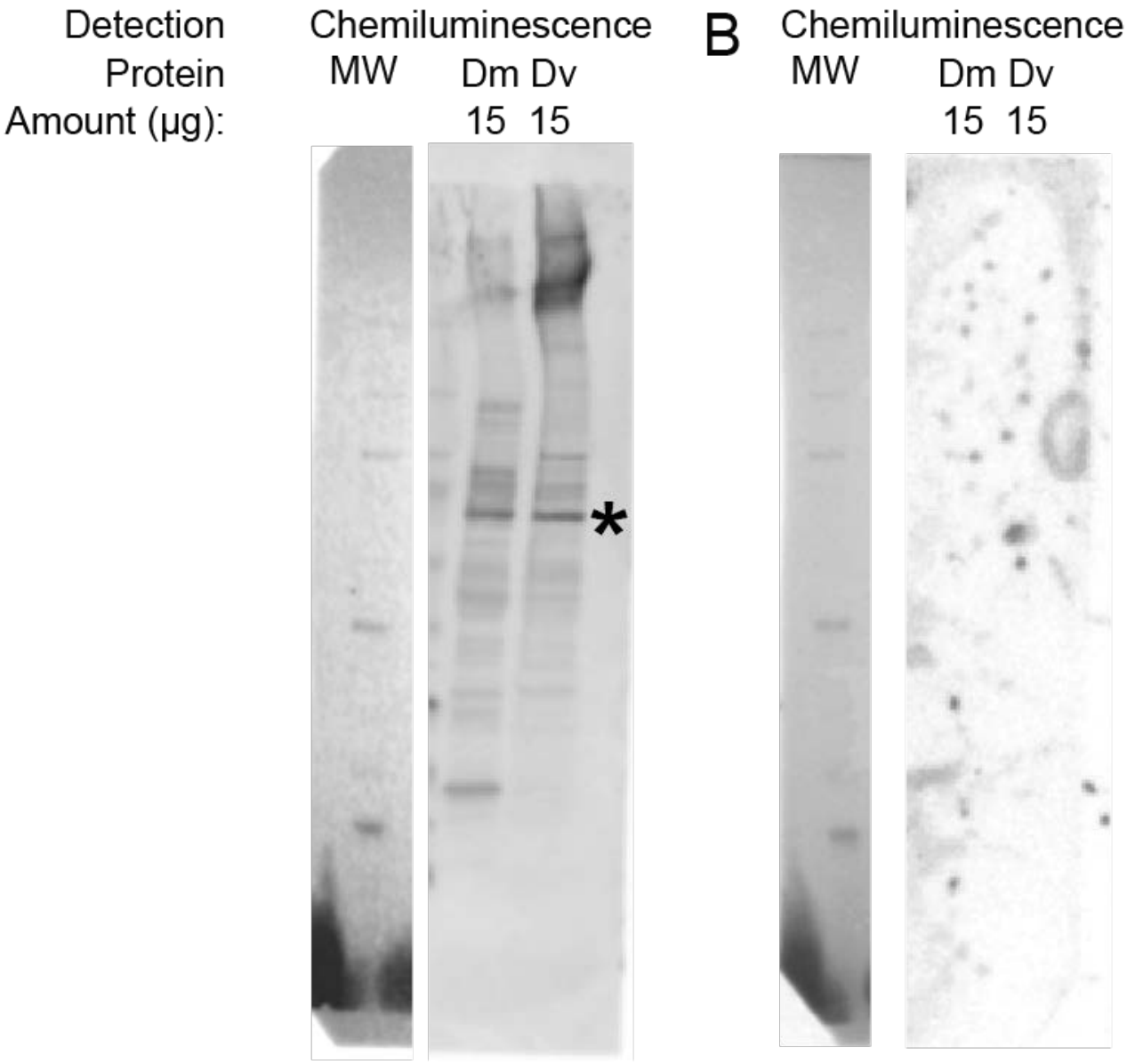


Figure S18. *D. virilis* anti-Oskar antibody validation. **A)** Chemiluminescent Western Blot with *D. melanogaster* (Dm) and *D. virilis* (Dv) ovary lysates incubated with anti-*Dvir* Oskar primary antibody. The amount of protein (*µ*g) that was loaded for each lane is listed under the species identifier for each lane. Lane with molecular weight markers are marked MW. Bands at expected product sizes are marked with an asterisk (*Dmel* Oskar ~69 kDa, *Dvir* Oskar ~69 kDa). **B)** Control blot with no primary antibody. Note that this control experiment is the same one used to validate a second antibody that was generated at the same time for a different project[6] , and is reported as such in Figure S6 therein.

Chimeric *oskar* mRNA enrichment (*osk* null background)			
Genotype	Sample size	Integrated posterior enrichment p-value	Pearson correlation p-value
Dm1234	19	n/a	n/a
Dm123Dv4	24	0.00107	0.08475
Dm124Dv3	8	0.12169	0.46363
Dm134Dv2	24	0.14356	0.00017
Dm234Dv1	24	0.00104	0.24710

Table S1. Statistical analysis of *oskar* mRNA posterior enrichment and Pearson correlation with HA in stage 10 oocytes expressing each Oskar chimera in the *oskar* RNA null background *w[1118]; Kr[If-1]/CyO; TI{w[+mC]=TI}osk[0.EGFP]*. P-values are estimated from the distribution of difference of means between sample and control from 100,000 simulated samples.

Pole cell count (*osk* null background)			
Genotype	**Sample size**	***μ***	**p-value**
Dm1234	37	22.22	n/a
Dv1234	21	0.00	0.00
Dm123Dv4	16	0.00	0.00
Dm12Dv34	15	1.13	0.00
Dm13Dv24	18	0.00	0.00
Dm23Dv14	20	1.55	0.00
Dm1Dv234	15	0.00	0.00
Dm3Dv124	21	0.00	0.00
Dm2Dv134	18	0.00	0.00
Dm4Dv123	21	25.19	0.04438
Dm14Dv23	23	30.61	6.49E-7
Dm34Dv12	32	9.88	4.14E-13
Dm234Dv1	21	9.33	0.00
Dm24Dv13	21	18.57	0.01105
Dm124Dv3	22	22.95	0.31977
Dm134Dv2	20	8.25	1.55E-15

Table S2. Statistical analysis of pole cell counts in stage 5 embryos expressing each Oskar chimera in the *oskar* RNA null background (*y[1] sc[*] v[1]; Kr[If-1]/CyO; TI{w[+mC]=TI}osk[0.EGFP]*). The p-values are estimated from the distribution of difference of means between sample and control from 100,000 simulated samples.

.

Germ plasm enrichment (*osk* null background)				
	Genotype	**Sample size**	**Integrated posterior enrichment p-value**	**Pearson correlation p-value**
Stage 10 oocyte: Vasa	Dm1234	49	n/a	
	Dv1234	43	0.20058	0.42069
	Dm123Dv4	63	6.38E-07	6.54E-12
	Dm12Dv34	26	6.33E-12	7.20e-13
	Dm13Dv24	116	0.00011	1.27e-08
	Dm23Dv14	75	1.55E-08	7.03e-09
	Dm1Dv234	77	8.99E-08	1.68e-05
	Dm3Dv124	101	0.0	8.17e-07
	Dm2Dv134	30	0.00121	0.00300
	Dm4Dv123	70	0.00141	6.92E-06
	Dm14Dv23	71	5.04E-11	0.08168
	Dm34Dv12	32	0.04972	0.00017
	Dm234Dv1	28	0.25847	0.00201
	Dm24Dv13	81	0.29487	0.00678
	Dm124Dv3	46	1.49E-06	0.23057
	Dm134Dv2	54	3.53E-10	0.39111
Stage 1–2 embryo: Vasa	Dm1234	54	n/a	
	Dv1234	26	1.07E-5	3.93E-13
	Dm123Dv4	32	0.03668	0.00014
	Dm12Dv34	11	0.12219	0.01178
	Dm13Dv24	35	0.00141	0.00
	Dm23Dv14	28	5.69E-5	7.67E-08
	Dm1Dv234	See Table Legend & Methods		
	Dm3Dv124	33	0.25939	0.00023
	Dm2Dv134	30	0.03191	0.00245
	Dm4Dv123	38	0.25513	8.31E-06
	Dm14Dv23	39	1.50E-8	0.00
	Dm34Dv12	56	0.12130	0.10232
	Dm234Dv1	24	0.49020	8.26E-7
	Dm24Dv13	32	0.10103	0.03315
	Dm124Dv3	35	0.07229	0.01482
	Dm134Dv2	35	0.41964	0.33832
Stage 1–2 embryo: *nanos*	Dm1234	60	n/a	
	Dv1234	30	0.17960	7.08E-14

	Dm123Dv4	20	0.00476	1.50E-09
	Dm12Dv34	9	2.01E-06	0.04266
	Dm13Dv24	25	0.00028	7.80E-25
	Dm23Dv14	23	0.14142	1.86E-15
	Dm1Dv234	See Table Legend & Methods		
	Dm3Dv124	39	3.40E-15	4.97E-34
	Dm2Dv134	30	0.24130	3.31E-19
	Dm4Dv123	37	0.15120	1.73E-06
	Dm14Dv23	32	0.00104	0.02030
	Dm34Dv12	32	0.00113	0.00112
	Dm234Dv1	42	8.97e-05	0.19292
	Dm24Dv13	22	0.39319	0.00110
	Dm124Dv3	47	7.80E-08	0.25014
	Dm134Dv2	33	1.73E-11	1.41E-07
Stage 1–2 embryo: *gcl*	Dm1234	56	n/a	
	Dv1234	24	0.03136	0.49283
	Dm123Dv4	29	0.07679	1.33E-11
	Dm12Dv34	9	0.00527	0.01495
	Dm13Dv24	33	0.44230	1.345E-05
	Dm23Dv14	21	0.03223	2.67E-14
	Dm1Dv234	See Table Legend & Methods		
	Dm3Dv124	46	0.06752	5.54E-21
	Dm2Dv134	21	0.00394	0.00545
	Dm4Dv123	37	0.00205	0.02295
	Dm14Dv23	36	0.00023	0.09993
	Dm34Dv12	23	0.08356	0.02337
	Dm234Dv1	59	0.00136	7.82E-11
	Dm24Dv13	25	0.14451	0.14037
	Dm124Dv3	36	0.06186	0.47409
	Dm134Dv2	74	0.19011	0.01637

Table S3. Statistical analysis of Vasa, *nanos*, and *gcl* posterior enrichment and Pearson correlation with HA in stage 10 oocytes and stage 1–2 embryos expressing each Oskar chimera in the *oskar* RNA null background *w[1118]; Kr[If-1]/CyO; TI{w[+mC]=TI}osk[0.E+]*. For the chimeric genotype with the Long Osk domain from *D. melanogaster* and the other three domains from *D. virilis* (Dm1Dv234), sufficient posterior HA enrichment was found in oocytes to pass our threshold for analysis of germ plasm enrichment, but no embryos had sufficient enrichment to be included in the analysis. P-values are estimated from the distribution of difference of means between sample and control from 100,000 simulated samples.

Pole cell count and axial patterning (endog. *osk* background)							
Genotype	Stage 5 embryo: Pole cell counts				1st instar larva: Cuticle patterning		
	Sample size	μ	With negative control p-value	With positive control p-value	Sample size	JSD negative	JSD positive
Dm1234	21	62.05	5.99E-18	n/a	46	0	n/a
Dv1234	21	27.86	1.95E-7	0.00	31	1	1
Dm123Dv4	20	37.15	0.04990	2.10E-15	60	0.04297	0.04297
Dm12Dv34	26	35.23	0.01277	0.00	53	0.00950	0.00950
Dm13Dv24	20	3.80	0.00	0.00	51	1	1
Dm23Dv14	20	49.80	0.00330	1.72E-5	47	0.09083	0.09083
Dm1Dv234	20	40.70	0.28557	2.77E-15	51	0.04037	0.04037
Dm3Dv124	20	37.80	0.06714	7.77E-16	45	0	0
Dm2Dv134	20	45.35	0.17532	1.25E-6	54	0.55964	0.55964
Dm4Dv123	20	51.55	0.00020	0.00010	53	0.00950	0.00950
Dm14Dv23	20	59.30	1.41E-9	0.18236	57	0.01777	0.01777
Dm34Dv12	30	57.03	3.47E-13	0.01352	50	0	0
Dm234Dv1	22	46.68	0.03862	8.50E-9	52	0.04983	0.04983
Dm24Dv13	20	64.30	1.39E-20	0.19133	51	0	0
Dm124Dv3	33	44.42	0.15442	1.80E-13	60	0.06094	0.06094
Dm134Dv2	20	38.30	0.07193	0.00	57	0.02683	0.02683
endog. *osk* only	34	42.15	n/a	0.00	55	n/a	0

Table S4. Left: Statistical analysis of pole cell counts in stage 5 embryos expressing one copy of each Oskar chimera in a background with endogenous *oskar* present. Right: Jensen–Shannon Divergence (JSD) calculated for the distribution of "WT," "Strong AP Defects," and "Partial AP Defects" phenotypes in each chimeric background compared to the distribution of these phenotypes in the negative (endogenous *oskar* only) and positive control (Dm1234).

Germ plasm enrichment (endog. *osk* background)				
	Genotype	Sample size	With negative control p-value	With positive control p-value
Stage 10 oocyte: Vasa	Dm1234	52	1.48E-10	n/a
	Dv1234	53	4.10E-21	0.11051
	Dm123Dv4	64	6.46E-15	0.37868
	Dm12Dv34	39	6.55E-8	0.20238
	Dm13Dv24	67	0.03216	3.17E-5
	Dm23Dv14	42	4.17E-7	0.07693
	Dm1Dv234	41	2.58E-18	0.08042
	Dm3Dv124	65	4.96E-7	0.14429
	Dm2Dv134	37	1.86E-31	0.00423
	Dm4Dv123	74	1.36E-5	0.00587
	Dm14Dv23	66	0.00073	0.00093
	Dm34Dv12	37	4.15E-5	0.10557
	Dm234Dv1	32	4.68E-6	0.01924
	Dm24Dv13	51	2.25E-8	0.11377
	Dm124Dv3	61	1.78E-9	0.10925
	Dm134Dv2	40	1.34E-22	0.03775
	endog. *osk* only	179	n/a	1.36E-10
Stage 1–2 embryo: Vasa	Dm1234	125	0.00056	n/a
	Dv1234	16	1.47E-6	0.00238
	Dm123Dv4	73	8.02e-9	0.00131
	Dm12Dv34	37	0.31201	0.01605
	Dm13Dv24	58	0.00016	0.20395
	Dm23Dv14	56	0.02356	0.21459
	Dm1Dv234	31	0.29723	0.03034
	Dm3Dv124	82	0.00159	0.44346
	Dm2Dv134	23	0.00578	0.24946
	Dm4Dv123	134	1.36e-5	0.15072
	Dm14Dv23	54	0.24605	0.00250
	Dm34Dv12	60	0.03906	0.15357
	Dm234Dv1	37	0.21932	0.02844
	Dm24Dv13	38	0.36906	0.00322
	Dm124Dv3	88	0.30718	9.40E-6
	Dm134Dv2	132	0.43041	1.13e-5
	endog. *osk* only	56	n/a	0.00052
Stage 1–2 embryo: *nanos*	Dm1234	49	4.03e-7	n/a
	Dv1234	31	4.44E-16	0.00
	Dm123Dv4	91	0.49110	2.66E-6
	Dm12Dv34	36	0.43363	0.00062

	Dm13Dv24	48	0.00	0.00
	Dm23Dv14	71	0.0927	0.00041
	Dm1Dv234	27	0.26759	0.00028
	Dm3Dv124	30	0.00459	2.84E-8
	Dm2Dv134	28	7.89E-7	1.28E-14
	Dm4Dv123	30	0.00275	0.18410
	Dm14Dv23	104	5.80E-7	0.29581
	Dm34Dv12	30	0.00017	0.39860
	Dm234Dv1	23	0.00167	0.23828
	Dm24Dv13	58	2.34E-5	0.13648
	Dm124Dv3	50	0.17035	0.00110
	Dm134Dv2	49	0.21680	6.42E-6
	endog. *osk* only	133	n/a	3.78E-7
Stage 1–2 embryo: *pgc*	Dm1234	49	1.38E-18	n/a
	Dv1234	31	4.24E-8	0.00
	Dm123Dv4	91	0.01503	1.04E-12
	Dm12Dv34	36	0.01208	1.62e-8
	Dm13Dv24	48	3.42E-6	0.00
	Dm23Dv14	71	1.13E-13	0.00
	Dm1Dv234	27	0.09671	6.85E-10
	Dm3Dv124	30	0.11079	5.83E-14
	Dm2Dv134	28	1.97E-5	0.00
	Dm4Dv123	30	1.09E-7	2.35E-5
	Dm14Dv23	104	6.03E-9	1.12E-8
	Dm34Dv12	30	5.70E-13	0.06107
	Dm234Dv1	23	0.00412	1.27E-5
	Dm24Dv13	58	4.75E-8	1.54E-5
	Dm124Dv3	50	2.55E-11	0.00144
	Dm134Dv2	49	2.76E-6	4.26E-6
	endog. *osk* only	133	n/a	0.00

Table S5. Statistical analysis of Vasa, *nanos,* and *pgc* enrichment in stage 10 *D. melanogaster* oocytes and stage 1–2 embryos expressing each Oskar chimera in a background with endogenous *oskar* present.

	Oskar-GFP enrichment (endog. *osk* background)			
	Genotype	Sample size	Integrated posterior enrichment p-value	Pearson correlation GFP-HA p-value
Stage 10 oocyte: GFP	Dm1234	25	n/a	n/a
	Dv1234	31	0.20564	0.28918
	Dm13Dv24	33	0.24297	0.02389
	Dm2Dv134	24	0.01444	0.28044
Stage 10 oocyte: HA	Dm1234		n/a	
	Dv1234		0.48413	
	Dm13Dv24		0.49845	
	Dm2Dv134		0.02964	
Stage 1–2 embryo: GFP	Dm1234	12	n/a	n/a
	Dv1234	12	0.21432	5.92E-5
	Dm13Dv24	32	0.19108	0.29510
	Dm2Dv134	21	0.03168	0.00045
Stage 1–2 embryo: HA	Dm1234		n/a	
	Dv1234		0.28852	
	Dm13Dv24		0.06833	
	Dm2Dv134		0.00187	

Table S6. Statistical analysis of Oskar-GFP posterior enrichment and Pearson correlation with HA in stage 10 oocytes and stage 1–2 embryos expressing each Oskar chimera in a background with endogenous *oskar* present and tagged with Oskar-GFP. P-values are estimated from the distribution of difference of means between sample and control from 100,000 simulated samples.

	Nanos enrichment (endog. *osk* bacgkround)			
	Genotype	Sample size	Integrated posterior enrichment p-value	Pearson correlation p-value
nanos mRNA	Dm1234	21	n/a	n/a
	Dv1234	24	2.53E-14	0.23452
	Dm13Dv24	27	8.23E-5	0.44211
	Dm2Dv134	17	0.25754	0.00032
Nanos protein	Dm1234	21	n/a	n/a
	Dv1234	24	0.19438	4.75E-27
	Dm13Dv24	27	0.33927	3.73E-38
	Dm2Dv134	17	0.00469	4.08E-7

Table S7. Statistical analysis of Nanos protein and *nanos* mRNA posterior enrichment and Pearson correlation with HA (proxy for chimeric Oskar protein) in stage 1–2 embryos laid by females expressing chimeric *oskar* in a background with endogenous *oskar* present. P-values are estimated from the distribution of difference of means between sample and control from 100,000 simulated samples.

Smaug enrichment (endog. *osk* background)			
Genotype	Sample size	Integrated posterior enrichment p-value	Pearson correlation p-value
Dm1234	12	n/a	n/a
Dv1234	12	0.15866	0.26754
Dm13Dv24	32	0.44401	0.35755
Dm2Dv134	21	0.28508	0.33941

Table S8. Statistical analysis of Smaug posterior enrichment and Pearson correlation with HA in stage 1–2 embryos expressing each Oskar chimera in a background with endogenous *oskar* present. P-values are estimated from the distribution of difference of means between sample and control from 100,000 simulated samples.

Par-1 enrichment (endog. *osk* background)			
Genotype	Sample size	Integrated posterior enrichment p-value	Pearson correlation p-value
Dm1234	31	n/a	n/a
Dv1234	23	0.43724	0.31283

Table S9. Statistical analysis of Par-1 posterior enrichment and Pearson correlation with HA in stage 10 oocytes expressing each Oskar chimera in a background with endogenous *oskar* present. P-values are estimated from the distribution of difference of means between sample and control from 100,000 simulated samples.

Par-1 enrichment (*osk* null background)			
Genotype	Sample size	Integrated posterior enrichment p-value	Pearson correlation p-value
Dm1234	19	n/a	n/a
Dm123Dv4	24	0.00517	3.45E-5
Dm124Dv3	8	0.30397	0.11840
Dm134Dv2	24	0.39665	0.49251
Dm234Dv1	24	0.00297	0.04158

Table S10. Statistical analysis of Par-1 posterior enrichment and Pearson correlation with HA in stage 10 oocytes expressing each Oskar chimera in the *oskar* RNA null background *w[1118]; Kr[If-1]/CyO; TI{w[+mC]=TI}osk[0.EGFP]*. P-values are estimated from the distribution of difference of means between sample and control from 100,000 simulated samples.

Radial Oskar localization	
Genotype	**Sample size**
D. mel osk null + *D. mel osk* transgene	25
D. mel osk null + *D. vir osk* transgene	24
D. melanogaster (Oregon R)	25
D. virilis	56
D. mel osk null + *Dm123Dv4* transgene	34
	p-value
D. mel osk null + *D. mel osk* transgene vs. *D. mel osk* null + *D. vir osk* transgene	1.21E-15
D. mel osk null + *D. mel osk* transgene vs. *D. melanogaster* (Oregon R)	0.05499
D. mel osk null + *D. mel osk* transgene vs. *D. virilis*	0.00103
D. mel osk null + *D. mel osk* transgene vs. *D. mel osk* null + *Dm123Dv4 osk* transgene	0.30309
D. mel osk null + *D. vir osk* transgene vs. *D. melanogaster* (Oregon R)	0.00
D. mel osk null + *D. vir osk* transgene vs. *D. virilis*	4.71E-8
D. mel osk null + *D. vir osk* transgene vs. *D. mel osk* null + *Dm123Dv4 osk* transgene	0.00
D. melanogaster (Oregon R) vs. *D. virilis*	2.40E-09
D. melanogaster (Oregon R) vs. *D. mel osk* null + *Dm123Dv4 osk* transgene	0.00202
D. virilis vs.*D. mel osk* null + *Dm123Dv4 osk* transgene	0.00127

Table S11. Statistical analysis of radial HA localization in cleavage stage embryos. The p-values are estimated from the distribution of difference of means between sample and control from 100,000 simulated samples.

Genetic background	Experiment	Primary antibody	Conc.	Secondary antibody/ stain	Conc.
Chimeras with endogenous *oskar* present	Vasa and HA in stage 10 oocytes	Rabbit anti-Vasa (gift from Akira Nakamura, Kumamoto University, Japan)	1:3000	Goat anti-rabbit Alexa 488 (Jackson ImmunoResearch)	1:500
		Mouse anti-HA (AbClonal)	1:50	Goat anti-mouse Alexa 647 (ThermoFisher)	1:500
		—		Hoechst 33342 (Sigma Aldrich)	1:2500 of 10 mg/mL stock
	Vasa and HA in stage 1–2 embryos	Chicken anti-Vasa (this paper)	1:1000	Goat anti-chicken Alexa 568 (ThermoFisher)	1:500
		Rat anti-HA (Millipore Sigma)	1:50	Goat anti-rat Alexa 647 (ThermoFisher)	1:500
				Hoechst 33342 (Sigma Aldrich)	1:2500
	nanos, pgc, and HA in stage 1–2 embryos	Mouse anti-HA (AbClonal)	1:50	Goat anti-mouse Alexa 488 (ThermoFisher)	1:500
				Hoechst 33342 (Sigma Aldrich)	1:2500
	Vasa, phalloidin, and HA in stage 5 embryos	Chicken anti-Vasa (this paper)	1:1000	Goat anti-chicken Alexa 568 (ThermoFisher)	1:500
		Mouse anti-HA (AbClonal)	1:50	Goat anti-mouse Alexa 647 (ThermoFisher)	1:500
		—		Alexa 488 phalloidin (ThermoFisher)	1:500
				Hoechst 33342 (Sigma Aldrich)	1:2500
	Osk-GFP, HA in stage 10 oocytes	Rabbit Anti-GFP conjugated to Alexa Fluor 488	1:250	—	—
		Rat anti-HA (Millipore Sigma)	1:50	Goat anti-rat Alexa 568 (ThermoFisher)	1:500
	Osk-GFP, HA, and Smaug in stage 1–2 embryos	Rabbit Anti-GFP conjugated to Alexa Fluor 488	1:250	—	—
		Rat anti-HA (Millipore Sigma)	1:50	Goat anti-rat Alexa 568 (ThermoFisher)	1:500
		Guinea pig anti-Smaug (gift from Howard Lipshitz, University of Toronto, Canada)	1:500	Donkey anti-guinea pig Cy5 (ThermoFisher)	1:500
	HA, *nanos,* and Nanos in stage 1–2 embryos	Rabbit anti-Nanos (gift from Akira Nakamura, Kumamoto University, Japan)	1:1000	Donkey anti-rabbit Alexa 647 (ThermoFisher)	1:500
		Rat anti-HA (Millipore Sigma)	1:50	Goat anti-rat Alexa 488 (ThermoFisher)	1:500
Chimeras in *oskar* RNA null background	Vasa and HA in stage 10 oocytes	Rabbit anti-Vasa (gift from Akira Nakamura, Kumamoto University, Japan)	1:3000	Donkey anti-rabbit Alexa 647 (ThermoFisher)	1:500
		Mouse anti-HA (AbClonal)	1:50	Goat anti-mouse Alexa 568 (ThermoFisher)	1:500
		—		Hoechst 33342 (Sigma Aldrich)	1:2500
	Vasa and HA in stage 1–2 embryos	Rabbit anti-Vasa (gift from Akira Nakamura, Kumamoto University, Japan)	1:3000	Goat anti-rabbit Alexa 568 (ThermoFisher)	1:500
		Rat anti-HA (Millipore Sigma)	1:50	Goat anti-rat Alexa 647 (ThermoFisher)	1:500

		—		Hoechst 33342 (Sigma Aldrich)	1:2500
	nanos and HA in stage 1–2 embryos	Rat anti-HA (Millipore Sigma)	1:50	Goat anti-rat Alexa 647 (ThermoFisher)	1:500
		—		Hoechst 33342 (Sigma Aldrich)	1:2500
	gcl and HA in stage 1–2 embryos	Rat anti-HA (Millipore Sigma)	1:50	Goat anti-rat Alexa 647 (ThermoFisher)	1:500
	Vasa, phalloidin, and HA in stage 5 embryos	Chicken anti-Vasa (this paper)	1:1000	Goat anti-chicken Alexa 568 (ThermoFisher)	1:500
		Rat anti-HA (Millipore Sigma)	1:50	Goat anti-rat Alexa 647 (ThermoFisher)	1:500
		—		Alexa 488 phalloidin (ThermoFisher)	1:500
		—		Hoechst 33342 (Sigma Aldrich)	1:2500
	Vasa and HA in stage 14 embryos	Rabbit anti-Vasa (gift from Akira Nakamura, Kumamoto University, Japan)	1:3000	Goat anti-rabbit Alexa 568 (ThermoFisher)	1:500
		Rat anti-HA (Millipore Sigma)	1:50	Goat anti-rat Alexa 647 (ThermoFisher)	1:500
		—		Hoechst 33342 (Sigma Aldrich)	1:2500
	Par-1, *osk,* and HA in stage 10 oocytes	Rabbit anti-Par-1 (gift from Daniel St. Johnston, Gurdon Institute, UK)	1:2500	Donkey anti-rabbit Alexa 647 (ThermoFisher)	1:500
		Mouse anti-HA (AbClonal)	1:50	Goat anti-mouse Alexa 488 (ThermoFisher)	1:500
Wild-type *D. melanogaster*	Vasa, Oskar, and actin in stage 10 oocytes	Rat anti-Oskar (Extavour Lab)	1:250	Goat anti-rat Alexa 647 (ThermoFisher)	1:500
		Rabbit anti-Vasa (gift from Akira Nakamura, Kumamoto University, Japan)	1:3000	Goat anti-rabbit Alexa 488 (Jackson ImmunoResearch)	1:500
		—		Rhodamine phalloidin (ThermoFisher)	1:250
				Hoechst 33342 (Sigma Aldrich)	1:2500
	Vasa and Oskar in stage 1–2 embryos	Rabbit anti-Oskar (gift from Anne Ephrussi, EMBL, Germany)	1:3000	Donkey anti-rabbit Alexa 647 (ThermoFisher)	1:500
		Chicken anti-Vasa (this paper)	1:1000	Goat anti-chicken Alexa 568 (ThermoFisher)	1:500
		—		Hoechst 33342 (Sigma Aldrich)	1:2500
	Vasa in stage 5 embryos	Chicken anti-Vasa (this paper)	1:1000	Goat anti-chicken Alexa 568 (ThermoFisher)	1:500
		—		Alexa 488 phalloidin (ThermoFisher)	1:500
				Hoechst 33342 (Sigma Aldrich)	1:2500
Wild-type *D. virilis*	Vasa, Oskar, and actin in stage 10 oocytes	Chicken anti-Oskar (this paper)	1:1000	Goat anti-chicken Alexa 647 (ThermoFisher)	1:500
		Rabbit anti-Vasa (gift from Akira Nakamura, Kumamoto University, Japan)	1:3000	Goat anti-rabbit Alexa 488 (Jackson ImmunoResearch)	1:500
		—		Rhodamine phalloidin (ThermoFisher)	1:250
				Hoechst 33342 (Sigma Aldrich)	1:2500
	Vasa and Oskar in stage 1–2 embryos	Chicken anti-Oskar (this paper)	1:1000	Goat anti-chicken Alexa 568 (ThermoFisher)	1:500
		Rabbit anti-Vasa (gift from Akira Nakamura, Kumamoto University, Japan)	1:3000	Goat anti-rabbit Alexa 488 (Jackson ImmunoResearch)	1:500
		—		Hoechst 33342 (Sigma Aldrich)	1:2500
	Vasa in stage 5 embryos	Rabbit anti-Vasa (gift from Akira Nakamura, Kumamoto University, Japan)	1:3000	Goat anti-rabbit Alexa 488 (ThermoFisher)	1:500

		—	Rhodamine phalloidin (ThermoFisher)	1:500
			Hoechst 33342 (Sigma Aldrich)	1:2500

Table S12. Antibodies and stains used in immunofluorescence experiments. “Conc.” = antibody or stain concentration.

Hybridization chain reaction probes			
Species	**Probe**	**Amplifier**	**Fluorophore**
D. melanogaster	*oskar*	B1	Alexa 488
	Nanos	B5	Alexa 555
	germ cell-less	B3	Alexa 594
	polar granule component	B4	Alexa 647
	oskar 3'UTR	B5	Alexa 555
D. virilis	*oskar*	B1	Alexa 488
	nanos	B5	Alexa 555
	germ cell-less	B3	Alexa 594
	polar granule component	B4	Alexa 647

Table S13. List of hybridization chain reaction (HCR) probes used in fluorescence *in situ* hybridization experiments.

Primer sequences	
Name	**Sequence**
pVAL22_gOsk_bridge2_R	CACCCTCAGCTCCAAAGCCTCGAGTGTTTTGCCATTTTACA
pVAL22_gOsk_bridge1_R	CACTAGTAGTACCAGCTTATAACTTCGTATAATGTGAATTGGGTACCGGGCC
pVAL22_gOsk_bridge2_F	TGTAAAATGGCAAAACACTCGAGGCTTTGGAGCTGAGGGTG
pVAL22_gOsk_bridge1_F	GGCCCGGTACCCAATTCACATTATACGAAGTTATAAGCTGGTACTACTAGTG
pVALIUM22_R6	GCTTTGGAGCTGAGGGTG
pVALIUM22_F6	ACATTATACGAAGTTATAAGCTGGTACTACTAGTG
Dmel_gOsk_HA_F1	GATGTTCCGGATTACGCTTAAGTTGGGTTCTTAATCAAGATACATATATG
Dmel_gOsk_HA_R1	GTATGGGTAACTACCATACTCCAGACTCGTTTCAATAACTTGC
HA_F1	GGTAGTTACCCATACGATGTTCCGGATTACGCT
Dmel_Dvir4_R1	TAATCCGGAACATCGTATGGGTAACTACCATAATACTCCAAGTTTTCTTCAATCATGTGC
Dmel_upstream_F1	CGCTTGGAGGAAAGTGATCCAATATTCTTG
Dmel_Dvir1_F1	GAATATTGGATCACTTTCCTCCAAGCGATGGCGACATTCAGAAGTGAATTC
Dmel_upstream_F2	CTGTTGAATTCACTTCTGAATGTCGCCATCGCTTGGAGGAAAGTGATCCAATATTCTTG
Dmel_Dvir1_F2	ATGGCGACATTCAGAAGTGAATTCAACAGCGTGCCGAACACTTACAACC
Dvir_Losk_F161	ATGACCATCATGGACAACACCTATATT
Dvir_int_R1	CCAGCAGTATGGAGCGTATTTCAG
Dvir_Losk_F261	GACAGTGTGAGCAACCCAATC
Dvir_Losk_F401	TCGGACTATGATGCATATCTATTGG
Dvir_Losk_F387	TCGTGTCCATCAACGCAAC
Dvir_int_F1	GTACATGGTTATGATTTCGAGGCT
Dvir_int_F2	CAAATCAACCGACTCCATTCCC
Dmel_gOsk_insert_F1	AACTGCTCACCGTTACTTCTGTTG
Dmel_Losk_R414	GTTAATCGTCAGCAGAGAATCGTTG
Dmel_Losk_R400	TAAAATCGTTGGCGTGGGC
Dmel_Losk_F140	ACCATCATCGAGAGCAACTATATATCCG

Dmel_Losk_gOsk_R1	CATCGCTTGGAGGAAAGTGATC
Dmel_Dvir4_R2	CCGGAACATCGTATGGGTAACTACCATAATACTCCAAGTTTTCTTCAATCATGTGC
Dmel_upstream_F3	GAATTCACTTCTGAATGTCGCCATCGCTTGGAGGAAAGTGATCCAATATTCTTG
Dmel_Dvir1_F2	ATGGCGACATTCAGAAGTGAATTCAACAGCGTGCCGAACACTTACAACC
Dvir_Losk_R386	CAACGTTGTTGGCGTGCGCG
Dm4_Dv3_F1	CGCGCACGCCAACAACGTTGACCAGTGGAACCTACAACGATTCTC
Dm4_HA_R1	CCGGAACATCGTATGGGTAACTACCATACTCCAGACTCGTTTCAATAACTTGC
Dvir_Losk_R260	GCGTTGTCGCTGCTGCAG
Dm3_Dv2_F1	TACTGCAGCAGCGACAACGCTACAGCAGCGGAGCTCCG
Dm3_Dv4_R1	TGTTGCGTTGATGGACACGATAAAATCGTTGGCGTGGGC
Dm2_Dv1_F1	GTGCAAGTATCACCAGCTCCAGCATGACCATCATCGAGAGCAACTATATATC
Dvir_Losk_R160	GCTGGAGCTGGTGATACTTGCAC
Dm2_Dv3_R1	TGGATTGGGTTGCTCACACTGTCGTCGCTGGTGCGCTCTTTC
Dm1_Dv2_R1	CCAATATAGGTGTTGTCCATGATGGTCATGTTGTTCTCGCTGGTGTTGCTG
Dm1_gOsk_F1	GAATATTGGATCACTTTCCTCCAAGCGATGGCCGCAGTCACAAGTG

Table S14. Primer sequences used for cloning *oskar* chimeras.

Supplemental References

1. Abramson, J. *et al.* Accurate structure prediction of biomolecular interactions with AlphaFold 3. *Nature* **630**, 493–500 (2024).

2. Rice, P., Longden, I. & Bleasby, A. EMBOSS: The European Molecular Biology Open Software Suite. *Trends Genet* **16**, 276–277 (2000).

3. Kubíková, J., Ubartaitė, G., Metz, J. & Jeske, M. Structural basis for binding of Drosophila Smaug to the GPCR Smoothened and to the germline inducer Oskar. *Proc. Natl. Acad. Sci.* **120**, e2304385120 (2023).

4. Suyama, R., Jenny, A., Curado, S., Berkel, W. P. & Ephrussi, A. The actin-binding protein Lasp promotes Oskar accumulation at the posterior pole of the Drosophila embryo. *Development* **136**, 95–105 (2009).

5. Anne, J. Targeting and Anchoring Tudor in the Pole Plasm of the Drosophila Oocyte. *PLoS ONE* **5**, e14362 (2010).

6. Repouliou, A., Srouji, J. R., Rivard, E. L., Leschziner, A. E. & Extavour, C. G. The LOTUS domain of Oskar promotes localisation of both protein and mRNA components of Drosophila germ plasm. *bioRxiv* 2025.05.02.651258 (2025) doi:10.1101/2025.05.02.651258.